Multimodal imaging of neuroinflammation in the living human brain

Riccardo De Marco

A thesis submitted in partial fulfilment of the requirements

of the Brighton and Sussex Medical School for the degree

of Doctor of Philosophy

February 2023

Abstract

Converging evidence implicates inflammation in the pathophysiology of depression. This has fuelled the development/ repurposing of novel and established immune-targeted agents as potential anti-depressant therapies. However, methods for assessing CNS target engagement for immunotherapeutics are currently limited. In this thesis, I aimed to determine whether an experimental model of acute inflammation (intravenous endotoxin) coupled with two different imaging modalities (MRI and PET), behavioural, physiological and immunological data could serve as a potential in-vivo model for assessing 'target engagement' for therapies targeting microglia.

To do this, participants (healthy young males) underwent two experimental sessions in which they received Lipopolysaccharide (LPS) (1 ng/kg) or saline in randomised order. Half received minocycline (a putative microglial inhibitor) prior to each session, and half an identical looking placebo. The primary neuroimaging technique used to assess effects on the brain was Positron Emission Tomography (PET) targeting the microglial marker 18-kDa Translocator Protein (TSPO). Diffusion-Weighted Magnetic Resonance Spectroscopy (DW-MRS), was later added for a subset of participants to investigate whether this novel MRI-based method was sensitivity to 'neuroinflammation'. Mood questionnaires and a reward/ punishment reinforcement learning task were used to assess psychological changes. Serial blood-draws and continuous physiological monitoring was used to assess physiological/ immunological responses.

Key findings include demonstrating that DWMRS is sensitive to LPS-induced changes in glial morphometry and showing that a simpler quantification of TSPO (using a

supervised clustering algorithm (SVCA) based pseudo-reference region) is sensitive to LPS-induced microglial activity. Though neither technique was significantly influenced by minocycline. Behavioural performance on the reward/punishment reinforcement-learning task was also modulated by inflammation (LPS), replicating findings observed using a milder inflammation model (Typhoid vaccination). Interestingly this LPS-induced motivational reorientation (increased sensitivity to punishments versus rewards) was significantly attenuated by minocycline.

Together, these data provide tentative support for LPS coupled with a reward/punishment reinforcement learning task as a potential method for assessing target engagement for novel neuroimmune therapeutics. They show that a simpler pseudo-reference region approach is suitable for TSPO PET using the [^{18}F]-DPA-714 tracer and provide proof-of-concept data for DWMRS as a potentially important new MRI based tool for quantifying neuroinflammation. Future studies will be required to further validate each of these approaches before they are considered for wider adoption.

Tables of contents

List of Tables

List of Figures

List of abbreviations

2TCM: Two-Tissue Compartment Model

5-HT: Serotonin

ACC: Anterior Cingulate Cortex

ADC: Apparent Diffusion Coefficient

AIF: Arterial Input Function

ALS: Amyotrophic Lateral Sclerosis

ANOVA: Analysis of Variance

AUC: Area Under the Curve

BBB: Blood Brain Barrier

BH4: Tetrahydrobiopterin

BMI: Body Mass Index

BP_{ND}: Binding Potential

Bq: Becquerel

CF: Calibration Factor

CNS: Central Nervous System

CRP: C-Reactive Protein

CSF: Cerebrospinal Fluid

D2R: Dopamine Receptor D2

DA: Dopamine

DVR: Distribution Volume Ratio

DW-MRS: Diffusion-Weighted Magnetic Resonance Spectroscopy

DWI: Diffusion-Weighted Imaging

fMRI: functional Magnetic Resonance Imaging

f_P: Plasma free fraction

fVAS: fatigue Visual Analog Scale

GM: Grey Matter

GR: Glucocorticoid Receptor

HABs: High Affinity Binders

HAM-D: Hamilton Depression Rating Scale

HPA: Hypothalamic-Pituitary-Adrenal

IDIF: Image-dDrived Input Function

IDO: Indoleamine 2,3-dioxygenase

IFN: Interferon

IL: Interleukin

KA: Kynurenic Acid

K_i: inhibitory constant

KP: Kynurenine Pathway

KYN: Kynurenine

LAB: Low Affinity Binders

LPS: Lipopolysaccharide

LTP: Long-Term Potentiation

MABs: Mixed Affinity Binders

MDD: Major Depressive Disorder

MDE: Major Depressive Episode

MRS: Magnetic Resonance Spectroscopy

MS: Multiple Sclerosis

NAA: N-Acetyl-Aspartate

NE: Noradrenaline

NMDA: N-methyl-D-aspartate

NODDI: Neurite Orientation Dispersion and Density Imaging

PAMP: Pathogen-Associated Molecular Patterns

PBIF: Population-Based Input Function

PET: Positron Emission Tomography

POB: Plasma-Over-Blood

POMS: Profile Of Mood State

QA: Quinolinic Acid

qMT: quantitative Magnetization Transfer

ROI: Region Of Interest

ROS: Reactive Oxygen Species

SEM: Standard Error of the Mean

SERT: Serotonin Transporter

SLE: Systemic Lupus Erythematosus

SNS: Sympathetic Nervous System

SPM: Statistical Parametric Mapping

SSRIs: Selective Serotonin Reuptake Inhibitors

Std: standard deviation

SUV: Standardized Uptake Value

SVCA: Supervised Clustering Algorithm

TAC: Time Activity Curve

TCAs: Tricyclic Antidepressants

TLR: Toll-like Receptor

TNF: Tumour Necrosis Factor

TR: Treatment Resistance

TRD: Treatment-Resistance Depression

TRP: Tryptophan

TSPO: Translocator Protein 18 kDa

VMAT2: Vesicular Monoamine Transporter 2

VOI: Volumes Of Interest

V_T: Volume of distribution

WBC: White Blood Cells

WM: White Matter

Acknowledgements

I would like to thank my supervisors Dr. Alessandro Colasanti, Professor Neil Harrison and Professor Mara Cercignani for the opportunity to take on this project and for their guidance throughout my PhD.

I also would like to thank my fellow PhD students Balazs Orzsik, Marisa Amato, George Tertikas, and Prince Nwaubani for their help and support during the participant recruitment phases, experiment sessions and ELISA experiments.

I would like to acknowledge the work of Professor Itamar Ronen and Dr. Francesca Branzoli. Their contribution was fundamental to start the DW-MRS scan acquisitions and to analyse and interpret the data collected.

I would also like to thank Dr. Julia Schubert and Dr. Mattia Veronese for their assistance in the analysis of PET images.

I am grateful to the volunteers that took part in this study.

Thanks to Rolf Cook for proofreading the manuscript.

Finally, I would like to thank my family for their constant support and encouragement.

Author’s Declaration

I declare that the research contained in this thesis, unless otherwise formally indicated within the text, is the original work of the author. The thesis has not been previously submitted to this or any other university for a degree, and does not incorporate any material already submitted for a degree.

Riccardo De Marco

February 2023

Statement of contribution

I wrote the ethics and Standard Operating Procedures (SOPs) necessary for the conducting the experiment.

I tested a series of laboratory equipment and run pilot experiments in order to start a radiochemistry laboratory to complement the PET imaging facility. Then I wrote the protocol for the experiment described here.

I managed the participant recruitment processes. I coordinated the data collection phase in all of its aspects. These included organizing experiment sessions, supervising of PET and MRI scans, administering of psychological questionnaires and tasks, and processing of blood samples for radiochemistry and immunological analysis.

I was entirely responsible for the data analysis for all of the PET, psychological, physiological and cytokine data, including that collected before the start of my PhD. I have also run a significant part of the MRI analysis.

I provided interpretation of the results and I was the principal author of the article that includes half of the results presented in Chapter 6.

I was also involved in the data collection for the first part of this project as part of my MSc. The start of the second phase of the data collection for this project coincided with the start of my PhD.

Publications derived from this work

Original research articles

- De Marco, R., Ronen, I., Branzoli, F., Amato, M.L., Asllani, I., Colasanti, A., Harrison, N.A., Cercignani, M., 2022. Diffusion-weighted MR spectroscopy (DW-MRS) is sensitive to LPS-induced changes in human glial morphometry: A preliminary study. Brain. Behav. Immun. 99, 256–265. https://doi.org/10.1016/J.BBI.2021.10.005.

- De Marco, R., Barritt, A.W., Cercignani, M., Cabbai, G., Colasanti, A., Harrison, N.A., 2023. Inflammation-induced reorientation of reward versus punishment sensitivity is attenuated by minocycline. Brain. Behav. Immun. 111, 320–327. https://doi.org/10.1016/J.BBI.2023.04.010

Chapter overview

Chapter 1

In this chapter I introduce the field of psychoneuroimmunology and review data linking inflammation and immunity with the pathophysiology of depression including clinical and pre-clinical evidence. I describe the principal mechanisms linking the immune system and the brain and outline the mechanisms through which this may ultimately result in impairment in mood. I emphasize the importance of distinguishing different depression phenotypes and how a better characterization of immune biomarkers may help fulfil unmet clinical needs.

Chapter 2

This chapter describes the neuroimaging techniques that have been used to investigate the effect of inflammation on the brain, with a focus on findings from studies on depressed patients or experiments that used immune challenges on healthy humans.

Chapter 3

Here, I describe the overarching methodology of the study which is relevant to each of the subsequent experimental chapters. This includes the experimental study design, the protocol adopted during the experiment sessions, participant demographics and the recruitment process.

Chapter 4

The first results chapter presents findings from all of the peripheral physiological and immunological responses to the immune challenge (LPS) and placebo (saline). The expected immune activation includes rapid changes in vital signs, differential white blood cells count and circulating cytokines.

Chapter 5

This chapter reports the psychological responses to inflammation. The main focus is on the results of a reinforcement learning task used to assess the effect of LPS on reward and punishment sensitivity. Using this cognitive test, I replicate previous results showing that inflammation induces motivational reorientation as indicated by enhanced sensitivity to punishment versus reward. Furthermore, I present new findings suggesting that minocycline can attenuate this inflammation-induced motivational reorientation. I highlight the relevance of these data for a particular subdomain of depression symptoms and the potential therapeutic implications.

In addition, the changes in mood and fatigue induced by the inflammatory stimulus as assessed through self-rating questionnaires are reported.

Chapter 6

DW-MRS is a novel neuroimaging technique that enables quantification of intracellular metabolite diffusion. Here I present results showing that DW-MRS is sensitive to microstructural brain changes induced by inflammation, as shown by the increased apparent diffusion coefficient of the glial metabolite choline. I provide an overview of the technical limitations of this technique, discuss the next

steps required to further validate this approach then consider how the emerging field of Immunopsychiatry may benefit from this new imaging tool.

Chapter 7

The final experimental chapter describes the TSPO PET experiments and is divided into two main sections. In the first I describe the implementation of a Supervised Cluster Algorithm (SVCA) approach to define a pseudo-reference region for the TSPO PET data analysis. I discuss the rational for using this technique and I show the outcomes, reflecting on differences with respect to the current gold standard method. This includes highlighting the practical advantage of using a non-invasive methodology. Results show that this technique is sensitive to the glial activation induced by the immune challenge. However, it is likely that the resulting signal is still underestimated.

The second section reports data from a smaller cohort collected and analysed using the current gold standard method, which includes full arterial blood and plasma sampling. I discuss how I established a radiochemistry laboratory specifically for this study. I focus on the methodological aspects of the data collection phase and emphasize the logistical and technical drawbacks of this approach. Effect of LPS-induced changes in radiotracer availability in the blood compartment is a central aspect of this section. To conclude I present the effect of inflammation on the TSPO PET results analysed using a kinetic model with an arterial blood input function.

Chapter 8

Here I draw together findings from each of the previous chapters. I describe the strengths and limitations of each technique. I suggest future experiments to complement my findings and to provide a more robust understanding of the effectiveness of each technique.

Chapter 1: Background

1.1 Brief history of the "inflammatory theory" of depression

Depressive disorders are a major public health problem. Globally, major depressive disorder (MDD) is the most prevalent mental illness and causes substantial impairment and large direct and indirect healthcare costs (Briley and Lépine, 2011). The World Health Organization ranks MDD as the leading cause of disability, affecting 4.4% of the global population (Friedrich, 2017).

Depression symptoms are heterogeneous, encompassing cognitive, behavioural and neurovegetative features. Its aetiology is considered multifactorial and includes genetic, biological, environmental and social factors. (Sullivan, Neale and Kendler, 2000)

The monoamine hypothesis has been the most widespread pathophysiological explanation for MDD. According to this hypothesis, lower level of dopamine, serotonin and norepinephrine represents the biological basis of depression. The hypothesis was based on the observations that reduced availability of monoamines, as a side effect of the antihypertensive drug reserpine, precipitated depression symptoms (Shore, Silver and Brodie, 1955), whereas administering monoamine precursors, or inhibition of monoamine degradation or reuptake, can improve depressive symptoms (Hirschfeld, 2000). Even today most available antidepressants exert their function by increasing the availability of monoamines (Harmer, Duman and Cowen, 2017). The only exception is esketamine, which was approved in 2019, which is the first treatment, since the 1950s, targeting a novel mechanism (Hashimoto, 2019). However, although it provides a biochemical basis of mood disorders and useful pharmacological applications, the monoamine theory

presents some limitations. For example, it does not account for the delay observed between the administration of antidepressants, with the consequent increased monoamine concentration, and their clinical response (Harmer, Duman and Cowen, 2017). Moreover, MDD is characterized by a relatively high incidence of patients (34-46%) that fail to achieve full remission after two courses of common antidepressants (Voineskos, Daskalakis and Blumberger, 2020). This subtype of MDD is termed treatment-resistance depression (TRD).

The diagnosis of MDD is made when a patient reports 5 of the 9 criteria of the DSM-5 over a 2-week period. At least one core symptom ("depressed mood" or "loss of interest or pleasure" (anhedonia)) is required for the diagnosis. The additional symptoms are: weight loss, insomnia, psychomotor agitation or retardation, fatigue, feeling of worthlessness or guilt, decreased ability to concentrate and recurrent thoughts of death or suicidal ideation. Based on the severity of the symptoms, depression is classified as mild, moderate or severe. Hence, patients with a remarkably different profile of symptoms might receive the same type of diagnosis and treatment.

The broad variability in symptoms and the different responses to drugs among patients has led to the hypothesis that a precision medicine approach would help to increase the clinical response of MDD patients. In this framework, the validation of biomarkers that provide information about the biological basis of certain depressive symptoms would enhance the selection of treatment for specific subtypes of depression.

Imbalances in the immune system are pathophysiological elements that have captured researchers' attention in the context of depression. The hypothesis that the connection between the immune system and the brain could have behavioural implications was

initially made based on studies on animals. Such behavioural changes (sickness behaviours) during viral or bacterial infection were interpreted as an adaptive response to conserve resources to fight a pathogen rather than a debilitating effect of the infection (Hart, 1988). The first evidence that linked MDD to inflammation in humans was data showing an increased blood concentration of acute phase protein in depressed patients (Maes, Scharpé, *et al.*, 1992). The inflammatory theory of depression links depression to heightened immune activity and propose depressive symptoms as a maladaptive sickness response. It suggests that there may be a biological basis for depression that complement the monoamine theory. Since the first observations of immune markers in MDD patients this theory has become increasingly influential and the immunopsychiatry field has grown substantially in the last two decades.

Despite exceptional progresses having been made in characterizing neuro-immune pathways that may mediate the onset of depression, a direct translational approach to treat depression targeting the immune system is still lacking. This unmet clinical need may be fulfilled by the identification of *in vivo* biomarkers able to quantify the neuroimmune activity in humans and to provide information about the efficacy of new antidepressant.

1.2 Sickness behaviour

It is well known that infections, regardless of the invading pathogen induce a set of stereotyped mood, motivational and behavioural changes in animals and humans. These behavioural consequences observed during the course of an infection include depressed mood, lethargy, loss of appetite, reduced social exploration, anhedonia, hyperalgesia and

decreased concentration. From an evolutionary point of view, these behavioural responses to sickness have been considered as an adaptive system to fight pathogens and environmental threats. For instance, energy conservation and social withdrawal allow to redirect priorities and resources towards fighting the invading pathogen and, possibly, keeping an infection from spreading across a group and protecting the individual from further pathogens exposure. Behavioural alterations observed during illnesses have been collectively termed "sickness behaviours". Noticeably, some sickness behaviours closely resemble clinical features of depression, such as anhedonia, anorexia, helplessness and low concentration. The overlap between sickness behaviours and depressive symptoms provided a rationale for investigating the role of the immune system in mental disorders with potential therapeutic strategies.

The behavioural and cognitive correlates of immune activation have long been studied using the peripheral or central administration of recombinant cytokines or immune challenges that induce the production of inflammatory mediators (Dantzer, 2001).

The interleukin-1 (IL-1) family cytokine and Tumour Necrosis Factor α (TNF-α), produced by monocytes, macrophages and microglia, have been considered candidates in the onset of sickness behaviour. Animals treated with proinflammatory cytokines or immune challenges that trigger their release display the full spectrum of sickness behaviours, such as decreased locomotor activity, food intake and social behaviour and impaired learning (Gibertini *et al.*, 1995; Kent *et al.*, 1996; Bluthé, Dantzer and Kelley, 1997). There has been a growing interest in characterizing the neuronal substrates that mediate the behavioural and cognitive changes during the course of inflammation. Of note, peripheral cytokines or experimental immunostimulants trigger the release of

cytokines by brain cells, mainly microglia. The expression of cytokines within the brain has been deemed a principal mediator of sickness behaviour (Dantzer, 2001). Moreover, intracerebroventricular injection of the proinflammatory cytokine IL-1β leads to an impairment of long-term potentiation (LTP) in hippocampal granule cells synapses (Vereker, O'Donnell and Lynch, 2000). In mice subjected to mild chronic stress, IL-1 mediated the depressive-like behaviour and decreased hippocampal neurogenesis (Goshen *et al.*, 2007). However, the specific pathway underlying this mechanism has yet to be fully defined.

Lipopolysaccharide (LPS), which induces the expression of proinflammatory cytokine has largely been used as an infection model to activate the innate immune response and consequently elicit the entire set of sickness behaviours (Pugh *et al.*, 1998).

Experimental induction of sickness behaviour in animal models has been used to investigate the potential antidepressant effect of drugs targeting a component of the immune system. For example, TNF-α inhibitors have been shown to reduce depressive-like and anxiety-like behaviour in mouse models of depression (Krügel *et al.*, 2013).

1.3 Cross-talk between the brain and the immune system

The inflammatory theory of depression has gradually gained support as understanding of the relationship between the Central Nervous System (CNS) and the immune system has increased. I will first review immune-to-brain communication pathways before moving to clinical and experimental evidence in support of the inflammatory theory of depression.

Over the last two decades the concept of CNS as an "immune-privileged" organ system has been largely challenged and re-evaluated. The role of CNS immune resident cells and the interplay between the peripheral immune system and the brain have been progressively characterized. Recent data suggest that microglia cells (resident CNS macrophages), whose functions have been investigated mainly in a pathological framework, exert an important tissue homeostatic role in the healthy CNS, for instance in the synaptic pruning (Schafer *et al.*, 2012) and in maintaining hippocampal neurogenesis (Ziv *et al.*, 2006).

1.3.1 Immune to Brain to pathways

The immune system interacts with the CNS through multiple different parallel pathways as illustrated in Figure 1.1. A pathway that has been characterized involves afferent fibres of the vagus nerve. The endings of the afferent fibres, that express IL-1β receptors and Toll-like receptors, can be activated upon systemic infection or LPS immune challenge (Pavlov and Tracey, 2012). The expression of the immediate early gene c-Fos, a marker of neuronal activation, is triggered during peripheral inflammation in the primary (the nucleus tractus solitarius (NTS)) and secondary projections (including the ventrolateral medulla, the hypothalamic paraventricular and supraoptic nuclei, parabrachial nucleus and the central amygdala) of the vagus nerve (Wan *et al.*, 1994). Studies in mice using endotoxemia (LPS administration) as a model of systemic infection have also suggested that vagal afferent fibres may be responsible for an increased production of IL-1β in the hippocampus and hypothalamus (Laye *et al.*, 1995). Afferent fibres of the vagus nerve are ultimately involved in the behavioural response to peripheral inflammation. In support

of this, subdiaphragmatic vagotomy in rats attenuated the detrimental effect of peripheral inflammation on social exploration (Luheshi *et al.*, 2000).

The humoral interoceptive pathway represents another mechanism that enables communication between the CNS and the immune system. Circulating cytokines can enter the brain through the circumventricular organs, regions of the brain with a highly fenestrated vasculature, which allows the uptake and the release of relatively large molecules that cannot normally cross the blood brain barrier (BBB). However, this mechanism only accounts for a small fraction of the cytokine leakage into the brain (Maness, Kastin and Banks, 1998). The binding to saturable transporter on the BBB constitutes the main route through which cytokines enter the brain (Banks, 2005). An active transport across the BBB has been observed for several cytokines, such as IL-1and IL-6 (Banks, Kastin and Gutierrez, 1994; Plotkin, BanksP and Kastin, 1996). However, the BBB passage is highly selective and some cytokines, IL-2 for example, cannot enter the brain by this route (Banks, Niehoff and Zalcman, 2004). The brain cytokines uptake is also variable across regions, with some cytokines that only access some particular areas and others that can access every region but with highly variable efficiency (Maness *et al.*, 1995; Banks, Moinuddin and Morley, 2001).

In addition, phagocytic cells in the choroid plexus release IL-1, which can diffuse within the brain (Quan, Whiteside and Herkenham, 1998). Perivascular macrophage-like cells in the circumventricular organs expressing Toll-like receptors (TLRs) are able to detect circulating PAMP (pathogen-associated molecular patterns) and respond releasing cytokines (Dantzer et al., 2008). Of note, cytokines (particularly IL-6), by binding the

brain endothelium receptors, trigger the release of prostaglandin E2 promoting fever (Evans, Repasky and Fisher, 2015).

The infiltration of activated monocytes into the brain has been proposed to be a third immune-to-CNS communication axis. The suggestion derives from evidence that depressive like behaviours in mice model with systemic inflammation are modulated by monocyte recruitment. This follows the observation that in a mouse model of hepatic inflammatory disease, peripheral TNF-α stimulated microglial release of Monocyte Chemoattractant Protein-1 (MCP-1/CCL2), a cerebral monocyte chemoattractant protein, leading to activated monocytes infiltration into the brain. By blocking the activated microglia-mediated monocyte recruitment the depressive-like behaviours induced by peripheral inflammation were significantly ameliorated (D'Mello, Le and Swain, 2009).

Peripheral myeloid cell invasion is triggered upon bacterial (Mildner *et al.*, 2008) and viral infection and axonal injury (Babcock *et al.*, 2003). Interestingly, the recruitment of peripheral monocytes, which promotes the inflammatory signalling within the brain, is not strictly a consequence of a trauma or pathology but can occur as a result of a psychological stressor (Wohleb *et al.*, 2013).

Numerous data have suggested that myeloid cells trafficking within the brain plays an important role in regulating behaviour and may account for anxiety and depressive-like behaviour following RSD (Repeated Social Defeat) (Wohleb *et al.*, 2015). Accordingly, a mouse model deficient in monocyte chemotactic system (CCR2 knockout) did not develop stress-dependent anxiety behaviour (Wohleb *et al.*, 2013).

Figure 1.1 summarizes the mechanisms by which the immune system communicates with the brain.

1.3.2 Brain to immune pathways

The CNS plays a regulatory role in cytokine release at the site of injury through the immune reflex, preventing the tissue damage that an unbalanced cytokine release would cause. This process consists of a negative loop dependent on the vagus nerve, whose afferent arm transmits inflammatory signals to the brain. The efferent fibres of the vagus nerve, by a cholinergic transmission, suppress the production of cytokines by macrophages via a pathway mediated by the α subunit of the acetylcholine receptor (AChR) (Tracey, 2007).

The brain also modulates systemic inflammation by activating of the hypothalamic-pituitary-adrenal (HPA) axis, which results in the release of glucocorticoids (Imura and Fukata, 1994). In fact, glucocorticoids are routinely used as immunosuppressive agents for autoimmune and inflammatory diseases (Webster and Sternberg, 2004).

The HPA axis and the sympathetic nervous system (SNS) activity can regulate the activation and recruitment of myeloid cells. SNS noradrenergic fibres innervate primary and secondary lymphoid tissues that express β-adrenergic receptors, including bone marrow, lymph nodes and spleen (Felten *et al.*, 1985); the SNS noradrenergic signal can directly affect myeloid cell behaviour in terms of migratory activity and cytokine production (Grisanti *et al.*, 2011).

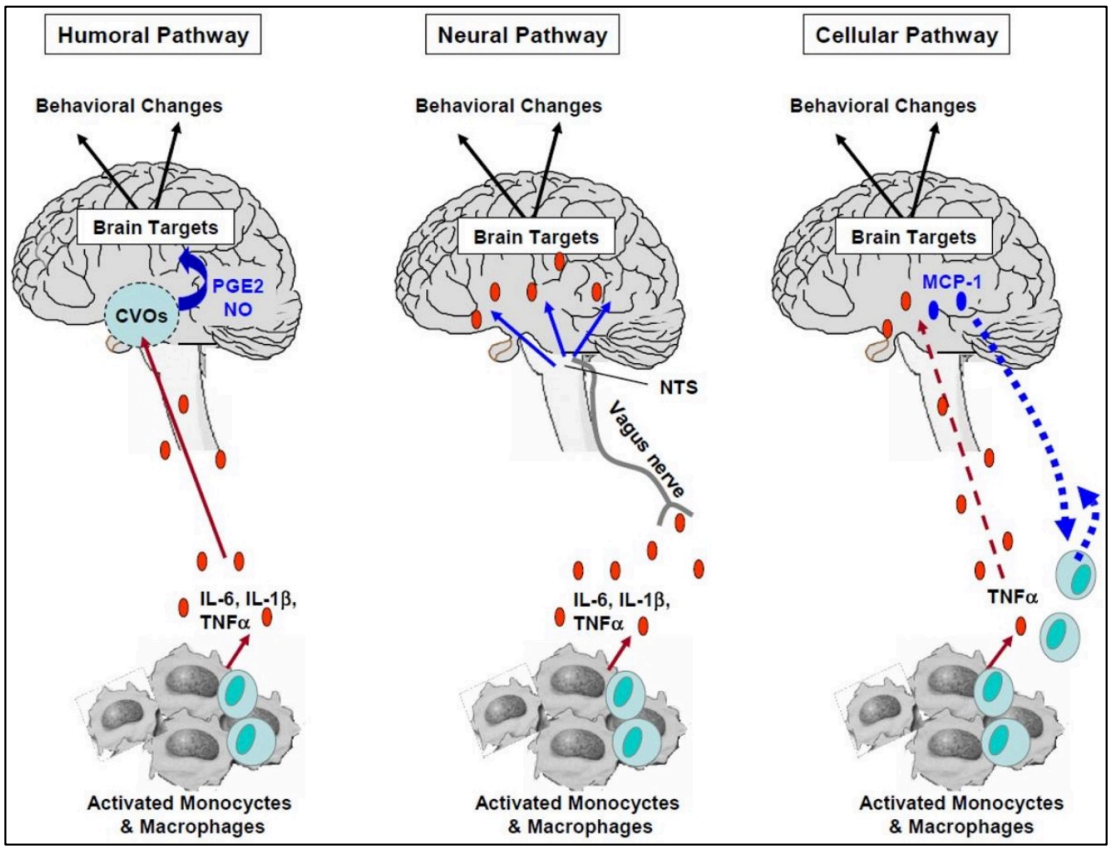

Figure 1.1 Immune system to brain pathways

Humoral pathways: circulating cytokines passively enter into the brain through the circumventricular organs (CVOs) and choroid plexus, or are actively transported by cytokine transporters of the endothelium. Neuronal pathways: proinflammatory cytokines (or LPS) activate fibres of the vagus nerve, which convey information to the brain. Cellular pathway: activated monocytes leak into the brain parenchyma following the gradient of microglial-derived Chemoattractant Protein-1 (MCP-1) (Figure taken from Capuron and Miller, 2011).

1.4 Immune biomarkers in depressed patients

Clinical data have consistently associated aberrations in immunological/inflammatory pathways with MDD. Meta-analyses of studies revealed elevated peripheral inflammatory

markers such as C-Reactive Protein (CRP), TNF-α and IL-6 in patients that meets DSM criteria for major depression (Alesci *et al.*, 2005; Raison, Capuron and Miller, 2006; Dowlati *et al.*, 2010; Haapakoski *et al.*, 2015). The origin of this raised level of inflammatory markers is not yet clear and several mechanisms have been described (Himmerich *et al.*, 2019). For example, risk factors for MDD that are linked with increased circulating cytokines include early life trauma, stress exposure and HPA axis imbalances (Pariante, 2017), social and environmental factors such as poverty and air pollution (Kristiansson *et al.*, 2015) and physical diseases such as obesity (Schmidt *et al.*, 2015), diabetes (Herder *et al.*, 2017) and autoimmune diseases (Kuwabara *et al.*, 2017).

Anomalous white blood cell count and trafficking have also been observed in MDD. Notably, depressed patients have been reported to have a significantly higher frequency of lymphopaenia (Kronfol, 2002; Mazza *et al.*, 2018). Conversely, total White Blood Cells (WBC) and neutrophils have been reported to be higher in depressed patients than in healthy controls (Maes, Lambrechts, *et al.*, 1992; Demir *et al.*, 2015). These data suggest that numerous immune pathways, which involve circulating immune messengers and immunocompetent cells, may contribute to the aetiology of depression.

Immune dysfunctions in the central nervous system (CNS) may also be involved in the pathophysiology of depression. A meta-analysis of 12 studies that investigated cerebrospinal fluid (CSF) cytokines levels in depression reported significantly increased IL-6, TNF-α and IL-8 concentrations in MDD patients. However, there was a high heterogeneity across the studies (Enache, Pariante and Mondelli, 2019). Furthermore, post-mortem analysis on brain samples from depressed patients that committed suicide showed increased microgliosis and the expression of immune related genes such as pro-

inflammatory cytokines, Toll-like receptors and chemokines involved in monocyte recruitment (Shelton *et al.*, 2011; Torres-Platas *et al.*, 2014; Pandey *et al.*, 2019).

The link between inflammation and depression has prompted researchers to evaluate whether common antidepressant drugs exert immunomodulating activities. Numerous studies investigated the relationship between antidepressant treatments and cytokine levels, with inconsistent results. Different Tricyclic Antidepressants (TCAs) and Selective serotonin reuptake inhibitors (SSRIs) suppress the production of the proinflammatory cytokine Interferon-γ (IFN-γ) and enhance the secretion of IL-10, the major anti-inflammatory cytokine, in T-lymphocytes and monocytes cultures (Kenis and Maes, 2002). However, a meta-analysis, including 17 in vitro studies and a total of 19 antidepressants, was unable to identify a unidirectional immunomodulatory effect. Instead, the pro- or anti- inflammatory effect may depend on the dose or the interaction with an inflammatory stimulus (Baumeister, Ciufolini and Mondelli, 2016). Results from longitudinal studies in MDD patients have yielded controversial results. Mirtazapine treatment was associated with decreased serum TNF-α (Gupta *et al.*, 2016). Conversely, Kast reported increased plasma TNF-α after mirtazapine treatment while bupropion decreased TNF-α (Kast, 2003). A meta-analysis reported a lower concentration of IL-1β but not of TNFα or IL-6 plasma after SSRI treatment (Hannestad, Dellagioia and Bloch, 2011). A more recent meta-analysis including a total of 827 MDD patients reported moderate effects of anti-depressants on circulating concentrations of IL-6, IL-1β, TNF-α, and IL-10 but no changes in IL-2, IL-4 or IFN-γ levels (Wang *et al.*, 2019). However, authors reported a large heterogeneity between studies in both meta-analyses. It is still not clear whether the immunomodulatory effects of anti-depressants are unintended consequences or represent a part of the mechanism of action for their clinical effect.

1.5 Effect of inflammation on the HPA axis

The hypothalamic-pituitary-adrenal (HPA) axis is a neuroendocrine system which regulates the release of glucocorticoid hormones. The HPA axis consists of interactions between the hypothalamus, pituitary gland and adrenal gland. The activation of the HPA axis results in cortisol release by the adrenal glands. Cortisol, the primary glucocorticoid hormone in humans, is involved in a wide range of homeostatic, metabolic and immune functions (Sapolsky, Romero and Munck, 2000). The HPA axis also plays a central role in behavioural response to stress (Smith and Vale, 2006). Cortisol release is regulated by a negative feedback: cortisol binds to the Glucocorticoid Receptor (GR) of the hypothalamus and pituitary gland, inhibiting its own secretion (Figure 1.2). The inhibition of HPA negative feedback (glucocorticoid resistance) causes HPA hyperactivity.

Glucocorticoid resistance, linked to alterations at GR level which results in HPA hyperactivity, is an important biological hallmark of depression, present in up to 80% of MDD patients, that has been studied since before the association between inflammation and depression was observed (Owens and Nemeroff, 1993; Heuser, Yassouridis and Holsboer, 1994).

Notably, the HPA axis exerts a regulatory role in preventing imbalanced immune reactions. Cortisol modulates inflammatory activity and glucocorticoid resistance can result in exaggerated immune activity (Silverman and Sternberg, 2012). As the relationship between inflammation and MDD emerged, there was growing interest in the potential link between inflammatory mediators and glucocorticoid resistance in MDD.

The interplay between inflammation and glucocorticoid resistance has been studied in clinical populations. In a small group of depressed patients, the IL-6 level was positively

correlated with the cortisol level after a dexamethasone suppression test, suggesting that inflammation was associated with impaired HPA axis regulation (Maes *et al.*, 1993). Transcriptomic analysis in depressed patients showed that patients with a higher expression of proinflammatory cytokines also exhibited lower leukocytes glucocorticoid receptor (GR) mRNA and a higher expression of FKBP5, which inhibits GR function (Cattaneo *et al.*, 2012).

Research investigating the molecular basis for this phenomenon have characterized possible mechanisms by which cytokines can lead to glucocorticoid resistance. In vitro studies have shown that proinflammatory cytokines can downregulate the expression and function of the GR in a variety of cell types, potentially leading to glucocorticoid resistance (Spahn *et al.*, 1996; Pariante *et al.*, 1999). Furthermore, the activation of the NLRP3 inflammasome can increase glucocorticoid resistance by triggering the caspase 1-mediated GR cleavage (Paugh *et al.*, 2015).

However, although associations between circulating cytokines and glucocorticoid resistance have been observed in depression, whether glucocorticoid resistance is a prerequisite of increased cytokines in depressed patients is still controversial and require further investigation (Perrin *et al.*, 2019).

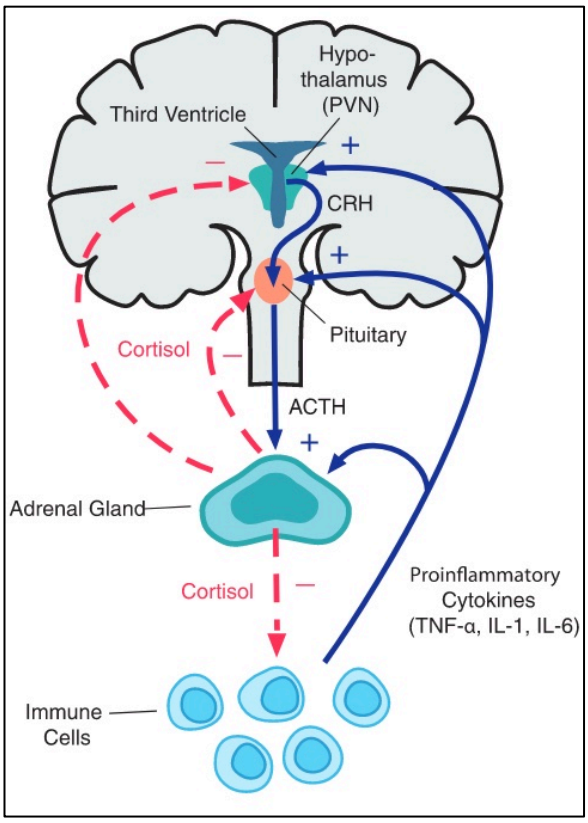

Figure 1.2 Cross-talk between HPA axis and cytokines

The hypothalamus releases the corticotropin releasing hormone (CRH) which induces the production of adrenocorticotropin hormone (ACTH) by the anterior pituitary gland. ACTH stimulates the secretion of cortisol by the adrenal glands. Cortisol inhibits proinflammatory activities of immune cells and binds to the glucocorticoid receptor on the hypothalamus and anterior pituitary gland regulating its own secretion. Glucocorticoid resistance leads to the failure of this feedback mechanism and increased cortisol level. Proinflammatory cytokines trigger the release of cortisol by stimulating all three levels of the HPA axis (Figure taken from Silverman and Sternberg, 2012).

1.6 Challenge studies

In order to investigate whether inflammation has a potentially causative role in the aetiology of depression, the effect of induced inflammation (be it experimentally or during immunotherapies) has also been assessed.

Various types of experimental immune challenges have been used to investigate the psychological implications of systemic inflammation. LPS and typhoid vaccination have been used in experimental settings, whereas Interferon-α (IFN-α) is used as a treatment in clinical contexts.

1.6.1 Endotoxemia as a tool to study inflammation-induced mood deterioration

LPS (also called endotoxin) is a component of the outer membrane of gram-negative bacteria. LPS represents a safe, well-established experimental paradigm to provoke inflammation-induced psychological changes that resemble depressive symptoms in humans, such as depressed mood, anxiety, anhedonia and fatigue. As such, it has been widely used in animals and humans as model of infection to assess the detrimental impact of inflammation on behaviour and cognition (Nava Catorce and Gevorkian, 2016; Lasselin, Lekander, *et al.*, 2020).

Systemic injection of LPS in mice and rats elicits typical sickness behaviours, such as anhedonia and decreased locomotor activity, food consumption and social interaction (Yirmiya, 1996).

LPS induces increased body temperature and a transient robust increase of cytokine concentration in the blood, which peaks at 2-3 hr after the administration and then rapidly decreases. Importantly, 0.8 ng/kg LPS induces raised CSF level of IL-6, which positively

correlates with a depressed mood in heathy humans (Engler *et al.*, 2017). The dose-dependent behavioural effects of LPS in humans generally arise within 1 hour post injection and peak at 2 hours (Grigoleit *et al.*, 2011; DellaGioia *et al.*, 2013; Lasselin, Elsenbruch, *et al.*, 2016). Interestingly, endotoxemia induces decreased ventral striatum activity in response to monetary rewards (Eisenberger *et al.*, 2010). Conversely LPS has been associated with enhanced neuronal response in the ventromedial PFC and ventral striatum to both positive and negative social feedbacks (Muscatell *et al.*, 2016). Thus, LPS has emerged as a valid tool in investigating the effect of inflammation on the neuronal activity of reward-related brain regions.

As it represents an immune challenge that can mimic features of depression, endotoxemia has been proposed as a model to test the effect of immunomodulant drugs on inflammation-associated depressive symptoms (Suffredini and Noveck, 2014). In support of this, animal studies have shown that endotoxemia could be used to evaluate the effect of drugs directed to modulate immune pathways or neuronal signalling imbalances that may be due to inflammation (O'Connor, Lawson, André, *et al.*, 2009; Walker *et al.*, 2013; Camara *et al.*, 2015).

Importantly, one of the advantages of using endotoxemia as a model of inflammation is that, even though the tolerated doses are in different order of magnitudes, the behavioural responses are conserved across species allowing the translation of results from animals to humans (Lasselin, Schedlowski, *et al.*, 2020). On the other hand, endotoxemia presents some limitations. Although LPS can elicit behavioural changes that mimic depression features, it is characterized by a very acute physiological and behavioural response, whereas in MDD symptoms last for at least 2 weeks. This time discrepancy complicates

the interpretation of the findings as the mechanisms by which LPS acutely induces mood deteriorations could differ from that which is present during a chronic disease like MDD.

The main rationale for using LPS in this study is its ability to elicit a robust systemic and central inflammatory response (as reviewed in the following sections and in Chapter 7) in healthy subjects. This allows testing the sensitivity of neuroimaging methods to central inflammation and the potential target engagement of immunomodulant agents.

The mechanisms by which LPS elicits the immune response and the physiological effects observed in this study are reported and discussed in Chapter 4.

1.6.2 Typhoid vaccination model

The association between inflammation and mood and cognitive deterioration in humans has also been reported following the administration of typhoid vaccine (Strike, Wardle and Steptoe, 2004; Harrison *et al.*, 2009). Compared to LPS, typhoid vaccination elicits a milder inflammatory reaction. Typhoid vaccine induces fatigue and mental confusion but not fever, aching joints or headaches (Brydon *et al.*, 2008). However, since the response to typhoid vaccine is very subtle compared to the one to endotoxemia, it might be difficult to use this model to test the sensitivity of novel techniques to index neuroinflammation.

1.6.3 IFN-α model

IFN-α is a cytokine implicated in the early immune response to viral infection. It has been used in the treatment of viral infections and cancer (Borden and Parkinson, 1998). IFN-α treatment induces the expression of other pro-inflammatory cytokines, such as IL-6, in the blood and in the CSF (Taylor and Grossberg, 1998; Raison *et al.*, 2009).

Studies investigating the effect of immunotherapies in the context of melanoma and hepatitis-C treatment have shown that the chronic peripheral administration of proinflammatory proteins like Interferon-alpha induce depressive symptoms within 8-12 weeks in up to 50% of patients (Musselman *et al.*, 2001; Lucile Capuron *et al.*, 2002; Udina *et al.*, 2012).

IFN-α has widely been used to investigate the possible neurobiological basis of inflammation-associated depressive symptoms (Felger, Li, *et al.*, 2013; Dowell *et al.*, 2016, 2019).

Of note, as IFN-α induces depressive symptoms only in ~50% of patients within 8-12 weeks of therapy, it offers the opportunity to design longitudinal studies with baseline measurement and symptoms evaluations at different times to evaluate potential predictors for the onset of depressive symptoms (Capuron *et al.*, 2003; Davies *et al.*, 2020). Nevertheless, its use is limited to the clinical population and animal models and cannot be used in a preclinical experiment in healthy humans for ethical reasons.

1.7 Inflammation and neurotransmitters

Dopamine (DA), serotonin (5-HT) and noradrenaline (NE) are monoamine neurotransmitters involved in neuronal pathways that regulate mood motivation and behaviour. Imbalances of monoaminergic systems are associated with depression and other psychiatric diseases. and common antidepressants exert their function by increasing 5-HT, NE or DA availability within the synaptic cleft (Delgado, 2000). Yet, the

monoamine theory of depression does not provide a comprehensive explanation for the molecular mechanisms that cause imbalances of monoaminergic signalling.

As inflammation has been deemed responsible for affecting mood and behaviour and inducing depressive symptoms, its impact on monoamine neurotransmitters systems has been investigated (Figure 1.3).

However, the monoaminergic pathways are not the only neuronal mechanisms thought to be involved in depression symptoms to be affected by the peripheral immune activation. Accumulating evidence has suggested that abnormalities in the glutamatergic system may also be involved in the pathophysiology of depression (Sanacora, Treccani and Popoli, 2012).

1.7.1.1 Serotonin

A lower plasma concentration of the amino acid tryptophan (TRP) is well documented in depression and is thought to lead to decreased 5-HT biosynthesis, since TRP is the principal precursor of 5-HT (Cowen, Parry-Billings and Newsholme, 1989; Maes *et al.*, 1990).

Experimentally induced tryptophan depletion is also known to induce depressive symptoms which correlate with a decreased glucose metabolism in the dorsolateral prefrontal cortex (Bremner *et al.*, 1997)

Indoleamine 2,3-dioxygenase (IDO) is the rate-limiting enzyme of the kynurenine pathway (KP). IDO is expressed in various tissues and organs including the brain. It breaks down TRP into kynurenine (KYN) and its activity, which is negligible under

normal conditions, is enhanced during systemic inflammation (Figure 1.3). Therefore, IDO has emerged as a pathophysiological link between inflammation and depression.

TFN-α, IFN-γ, IFN-α, IL-6 and LPS upregulate the expression of IDO (Maes *et al.*, 2011). Indeed, immunotherapies (IL-2 or IFN-α) in cancer patients cause a drop in the plasma TRP level. Of note, the TRP metabolism is correlated with the severity of depressive symptoms during the therapy (Capuron et al., 2002).

The pivotal role of IDO in the inflammation-associated depressive symptoms was corroborated by preclinical studies in animals. Inhibition of IDO activity attenuated the LPS-induced decrease in TRP plasma concentration and prevented depressive-like behaviours without affecting the cytokine levels (O'Connor, Lawson, Andre, *et al.*, 2009; O'Connor, Lawson, André, *et al.*, 2009).

Other mechanisms that can potentially mediate the link between inflammation and impaired serotoninergic systems in the brain have been described: in mice cultured neurons and synaptosomes, TFN-α and IL-1β induced the activation of the p38 mitogen-activated protein kinase (MAPK) which leads to an increased expression and function of the 5-HT transporter (SERT) in a dose-dependent manner, resulting in increased 5-HT uptake (Zhu, Blakely and Hewlett, 2006). The observation that cytokines directly regulate serotonin availability within the synapses was corroborated by animal experiments: the intraperitoneal injection of LPS in mice provoked an increased SERT activity; interestingly, in SERT knockout mice LPS administration did not induce depressive-like behaviour such as immobility, suggesting that increased 5-HT uptake is at least in part responsible of LPS-induced behavioural changes (Zhu *et al.*, 2010).

1.7.1.2 Dopamine

The mesolimbic circuit consist of dopaminergic neurons in the ventral tegmental area (VTA) of the midbrain which send inputs to the ventral striatum. Its activity is involved in mood and motivation processing and has been associated with mood disorders. In particular, given its role in reward processing, dopaminergic neurotransmission has been linked to depressive symptoms, such as anhedonia, reduced motivation and energy level (Nestler and Carlezon, 2006).

There is compelling evidence of an effect of the immune system on DA signalling.

Inflammation can lead to a reduction in DA through a blockade of tetrahydrobiopterin (BH4), a key enzyme co-factor in DA synthesis. BH4 is necessary for the conversion of L-phenylalanine to L-tyrosine and L-tyrosine to L-DOPA, the precursor of DA. BH4 is oxidation-labile, therefore inflammation-induced reactive oxygen species (ROS) can readily reduce the BH4 level and ultimately inhibit DA synthesis (Neurauter *et al.*, 2008; Felger and Miller, 2012) (Figure 1.3). Supporting the role of inflammation with DA availability in humans, chronic IFN-α treatment in hepatitis-C patients has been shown to reduce plasma L-phenylalanine turnover (reflecting lower BH4 concentration) which negatively correlated with the CSF DA concentration. Moreover, a decreased CSF BH4 concentration correlated with increased CSF IL-6 (Felger, Li, *et al.*, 2013).

The DA vesicular package is another mechanism by which inflammation can alter the synaptic DA availability. An in vitro experiment using Enterochromaffin-like cells have shown that proinflammatory cytokines (IL-1β and TNF-α) inhibit the expression of vesicular monoamine transporter 2 (VMAT2), a transporter necessary for monoamine synaptic vesicles formation (Kazumori *et al.*, 2004).

The effect of cytokines on DA brain metabolism was assessed using [^{18}F]-DOPA Positron Emission Tomography (PET) in patients with chronic hepatitis C virus (HCV) treated with IFN-α and untreated patients. Patients undergoing IFN-α treatment exhibited increased [^{18}F]-DOPA uptake and a lower turnover. Interestingly, the IFN-α-induced anomalous DA metabolism was observed in the ventral striatum which also showed reduced activity in functional magnetic resonance imaging (fMRI) during a reward task (Capuron, 2012). A study investigating the effect of chronic IFN-α treatment in in nonhuman primates reported enhancement in the release of DA after 2 weeks of treatment, but this increase was reversed after 4 weeks. Interestingly, the reduced DA release was correlated with decreased sucrose consumption, an index of anhedonia-like behaviour. The same study, using PET with [^{11}C]-raclopride (a radiotracer for the DA receptor D2 (D2R)) found decreased D2R binding after 4 weeks of treatment (Felger, Mun, *et al.*, 2013). In humans endotoxemia (0.8 ng/kg) lead to an increase of stimulated dopamine release in the dorsal striatum (Petrulli *et al.*, 2017).

Moreover, LPS injection (0.8 ng/kg) in healthy volunteers reduced ventral striatal activity in response to reward cues, consolidating the notion that peripheral inflammation can alter the activity of dopaminergic circuits (Eisenberger *et al.*, 2010).

Taken together these data may suggest that inflammation-associated changes in dopamine neurotransmission may be region specific (ventral versus dorsa striatum) and can depend on alteration in DA release as well as DA receptor expression.

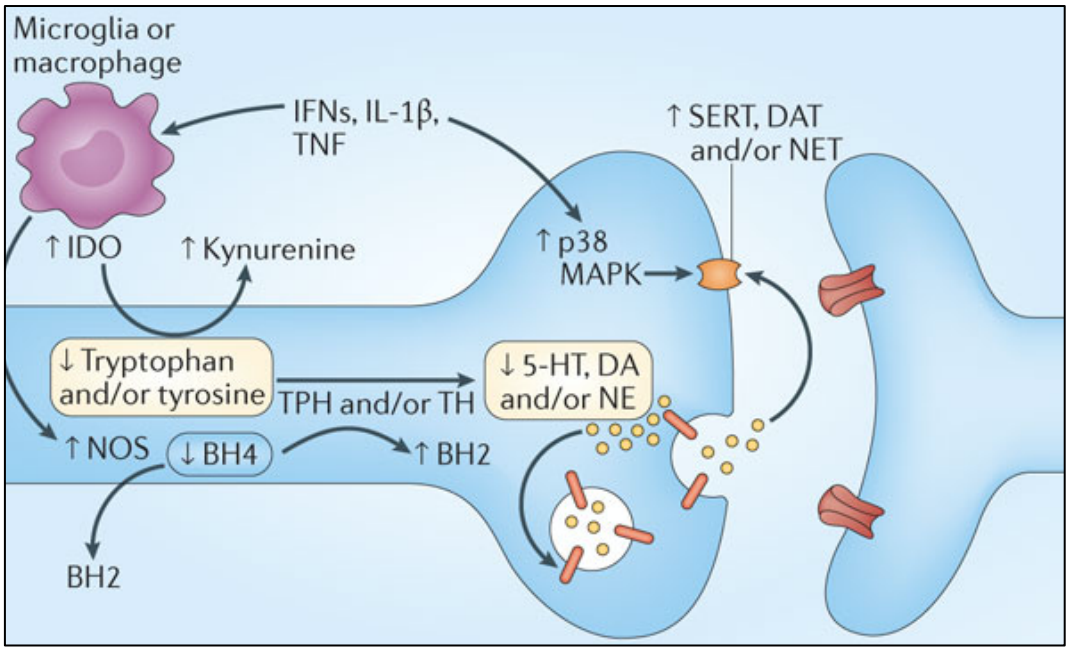

Figure 1.3 Effect of inflammatory mediators on monoamine metabolism
Inflammation can affect the monoaminergic circuits by reducing neurotransmitters synthesis and synaptic availability leading to behavioural changes that resemble depression symptoms (Figure taken from Miller and Raison, 2016).

1.7.1.3 Glutamate

The premise that glutamatergic imbalances may be involved in the pathophysiology of depression aligns well with the inflammatory theory of depression as glutamate signalling is known to be affected by inflammation (Sanacora, Treccani and Popoli, 2012).

The kynurenine pathway (KP) is one of the candidate mechanisms by which inflammation can alter glutamate signalling. As outlined above, the enzyme IDO, ubiquitously expressed can cause TRP depletion, which may in turn impair serotonin availability. However, IDO's activity, significantly enhanced by inflammation, can also lead to an impairment of glutamatergic neurotransmission. The enzymatic activity of IDO produces,

as a first metabolite, KYN, both in the periphery and in the brain; of note, systemic KYN efficiently crosses the BBB (Fukui *et al.*, 1991). KYN can then be metabolized in the brain, by activated microglia (or infiltrating monocytes) and astrocytes, into quinolinic acid (QA) or kynurenic acid (KA). In microglia, this is oriented towards the QA pathway, whereas astrocytes mainly produce KA (Schwarcz and Pellicciari, 2002). It has been shown, for instance, that HIV-1 infection in humans significantly increases the CSF level of QA, which correlates with the severity of cognitive symptoms (Heyes *et al.*, 1991). QA is an endogenous neurotoxin, which substantially affects glutamatergic signalling. QA directly activates N-methyl-D-aspartate (NMDA) receptors, increases glutamate release and inhibits glutamate reuptake by astrocytes (Tavares *et al.*, 2002), whereas KA is an NMDA antagonist (Schwarcz and Pellicciari, 2002) (Figure 1.4). Of note, elevated plasma levels of KYN have been associated with multiple psychiatric diseases, including anxiety and depression (Stone, 2001).

In addition to amplifying glutamatergic transmission by producing QA, inflammation can directly alter glutamate synaptic and extrasynaptic concentration. Inflammatory cytokines (IL-1, TNF-α and IFN-γ) can trigger the release of glutamate by astrocytes (Ida *et al.*, 2008). It has also been suggested that inflammatory cytokines can downregulate the expression of astrocytes glutamate transporters which can cause further increase of glutamate for synaptic signalling (Tilleux and Hermans, 2007).

Neuroimaging studies have provided further evidence that inflammation could account for glutamatergic dysfunction in depression. Patients undergoing IFN-α immunotherapy, exhibited a higher glutamate concentration, measured using Magnetic Resonance Spectroscopy (MRS), within the basal ganglia and the dorsal anterior

cingulate cortex (dACC) that was positively correlated with depressive symptoms (Haroon *et al.*, 2014). Targeting the glutamatergic system has become an important therapeutic approach for patients that do not respond to monoaminergic-based antidepressants. In fact, esketamine (an NMDA receptor antagonist) nasal spray was approved in 2019 and, although the molecular mechanisms are still unclear, it has shown rapid antidepressant effects in treatment-resistant patients (Hashimoto, 2019). Taken together, this evidence supports the notion that MDD is not necessarily correlated with neuronal patterns that depend on monoamine neurotransmitters but may be linked to an anomalous activity of glutamatergic pathways. Since inflammation is implicated in glutamatergic imbalances, these data have strengthened the role of the immune system in the pathophysiology of depression.

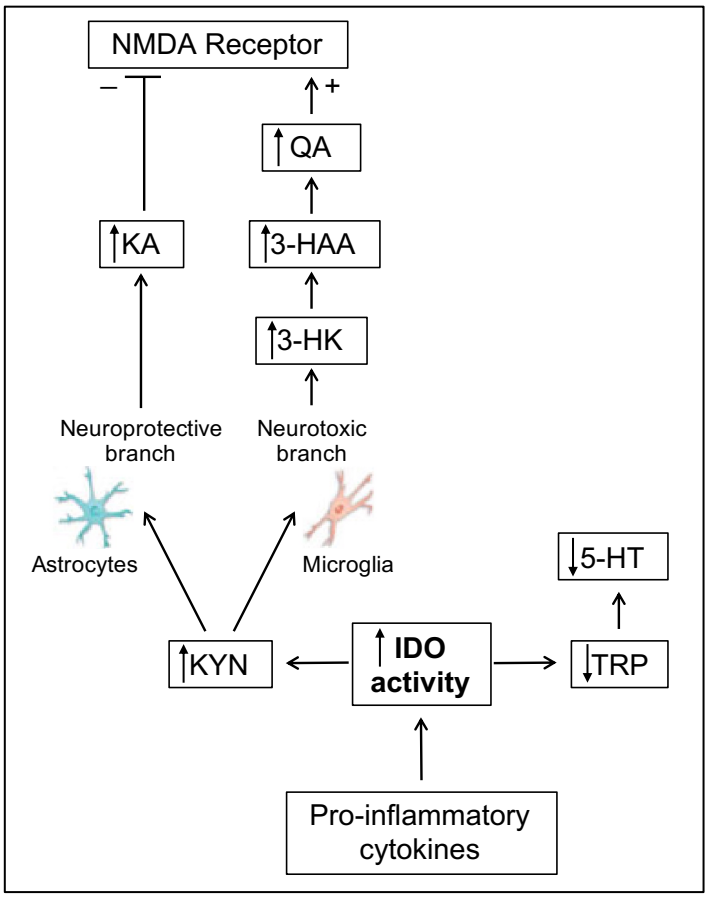

Figure 1.4 Kynurenine pathway

Proinflammatory cytokines induce upregulation of the enzyme IDO which metabolize TRP into KYN, decreasing serotonin synthesis. In the brain KYN is metabolized into KA by astrocytes (neurotrophic branch) and into QA, 3-hydroxy-kynurenine (3-HK), 3-hydroxyanthranilic acid (3-HAA) by microglia (neurotoxic branch). 3-HK and 3-HAA are two neurotoxins that can produce reactive radicals leading to oxidative stress (Goldstein *et al.*, 2000). QA and KA can bind to the NMDA receptor as an agonist and antagonist respectively, regulating glutamatergic circuits (Figure adapted from Gabbay et al., 2012).

1.8 Role of microglial cells in MDD

1.8.1 Microglial cells physiology

Microglia are the CNS immunocompetent cells, which are evenly distributed throughout the brain. They mediate the response to tissue homeostatic imbalances, for instance in brain injuries and disease, and are the principal cellular component of brain inflammatory processes and cellular debris phagocytic clearance. Microglia derive from primitive yolk sac myeloid cells and migrate into the nervous system before the formation of the blood brain barrier, thus unlike the rest of the CNS cells they have a mesodermal origin. Although their role in normal neural parenchyma has long been unclear and their status as been classically described as "resting" in a normal brain, they appear to have a critical function in CNS development and in tissue homeostasis maintenance (Kettenmann *et al.*, 2011). Morphologically microglial cells are characterized by a small soma and multiple elongated cell processes, through which they dynamically patrol non overlapping areas of the brain parenchyma (Nimmerjahn, Kirchhoff and Helmchen, 2005). Therefore, their normal behaviour seems to be "surveying" rather than "resting". In this state microglia play critical roles in fundamental processes, such as neural plasticity, that are believed to underlie learning, memory and brain development (Li and Barres, 2017).

Microglia also exist in a variety of distinct morphological states in the healthy brain. Upon pathological signals due, for example, infection, trauma, ischemia or neurodegenerative diseases, they can rapidly switch to a different, so-called *activated* state, involving substantial changes in cell morphology, proliferation, gene expression and functional behaviour (Figure 1.5). Once activated, microglia can acquire either a proinflammatory

(neurotoxic) or neuroprotective function. These cells are endowed with a variety of receptors (such as Nucleotide oligomerization domain (NOD)- and TLRs-like receptors, complement receptors and many phagocytic receptors) that recognize harmful stimuli and initiate an inflammatory response (Neumann, Kotter and Franklin, 2009). From a morphological point of view, activated cells take on an amoeboid appearance, undergoing a reduction in the characteristic finger-like processes and an increase in cell body volume (Figure 1.5) (Kettenmann *et al.*, 2011). When activated, microglial cells exhibit increased mobility due to the rapid cytoskeleton rearrangement and the expression of membrane receptors, such as chemokines and purinergic receptors, that allow them to migrate along the molecular gradients towards the site of injury or inflammation (Nam *et al.*, 2018; Franco-Bocanegra *et al.*, 2019). After CNS injuries microglia proliferation is regulated by the increased concentration of colony-stimulating factors (CSFs). Furthermore, activated microglia display enhanced phagocytic activity, especially in a context of neuronal damage (Kreutzberg, 1996; Kettenmann *et al.*, 2011). Another hallmark of microglia activation is the antigen-presenting activity. The Major Histocompatibility Complex class II (MHCII) is considered a marker of microglial activation and enable microglial cells to interact with infiltrating T-cells (Schetters *et al.*, 2018).

As in the case of their peripheral counterparts (macrophages), the activation of microglia has been broadly categorized into two different phenotypes: the proinflammatory M1 and the neuroprotective M2. Though, this is an oversimplification of what is more likely to be a gradient of phenotypes. The anti-inflammatory phenotype has been further subdivided into “alternative activated” (M2a; induced by IL-4) and “acquired deactivated” (M2c; induced by IL-10) (Lam, Lively and Schlichter, 2017). Therefore,

microglia activity exhibits great heterogeneity and seems to be stimulus-dependent. Upon encounter with pro-inflammatory stimuli, such as treatment with the proinflammatory cytokine IFN-γ or with LPS, these cells, as well as infiltrating macrophages, switch towards the M1 phenotype, producing proinflammatory cytokines (for example TNF-α, IL-1β and IL-12), chemokines and ROS, and expressing high levels of inducible nitric oxide (iNOS). Peripheral macrophages initiate this mechanism to fight an infection. In the sterile brain parenchyma this type of response also occurs as a result of trauma or chemical exposure (Orihuela, McPherson and Harry, 2016). On the other hand, M2 cells are believed to exert a neuroprotective/repair effect and to promote neurogenesis an tissue repair through the release of anti-inflammatory factors and the synthesis of polyamines and collagens (Cherry, Olschowka and Banion, 2014). Despite the remarkably different functions of the M1/M2 polarizations, it is still unclear whether these two phenotypes exhibit different morphological features and could coexist under pathological circumstances.

Microglial activation is a common pathological feature in a number of brain diseases. Therefore, inhibiting the microglial proinflammatory activity has emerged as a potential strategy in the treatment of neuroinflammatory-related pathologies. However, it may be necessary to characterize biomarkers specific for distinct microglial phenotypes, in order to assess the activity of potential pharmacological treatment.

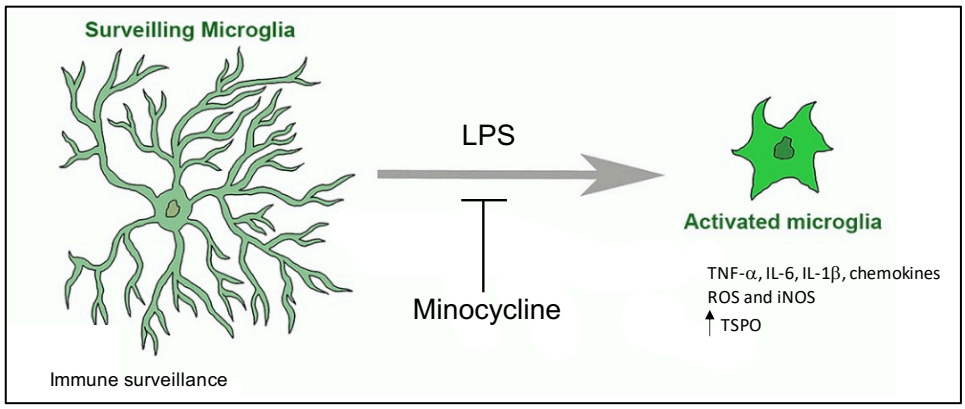

Figure 1.5 Microglial activation

LPS induces microglial transient proinflammatory activation, leading to morphological changes, cytokine release and increased expression of the inflammatory marker TSPO (discussed in detail in the next sections).

1.8.1.1 Microglial activity in depression

Given the importance of peripheral inflammation in the pathogenesis of depression, and the interplay between systemic and central immune responses, the role of microglial cells in the onset of depressive symptoms has progressively gained interest. Microglial cells are thought to translate and amplificated peripheral immune activity to the brain, inducing mood and cognitive impairments linked with depression (Ishikawa and Furuyashiki, 2021). These effects are normally transient but can become long-lasting in chronic inflammatory states. There is accumulating evidence for the role of microglia in inflammation-related depressive symptoms. LPS, peripherally or centrally administered, is well known to induce elevated blood levels of inflammatory cytokines, microglial activation and depressive behaviours in mice (Yirmiya, Rimmerman and Reshef, 2015). Seemingly, microglial activation and concurrent depressive behaviour have also been reported in response to psychological stressors, such as repeated social defeat or foot

shock (Calcia *et al.*, 2016). Psychological chronic stress can trigger proinflammatory microglia activation within the medial prefrontal cortex (mPFC) and lead to working memory deficits. Of note, the cognitive impairments were ameliorated by minocycline, a putative inhibitor of microglial activation (Hinwood *et al.*, 2013).

Interestingly, microglia activation has been correlated to MDD even in the absence of comorbid pathologies or immune challenges. Several histopathological studies showed an abnormal level of activated microglia in patients with psychiatric disorders. For example, post-mortem cellular morphological analysis of depressed suicides revealed an increased number of amoeboid microglia, indicative of proinflammatory activation, in the white matter of the dorsal anterior cingulate cortex (dACC) (Torres-Platas *et al.*, 2014). As described above, activated microglia play a pivotal role in the kynurenine pathway, breaking down TRP to create kynurenic acid, which is converted to the NMDA receptor agonist QA. A significant increase in QA immunoreactivity was observed in the subgenual anterior cingulate cortex (sACC), anterior mid-cingulate cortex (aMCC) and pregenual anterior cingulate cortex (pACC) of depressed suicides when compared to matched non-psychiatric controls (Steiner *et al.*, 2011). The kynurenic pathway is thought to be one of the principal molecular mechanisms by which microglial cells can ultimately lead to the onset of depression. However, other putative mechanisms that may underlie depressive symptoms are associated with microglial activity. Preclinical studies have linked depression with impaired neurogenesis (Jacobs, Van Praag and Gage, 2000). Microglial activation has been suggested to play a central role in the inhibition of neurogenesis in the hippocampus and consequently in impaired cognition and depression-like effects (Yirmiya, Rimmerman and Reshef, 2015).

1.8.2 Minocycline

Minocycline is a broad spectrum, second-generation, tetracycline antibiotic commonly used to treat conditions such as acne and infections of the respiratory system. Minocycline has long been used in in-vitro and animal studies as an inhibitor of microglial proinflammatory activity (Kobayashi *et al.*, 2013). Minocycline can efficiently cross the BBB and exerts neuroprotective, anti-apoptotic anti-inflammatory effects on the CNS independently of the antibiotic activity (Plane *et al.*, 2010). Minocycline increases neuronal survival and inhibit microglial activation in animal models of ischemic stroke and neurodegenerative diseases (Yrjänheikki *et al.*, 1998; Noble *et al.*, 2009). Accordingly, minocycline attenuated LPS-induced depressive-like behaviour in mice by inhibiting microglial activation (Henry *et al.*, 2008).

Given its neuroprotective functions, minocycline has emerged as a candidate drug to treat depression by targeting microglia.

Chapter 5 of this thesis presents new data on the effect of minocycline on inflammation-associated depressive symptoms. It also provides a brief literature review of the possible molecular mechanisms of action and results of recent trials using minocycline treatment in depression.

1.9 Towards a precision medicine approach for depression

Accumulating data have shown associations between central and peripheral inflammation with psychiatric diseases and have suggested that inflammation can interfere with the mechanisms of action of common antidepressants, such as availability of monoamine

neurotransmitters. With the premises that inflammation could affect the regulation of neuronal circuitries, brain tissue homeostasis and cytoarchitecture, these data, have spurred the research in immunotherapies for depression, with the underlying idea that inhibiting inflammation and in particular neuroimmune activation could have beneficial effects for depressed patients.

1.9.1 Inflammation and depression heterogeneity

As explained above, depression is characterized by heterogenous clinical profiles. Moreover, mounting evidence has shown that it may be crucial to differentiate subtypes of patients according to immune biomarkers and response to common antidepressants. There is growing interest in the potential association between distinct depressive features, biological characteristics and treatment responsiveness.

Recent studies have reported association between immune markers and specific depressive symptoms. For example IL-6 and CRP in depressed patients were associated with anhedonia, fatigue and altered sleep and appetite (Milaneschi *et al.*, 2021). A mendelian randomization study found association between IL-6 and suicidality and between body mass index (BMI) and anhedonia, tiredness and changes in appetite (Kappelmann *et al.*, 2021). These data highlight the heterogeneity of depressed patients and suggest that different immune-metabolic profiles may account for a particular subset of depressive symptoms.

The potential role of inflammation on a distinct pattern of symptoms is also supported by the residual symptoms observed after SSRI treatment in patients undergoing INF-α therapy.

Despite the improvement in mood symptoms, fatigue and psychomotor retardation are less likely to be ameliorated by SSRIs (Lucile Capuron *et al.*, 2002). It has been suggested that these residual symptoms may reflect specific inflammation-mediated depressive effects that depend on pathways which are not primarily serotoninergic (Felger, Li, *et al.*, 2013).

1.9.2 Inflammation and treatment resistance

Treatment resistance (TR) depression, which is defined as the lack of response to two courses of common antidepressants, occurs in one third of depressed patients (Voineskos, Daskalakis and Blumberger, 2020). The causes of the unresponsiveness have long been unknown. As the association between immune markers and depression has become evident, it has been investigated whether clinical features, including inflammation, could predict the treatment unresponsiveness. To test this the concentration of circulating inflammatory biomarkers of TR patients has been compared with treatment-responsive, untreated patients and healthy controls. TR has been associated with higher proinflammatory cytokines when compared to responsive patients (Maes *et al.*, 1997; Lanquillon *et al.*, 2000). More recent data showed that CRP is significantly higher in TR patients but not in responsive patients and was associated with vegetative depressive symptoms and high BMI (Chamberlain *et al.*, 2019). mRNA analysis of whole-blood samples, that considered genes encoding for cytokines, and purinergic and glucocorticoid receptors, found a different genes expression pattern in TR patients when compared to responsive patients (Cattaneo *et al.*, 2020).

In this framework it has become increasingly evident that a precise medicine approach could address the unmet therapeutic needs of depression patients by targeting a selective

class of symptoms and a particular subgroup of patients that are more likely to benefit from immunomodulating therapies.

1.9.3 Patient stratification and trials outcomes

The potential role of inflammation in a particular subset of depressed patients and in some specific symptoms may offer new therapeutic approaches that target neuroimmune components. Thus, it has been suggested that stratification for baseline immune activation should be considered when recruiting patients for a clinical trial testing a new antidepressant, particularly when the novel medication is intended to act on an immune system component. In addition, a wide range of outcomes variable should be considered a priori in order to maximize the likelihood of capturing a potential effect on a distinct subdomain of symptoms. An assessment of a symptom at least in part regulated by the putative targeted pathway should be included (Drevets *et al.*, 2022). It has been suggested that the lack of precise outcome variables in clinical trials may yield data impossible to interpret with potential false negative results (Lucido *et al.*, 2021).

To date, few studies have assessed the effect of immune-modulating drugs on depression after patient stratification for systemic inflammation. A randomized controlled trial (RCT) on 60 MDD patients using infliximab, a monoclonal TNF-α antibody, showed no depression improvement in TR depression. However, post-hoc analysis indicated an improvement in the cohort of patients whose CRP level was higher (>5mg/L) (Raison *et al.*, 2013).

Similarly, a recent study investigated the effect of augmentation therapy with minocycline in TR MDD patients considering the low-grade peripheral inflammatory status. Patients

with elevated baseline CRP (>3mg/L) exhibited an improvement in the Hamilton Depression Rating Scale (HAM-D-17) after minocycline treatment, whereas patients with low CRP level did not benefit from minocycline (Nettis *et al.*, 2021).

The importance of differentiating MDD patients based on inflammatory markers has also been confirmed by fMRI observations, showing increased corticostriatal activity following L-DOPA treatment only in patients with high baseline CRP (>2mg/L). The change in the corticostrial circuit, a pathway associated with reward, was associated with reduced anhedonia. These data provide further evidence that patients stratification may be crucial to interpret the effect of a pharmacological treatment (Bekhbat *et al.*, 2022).

Trial designs have not been the only limiting step in the development of novel antidepressants. Novel medications, directly targeting activated brain microglia are currently being investigated (Bhattacharya and Ceusters, 2020). However, though it is known that some of these drugs block microglial activation in rodents there is currently no direct way of measuring this in humans. Hence, there is a pressing need to develop methods for determining drug target engagement in humans.

Chapter 2: Imaging effects of peripheral inflammation on the human brain

Preclinical models have provided compelling evidence of, and explanations for the interplay between peripheral and central immune activation and the potential behavioural implications. Studies in animal models have also presented pharmacological agents, targeting brain immunocompetent cells (microglia), that improved inflammation-mediated behavioural impairments (Henry *et al.*, 2008; Bhattacharya and Biber, 2016).

Nevertheless, the extent to which findings from studies on animal models can reliably be translated to humans is often unknown. Neuroimaging techniques have helped to bridge the translational gap, providing important insights into the effect of inflammation on brain connectivity, homeostasis, morphology and neurochemistry, and to dissect the cognitive consequences of inflammation. However, the various modalities have their own compromises in terms of accessibility and specificity to immune biomarkers.

2.1 MRI methods

Several MRI methods have been tested in MDD patients or in a context of experimentally-induced inflammation, to disentangle the relationships between peripheral inflammation, imaging markers and inflammation-related cognitive impairments. Each MRI method presents advantages and drawbacks, but there is still no consensus on an imaging technique sensitive to peripheral inflammation that could potentially test the target engagement of a novel immunomodulating drug.

Structural neuroimaging studies have shown associations between volumes changes in particular brain regions and immune markers. For example, the hippocampus, sACC and caudate volumes correlated with the expression of immune genes in depressed patients (Savitz *et al.*, 2013). In addition, another study showed that the activation of the kynurenine pathway, often observed in depression, was inversely correlated with striatal volume (Savitz *et al.*, 2015).

The effect of systemic inflammation on neuronal networks has been investigated using functional magnetic resonance imaging (fMRI). fMRI studies on experimentally induced inflammation have identified impairments in neuronal pathways during the course of inflammation. Interestingly, acute systemic inflammation selectively affected the neurovascular reactivity of dopaminergic networks known to mediate reward and psychomotor functions, which are often impaired in depressed patients (Brydon *et al.*, 2008; Eisenberger *et al.*, 2010). Resting state fMRI also showed abnormal global network connectivity after INF-α challenge (Dipasquale *et al.*, 2016). Moreover, in depressed patients, the high level of peripheral CRP has been associated with an impaired functional connectivity in corticostriatal reward circuitry and within nodes of the default mode network (Felger *et al.*, 2016; Kitzbichler *et al.*, 2021).

However, despite being able to define brain regions involved in inflammation-related depressive symptoms, fMRI and structural MRI cannot provide precise information about the mechanistic biological basis of the effect of inflammation on the brain.

Proton Magnetic Resonance Spectroscopy (MRS) is a powerful tool that enables quantification of a number of different brain metabolites such as N-Acetyl-Aspartate

(NAA), choline, myo-inositol, γ-aminobutyric acid (GABA) and glutamate. MRS studies have reported effects of peripheral inflammation on brain glutamate concentration and its potential implication in depression. INF-α treatment induced a higher glutamate concentration in the basal ganglia and the dACC. Interestingly, glutamate concentration was correlated with impaired motivation, a symptom of depression often associated with inflammation (Haroon *et al.*, 2014). Moreover, MDD patients with high CRP (>3mg/L) exhibited a higher glutamate concentration in the left basal ganglia when compared to patients with low CRP (<1mg/L). The same study found a positive correlation between plasma CRP and concentration of myo-inositol, a putative astrocytic marker, suggesting abnormal glial activity (Haroon *et al.*, 2016). MRS has emerged as a potentially useful technique to detect changes in glutamate signalling during systemic inflammation and therefore could serve as a tool for testing putative drugs targeting the glutamatergic system. However, the majority of glutamate resides in the intracellular space and MRS does not distinguish between intracellular and extracellular concentration, confounding the interpretation of the results. Other limitations of MRS are that it allows to acquire only one voxel at the time and it does not provide information about the cellular mechanisms underlying the observed changes.

The potential role of inflammation in altering the tissue microstructure has been investigated using Diffusion-Weighted Imaging (DWI) techniques, which measure water molecule diffusion properties. Water diffusion is influenced by tissue integrity and complexity, which limit the free movement of water molecule. Thus, free water increases in a context of tissue damage or oedema. Neurite Orientation Dispersion and Density Imaging (NODDI) provide information about water diffusion in intracellular and extracellular space. In patients undergoing INF-α therapy changes in the striatum Neurite

Density Index (NDI), measured with NODDI, which could reflect changes of the water movement in the intracellular space, predicted the onset of fatigue, a symptom of depression often associated with inflammation (Dowell *et al.*, 2019). However, as water is present in each cell type, DWI modalities lack cell-specificity.

Another MRI technique that seeks to assess brain tissue microstructure integrity is quantitative Magnetization Transfer (qMT), which measures the magnetization transfer between free and macromolecular-bound protons. qMT was able to detect microstructural changes within the insula in healthy volunteers receiving typhoid vaccination, which correlated with inflammation-induced fatigue (Harrison *et al.*, 2015). In line with this, qMT also showed microstructural changes in the striatum of patients receiving INF-α which predicted the emergence of fatigue (Dowell *et al.*, 2016). Unlike conventional MRI techniques, which only measure free water, qMT can identify inflammation-modulated biochemical changes in tissue. Even though the cellular and molecular substrate is not completely understood, it has been suggested that qMT measurement in grey matter areas is affected by the density of protein and of hydrophilic molecule, such as lactate. Thus qMT might provide information about biochemical and metabolic changes during inflammation (Harrison *et al.*, 2015). Although, similarly to DWI techniques, the microstructural changes cannot be attributed to particular cell types.

In this thesis, Chapter 6 presents recently collected data using Diffusion-Weighted Magnetic Resonance Spectroscopy (DW-MRS), a novel MR method that combines characteristics of DWI and MRS.

2.2 TSPO PET

TSPO PET is considered the gold standard method to measure neuroinflammation (specifically microglial activation) *in vivo*. It has been employed in a wide range of neurological and psychiatric diseases as well as experimental models of neuroinflammation. It is based on the quantification of translocator protein 18 kDa (TSPO), putative markers of microglial proinflammatory activation.

2.2.1 PET imaging, general concepts and methodology

Positron Emission Tomography (PET) uses the intravenous injection of a radiotracer. Radiotracers are compounds labelled with a radioactive atom, which decays emitting a positron. The positron collides with an electron in the tissue, in a process called "annihilation" generating two gamma rays that travel in opposite directions. The PET scanner detects the two gamma rays and locates the annihilation site, producing quantitative images of radioactivity at different time frames. The radioactivity of every time frame as a function of time is the Time Activity Curve (TAC). Quantitative PET imaging uses tracers designed to bind to a molecular target. Therefore, the amount of radioactivity is proportional to the tissue density of the molecular target.

The recorded radioactivity is due to a combination of signals: the specific signal given by the radiotracer bound to its molecular target and the non-specific signal, due to the unbound radiotracer in the blood or in the parenchyma, or to the radiotracer bound to other macromolecules. Semi-quantitative analyses that normalize the measured radioactivity for injected activity and body weight of the subject provide a measure of

radiotracer uptake but do not distinguish the proportion of specific and non-specific signals.

The contribution of the specific signal can be calculated using compartmental kinetic models: mathematical models that decompose the tissue into different compartments and calculate the constant rates of tracer exchange between them. Tissue compartments that most models generally include are the non-displeacable (free and non-specifically bound tracer) and specific (tracer bound to its molecular target) compartments. The models are fitted to the measured PET data to calculate the constant rates of tracer exchange, which are used to compute the parameter that describe the amount of specific binding. Compartmental models generally use an arterial input function that describes the concentration of the radiotracer in the blood compartment as a function of time to provide information about tracer availability. In the blood compartment the tracer can be bound to blood cells. Since only the free tracer in the plasma can enter the tissue, the input function has to account for the ration of plasma over the total blood tracer concentration. The input function also has to account for the unchanged fraction of the radiotracer. In fact, the metabolism of the radiotracer, which is mainly due to the enzymatic activity of hepatic cells, causes the concentration of the unchanged (parent) radiotracer to decrease during the scan and, concurrently, the concentration of different metabolites to increase. Radiometabolites generally lack binding affinity for the tracer molecular target and do not efficiently cross the BBB. However, they contain a radionuclide, therefore their activity is still detected. Hence, the portion of signal in the blood given by radiometabolites represents an error that the analysis method should account for.

An alternative to models that use an input function are reference region-based methods. A reference region is defined as a region devoid of specific binding. Semi-quantitative analyses use the measured activity of the reference region to correct the activity of target regions for the non-specific binding. Reference tissue models do not require an arterial input function but use the TAC of the reference tissue to estimate the rate constants.

2.2.2 Translocator protein: a marker of neuroinflammation

TSPO, which was formerly known as the peripheral benzodiazepine receptor (PBR), has largely been used to index glial activity in the brain. Its structural and physiological characteristic are different from those of the benzodiazepine receptor found in the brain, which are ligand gated ion channels. The TSPO is a five transmembrane domains protein found on the outer mitochondrial membrane. TSPO is expressed at different levels throughout the body in a wide variety of cell types. Glandular tissues exhibit the highest levels, the kidneys and heart show intermediate values, whereas, under normal physiological conditions, the liver and brain express lower levels (Anholt *et al.*, 1986; Gavish *et al.*, 1999). TSPO is also found in blood cells, in particular, in monocytes (Canat *et al.*, 1993).

Several functions are associated with TSPO, first of which is cholesterol transport into the mitochondria, where the synthesis of steroids take place (Owen *et al.*, 2017). Other physiological mechanisms are attributed to TSPO, including mitochondria respiration, redox regulation, the import of protein into the mitochondria, calcium homeostasis, control of apoptosis, cell proliferation and regulation of inflammatory pathways (Papadopoulos *et al.*, 2006; Gut, Zweckstetter and Banati, 2015; Betlazar *et al.*, 2020). Nevertheless, despite TSPO has is widely used as a marker of neuroinflammation we still

do not have a complete understanding of its physiology and its precise role in immune functions.

The low expression TSPO in the brain under normal conditions, and its relatively selective expression in glial cells have led to consider it a biomarker of neuroinflammation (microglial activation). TSPO was demonstrated to be a sensitive PET target for a wide array of neurological and psychiatric diseases (Colasanti *et al.*, 2014; Kreisl *et al.*, 2020; Meyer *et al.*, 2020). The extent to which astrocytes and microglia contribute to the TSPO signal seen in human PET imaging remains a topic of debate. (Venneti, Lopresti and Wiley, 2006). However, studies in glial cells line and in animals have strengthened the hypothesis that TSPO represents a marker for activated microglia. Autoradiography and immunohistochemical data on microglial cell lines have demonstrated that TSPO is significantly increased in LPS-induced M1-activation whereas in IL-4-induced M2 microglia the TSPO expression does not differ from the controls (Beckers *et al.*, 2018). *In vivo* animal studies have shown that TSPO expression reflects activated microglia in various model of brain pathology (Banati, 2002). TSPO expression has been shown to be a valuable biomarker of acute neuroinflammation (intracranial LPS injection) in mice, reflecting microglia activation, as demonstrated by post-mortem immunohistochemical analysis (Dickens *et al.*, 2014). Furthermore, in nonhuman primates TSPO density was increased following LPS administration and immunohistochemistry analysis showed that TSPO immunoreactive cells were microglia and not astrocytes (Hannestad *et al.*, 2012) (Figure 2.1).

Despite the widespread use of TSPO as a neuroinflammatory marker in clinical research its physiological role and the pathways that trigger its upregulation following a harmful

stimulus are still poorly characterized. In vitro studies showed that TSPO is upregulated in response to proinflammatory cytokines. Since activated microglia secrete proinflammatory cytokines, the observed increase in TSPO expression has been speculated to reflect a role of TSPO in cytokine production regulation or in an autocrine cellular feedback system (Papadopoulos *et al.*, 2006; Rupprecht *et al.*, 2010). Some TSPO ligands have been shown to exert neuroprotective functions and to regulate microglial proliferation in models of neuroinflammation without neuronal death, strengthening the hypothesis that TSPO functions as a sensor and regulator of neuroinflammation (Veiga *et al.*, 2007).

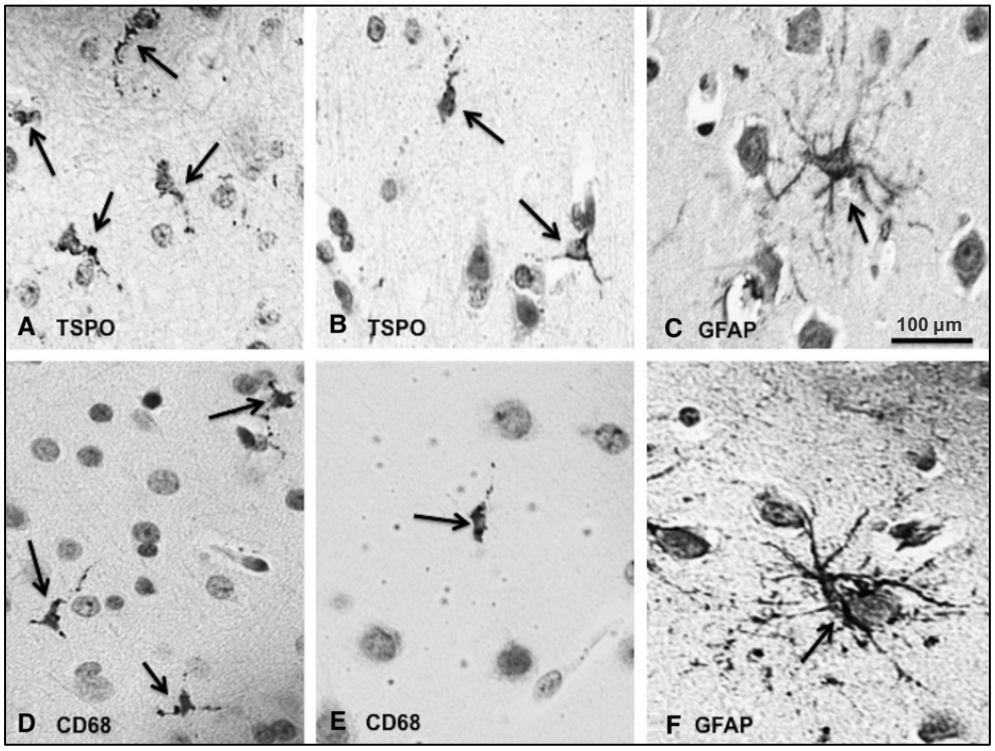

Figure 2.1 TSPO immunoreactivity in baboon frontal lobe after LPS injection
Hannestad et al. have shown that TSPO density increased at 1 hr and 4 hr, post LPS challenge in nonhuman primates. In order to investigate the cellular source of the observed increase in TSPO expression, one baboon was euthanized at 6hr post LPS. Post-mortem analysis showed that TSPO immunoreactive cells (A,B) have a symilar

morphology to cells that expressed the microglial marker CD68 (D,E). TSPO expression was not observed in astrocytes (GFAP immunoreactive cells) (C,F), suggesting that LPS induces TSPO expression selectively in microglial cells (figure taken from Hannestad et al., 2012).

2.2.3 TSPO in Depression

Since TSPO is believed to represent a reasonably reliable marker of microglial activation in neurological pathologies, it has been used to investigate whether microglial activation is also present in depressed patients; given the association between depression and central and peripheral inflammation.

In patients with Multiple Sclerosis (MS), elevated hippocampal TSPO density was associated with both depression score, assessed using the Beck Depression Inventory (BDI), and altered hippocampal functional connectivity (Colasanti *et al.*, 2016).

In depressed medication-free subjects experiencing a Major Depressive Episode (MDE) at the time of scanning, TSPO density, measured with the radiotracer [^{18}F]-FEPPA, was significantly elevated in the prefrontal cortex, Anterior Cingulate Cortex (ACC), and insula. Of note, TSPO density in the ACC was positively correlated with the severity of depressive symptoms (Setiawan *et al.*, 2015). Similar results were obtained using the TSPO radiotracer [^{11}C]-PK11195: TSPO binding was higher, particularly within the ACC, in MDE patients with suicidal thoughts (Holmes *et al.*, 2018). In line with these results, increased TSPO expression in depressed patients has also been reported in recent studies (Richards *et al.*, 2018; J. Schubert *et al.*, 2021). A recent meta-analysis of TSPO imaging in MDD, including 8 studies and a total of 238 patients and 164 controls, has

reported a ~18% increase in brain TSPO binding in MDD patients (Eggerstorfer *et al.*, 2022).

These data have strengthened the role of anomalous neuroinflammatory activity in depression and the notion that TSPO can serve as a marker for microglial activation.

2.2.4 TSPO radiotracers

[^{11}C]-PK11195, an isoquinoline–carboxamide derivative was the first radiotracer used to investigate neuroinflammation *in vivo*. [^{11}C]-PK11195 is sensitive to inflammatory processes as shown by results in a number of brain pathologies such as stroke, neurodegeneration and traumatic brain injury (Cagnin *et al.*, 2001; Chen and Guilarte, 2008; Turkheimer *et al.*, 2015). However, TSPO quantification with [^{11}C]-PK11195 has numerous limitations. Notably, [^{11}C]-PK11195 is characterized by a low brain permeability, low affinity (K_i=9.3 nM) and a significant amount of non-specific binding (Venneti, Lopresti and Wiley, 2006; Chauveau *et al.*, 2008). In particular, [^{11}C]-PK11195 displays substantial binding to acute phase plasma proteins, especially to α 1-acid glycoprotein (Lockhart *et al.*, 2003). This can bias the tracer binding quantification in the brain parenchyma. BBB damage can lead to a leak of the tracer bound to plasma protein into the brain tissue, generating non-specific signal, while systemic inflammation can increase plasma protein concentration, reducing the free plasma tracer availability, leading to inaccurate results. In addition, the use of short-half-life ^{11}C-labelled molecules requires that the scan must be carried out in the same facility as the cyclotron, thus limiting its clinical use.

The increased interest in microglial activity in different pathologies has stimulated the development of second-generation radiotracers with a higher brain permeability and lower non-specific binding, hence higher signal-to-noise ratio, to improve TSPO imaging (Banister *et al.*, 2013). Second-generation tracers include fluorinated (^{18}F) radioligands, which have a longer half-life than the commonly used ^{11}C-labelled tracers, thus allowing its use in facilities that do not have a cyclotron at their disposal.

The binding affinity of all second-generation radiotracers is confounded by the non-conservative rs6971 single-nucleotide polymorphism (SNP) of the *TSPO* gene. This SNP generates two TSPO isoforms with high and low binding affinities (Owen *et al.*, 2011). Homozygous individuals carrying the high affinity variation on both alleles have been called High Affinity Binders (HABs), individuals with the low binding variation on both alleles have been called Low Affinity Binders (LABs), while heterozygous individuals (with one "high binding" allele and one "low binding" allele) are referred to as Mixed Affinity Binders (MABs). An ~4-fold difference in binding affinity between HABs and LABs was observed for [^{11}C]-DPA-713, a second-generation radiotracer with a molecular structure similar to [^{18}F]-DPA-714. Generally, studies using second generation tracers have excluded LABs (9% in the Caucasian population) for their negligible specific signal.

The radiotracer used in this work is [^{18}F]-DPA-714 (N,N-diethyl-2-(2-(4-(2-fluoroethoxy)phenyl)-5,7-dimethylpyrazolo[1,5-α]pyrimidin-3-yl)acetamide), a second-generation radiotracer with medium affinity (K_i=7.0 nM) (James *et al.*, 2008). [^{18}F]-DPA-714 was shown to perform better, in terms of signal-to-noise ratio, than [^{11}C]-PK11195 and [^{11}C]-DPA-713 in a rat model of acute inflammation (AMPA intracranial injection). In fact, Chauveau et al. demonstrated that the second-generations tracers [^{11}C]-DPA-713

and [^{18}F]-DPA-714 had significantly higher TSPO binding than [^{11}C]-PK11195 in the post-mortem autoradiography (Chauveau *et al.*, 2009). [^{11}C]-PK11195 and [^{18}F]-DPA-714 have a similar kinetic, with a TAC peak in the inflamed and in the intact area at 2 min after the bolus injection, followed by exponential washout and a stationary phase. The peak observed after the injection is thought to reflect the high concentration of the tracers within the blood, indicating a mostly non-specific signal. The stationary phase after the peak indexes the equilibrium phase of the binding between the tracer and its molecular target. However, the uptake of [^{18}F]-DPA-714 at 62.5 min was significantly higher than that of [^{11}C]-PK11195, indicating a higher binding affinity (Chauveau *et al.*, 2009).

The presence of TSPO on vascular endothelial cells complicates the quantification of glial TSPO in the parenchyma. Kinetic models that account for the vascular component have been used to improve the quantification of parenchymal TSPO density (Wimberley *et al.*, 2021). [^{11}C]-PBR28 has been widely used and is characterized by a high affinity for TSPO: Ki=2.5 nM, higher than both [^{11}C]-PK11195 and [^{18}F]-DPA-714 (Banister *et al.*, 2015). A caveat for this study is that, as shown by kinetics analyses comparing [^{11}C]-PK11195, [^{18}F]-DPA-714 and [^{11}C]-PBR28, the endothelial binding is proportional to the tracer affinity. Higher binding to the endothelium can result in a diminished contrast between tissue types (grey versus white matter). This has implications when a supervise clustering method to automatically extract a reference tissue is used. The supervise clustering method relies on the ability of a tracer to distinguish different kinetics of specific tissue types. Therefore, this method has been suggested to be suitable for low- and middle-affinity tracer, such as [^{18}F]-DPA-714, that display high tissue contrast and not for high-affinity tracer with low tissue contrast (Rizzo *et al.*, 2019).

The [^{18}F]-DPA-714 metabolic profile showed three major radiometabolites. [^{18}F]-DPA-714 radiometabolites are more hydrophilic than the parental radiotracer, thus their permeability into the brain is reduced. (Peyronneau *et al.*, 2013). [^{18}F]-DPA-714 is metabolized more slowly when compared to [^{11}C]-PK11195: radioactive metabolites found in plasma were reported be the source of only ~35% of PET signal in the brain at 60 min after the tracer injection in healthy humans for [^{18}F]-DPA714 (Arlicot *et al.*, 2012), while they account for ~55% of the signal for [^{11}C]-PK11195 (Greuter *et al.*, 2005)

In recent studies [^{18}F]-DPA-714 has been successfully used to quantify neuroinflammation in neurodegenerative and psychiatric diseases in humans (Golla *et al.*, 2015; Yaqub *et al.*, 2018).

The gold standard model for the quantification of specific [^{18}F]-DPA-714 binding is the reversible Two-Tissue Compartment Model (2TCM) with a metabolite-corrected arterial input function. Chapter 7 presents results on TSPO quantification obtained using an alternative, non-invasive, approach in a large cohort; on a smaller cohort TSPO binding was measured with the gold standard approach.

2.3 Aims of the project

The aims of my PhD thesis were to:

1. Examine the effect of inflammation on the brain using two different imaging techniques and a behavioural task;
2. Investigate whether minocycline inhibits LPS effects on glial cells and behavioural outcomes.

The neuroimaging tools that I used were TSPO PET and DW-MRS.

TSPO PET has long been used to measure microglial activity, it requires costly and invasive procedures in order to obtain a metabolite-corrected input function used for the brain binding quantification. Here I sought to validate an alternative, non-invasive, quantification approach to measure TSPO density following LPS injection in healthy humans.

DW-MRS is a novel, non-invasive, neuroimaging technique that has recently been used in the context of neurodegenerative and neuroinflammatory diseases. I applied it, for the first time, during acute inflammation in healthy participants to investigate its sensitivity to LPS-induced brain tissue microstructural changes.

Inflammation is associated with symptoms that resemble symptoms of depression, such as motivational changes, low mood and fatigue. Here I investigated the LPS effect on these depressive-like symptoms with subjective questionnaires and a reinforcement learning task.

New techniques sensitive to the brain response to inflammation could potentially be useful when evaluating target engagement for drugs that inhibit neuroimmune activity.

Chapter 3: General methods

3.1 Study design

I adopted a randomised, placebo-controlled crossover, repeated measure, study design. Participants (N=20) received LPS (1 ng/kg) and saline (placebo), in a randomized order, during two separate experiment sessions (Figure 3.1). Sessions were separated by a minimum of 1 week (Figure 3.1).

In addition, as a between-subject factor, a subgroup of participants was treated with a short course of an anti-inflammatory drug (minocycline, 100mg bd for 3½ days) (Figure 3.1). Minocycline or placebo was administered via tablets (100mg) twice a day for the 3 days before each session. One last tablet was administered on the morning before the start of the experiment session. Dose and duration of minocycline or placebo pre-treatment was identical before the two session (saline/LPS).

My study initially employed randomization to assign participants to different sessions order of saline/LPS and treatment group (placebo/minocycline). The randomization process was performed by another researcher using a number generator in MATLAB. I was blinded to the randomization order until after the data analysis. However, throughout the course of the study, a number of participants experienced dropouts, which required to reorganize the calendar and make adjustments to the initially created randomization table. These changes were implemented in order to avoid wasting scheduled sessions and to maintain the overall feasibility of the study. In addition to participant dropouts, I

encountered logistical challenges during the course of the study that led to the cancellation of a number of sessions. These logistical issues were primarily related to the radiotracer delivery supply, and as a result, the study calendar was further rearranged. This rearrangement subsequently impacted the original randomization table that had been created.

The study took place at the Clinical Imaging Science Centre (CISC), Brighton.

The study was approved by the London Queen Square Research Ethics Committee (REF 17/LO/0936).

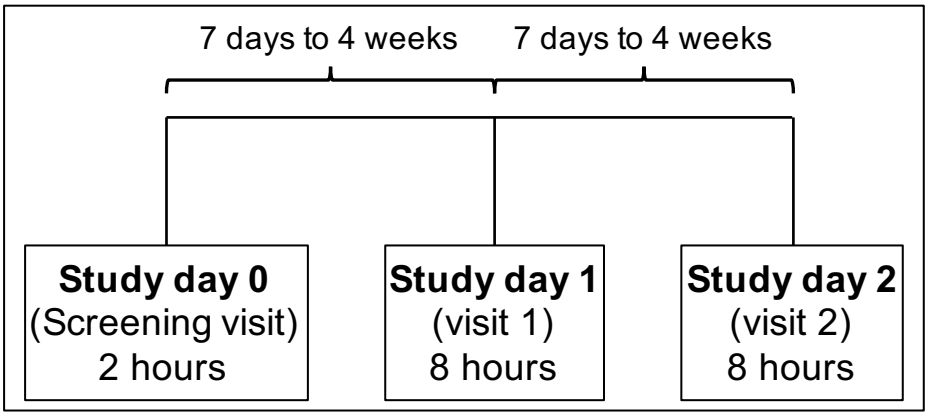

Figure 3.1 Study design

3.2 Study Protocol

Participants were invited at CISC for both experimental sessions. Upon arrival, a medical doctor interviewed each subject to check there had been no change in health since the screening visit.

Participants' heart rate, systolic and diastolic blood pressure and body temperature were constantly monitored throughout the experiment sessions. The values of vital signs were reported at baseline and several timepoints after receipt of LPS or saline injection (5 min, 15 min, 30 min, 60 min, 90 min, 2 hr, 3 hr, 3.5 hr, 4 hr, 5 hr, 6 hr and 7 hr). Blood samples were collected at baseline, 3 hr and 6 hr for haematological and plasma cytokines analysis. Participants underwent a 1 hr PET scan 3½ hr post LPS/saline injection. The MRI scan was completed at 5-5½ hr after injection. Participants completed a laptop-based reward learning task at 6 hr post injection and were monitored for another hour before the medical doctor agreed their discharge. Figure 3.2 illustrates a schematic version of the experimental protocol.

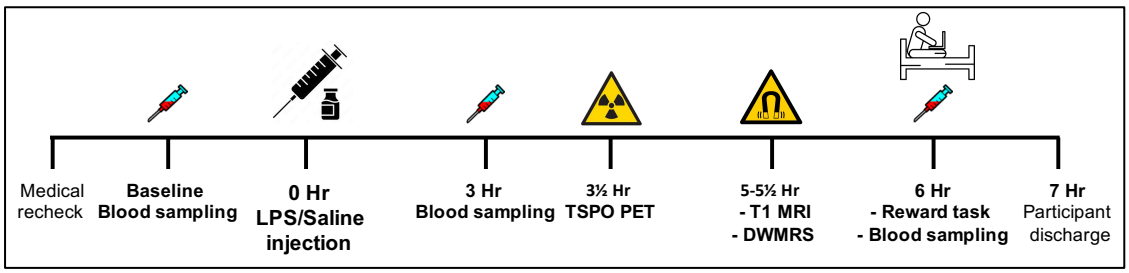

Figure 3.2 Experiment session flowchart

3.3 LPS administration

The E. coli endotoxin (1 ng/kg) or a placebo (5mL 0.9% saline) were administered intravenously (i.v) 3½ hr before the PET scan. Each LPS vial (1000 ng) was reconstituted with 1 mL of sterile H_2O and shaken for 30 minutes. 0.5 mL of the resulting solution was drawn and diluted to 10 mL in H_2O, to obtain a 50 ng/mL solution. Participants were injected with 0.02 mL/kg of the resulting solution.

3.4 Participant recruitment

Volunteers responded to electronic or posted advertisements around the Brighton area. Potential participants were asked to read the study information sheet before arranging a screening to assess their eligibility.

Only male subjects were included for ethical constraints related to the administration of a radioactive compound ([^{18}F]-DPA-714).

To participate in this study, male subjects had to meet all of the following criteria:

- Age between 18 and 55 years inclusive
- Non-smokers
- Participants must be in good health as determined from their medical history, physical examination, vital signs and clinical laboratory test results including renal and liver function and full blood count
- Participants that are high (HABs) or mixed affinity binders (HABs/MABs) determined from TSPO genotype.

Participants meeting any of the following criteria were excluded from participation in the study:

- In the opinion of the investigator, participants with a history of cancer, diabetes or other clinically significant cardiovascular, respiratory, metabolic, renal, hepatic, gastrointestinal, haematological, neurological, psychiatric or other major disorders, including HIV and hepatitis B or C infection.
- Participants who have had a clinically significant illness within 4 weeks of testing

- Subjects taking regular medicines including NSAIDs, antibiotics, aspirin or anticoagulants
- Any clinically significant abnormal laboratory test results at screening
- Participants with a heart rate at screening after resting for 10 minutes outside the range 50-90 beats per minute
- Participants with a supine blood pressure at screening, after resting for 10 minutes, higher than 149/89 mmHg or lower than 106/66 mmHg
- Participants who had received any prescribed systemic or topical medication (other than contraception) within two weeks prior to the study
- Limited use of paracetamol or non-steroidal anti-inflammatory drugs (NSAIDs) prior to the beginning of the study did not necessarily require exclusion, unless there was an on-going requirement for these medications
- Contraindications to MRI scanning, as assessed by the MRI safety questionnaire (e.g. cardiac pacemaker, metal implants or fragments from previous injury, history of claustrophobia)
- Participants with mental incapacity or language barriers which preclude adequate understanding.

As a first step during the screening, I ascertained that volunteers had read the information sheet and were fully aware of what the study involved.

The eligibility criteria were assessed as follow:

- MRI safety questionnaire
- Interview about medical history and regular use of medication use
- Completion of the MINI (Mini Neuropsychiatric Inventory)

- Physical examination
- 12 lead ECG
- Recording of vital signs: pulse, blood pressure and body temperature (auditory canal)
- Check for concomitant medication
- Blood sampling for haematology, clinical chemistry (liver function test and thyroid function test) and TSPO genotype (rs6971 SNP).

All subjects provided their written informed consent. Participants received financial compensation after completing the study. Participants that withdrew from the study were reimbursed based on the time they were involved.

3.5 Study cohorts

The study group was made up of two separate cohorts.

Initially 16 subjects were recruited. One did not complete the second session due to an incidental finding. Fifteen subjects underwent behavioural testing and TSPO PET scans. The last 7 subjects of this cohort were also tested using a new MRI technique (DW-MRS). This cohort was randomised to receive minocycline or a placebo.

Another smaller cohort of 5 subjects was more recently recruited to be tested with an improved PET imaging protocol. The experimental design was unchanged but without the minocycline/placebo randomization. Some additional eligibility criteria were included as a safety measure for the arterial cannulation. These were an Allen's test and

additional blood sample taken for the coagulation test. As I adopted a more invasive and logistically complicated procedure during the testing sessions of the second cohort (as explained in Chapter 7), it was not possible to collect behavioural data and venous blood samples for white blood cell count and cytokine analyses.

The total number of subjects that took part in each type of experiment (and their demographic data) will be specified in the relative result section. Figure 3.3 provides a visual representation of which subgroup was included in each experiment.

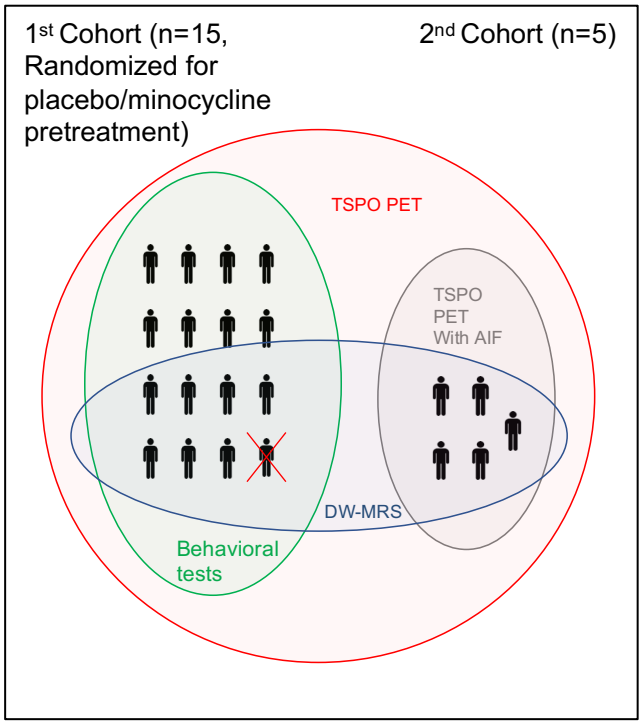

Figure 3.3 Study subgroups

The study population that underwent the experiment, receiving saline and LPS (within-subjects factor) on two different sessions, consisted of two cohorts. The first cohort was randomly assigned to receive either placebo or minocycline (100mg bd for 3½ days before each session) (between-subjects factor). One subject of the placebo arm was excluded due to an incidental finding. The subjects of the second cohort recruited to be

tested with an improved PET imaging protocol did not received placebo/minocycline pre-treatment.

3.6 Sample size calculation

An approximate sample size calculation of the first cohort was performed based on data from published studies with a similar design. However, the feasibility of the study was also taken into consideration, meaning that practical constraints such as availability of participants, resources, and time were taken into account when deciding on the sample size.

TSPO PET imaging of microglia (the current gold standard) has demonstrated a (mean±SEM) 46±8% increase in whole brain TSPO binding following LPS injection (1 ng/kg) in a study of 8 healthy human participants using a similar within-subjects design (Sandiego *et al.*, 2015). This gave an estimated effect size of 2.03 for this technique.

On the basis of this study, using 8 participants in the placebo treated arm there was >99% power to detect an increase in microglial activity (TSPO binding) following LPS compared to saline injection (alpha 0.05, one tailed).

There are currently no human studies on the effect of minocycline on LPS-induced microglial activation in humans. However, rodent studies using different markers of microglial activation (TLR-2 expression and IL-1β mRNA) give effect sizes of 1.74 and 1.17 respectively (Henry *et al.*, 2008). Taking the mean effect size from these studies (1.46), there was 87% power to detect a significant reduction in LPS-induced microglial activation in the minocycline group (alpha 0.05, one tailed).

However, we were aware that, how discussed later, the mentioned study used a different quantification analysis approach to determine TSPO binding in humans that could have resulted in a different effect size. Similarly, the effect of minocycline found in animal models may differ from the effect in humans.

Chapter 4: Physiological effects of LPS

4.1 Introduction

Lipopolysaccharide (LPS) administration has historically been used to induce fever in order to treat infections such as gonorrhoea and neurosyphilis. Endotoxemia (LPS administration) was then largely used to understand the mechanism that underlies the response to pathogens infection in both animals and humans (Bahador and Cross, 2007).

LPS, also called endotoxin, is a large glycolipid that is located on the outer membrane of gram-negative bacteria, that can trigger the activation of the innate immune system. In the past two decades, over a thousand healthy volunteers have taken part in studies involving LPS administration, to investigate its effects on the immune response (Bahador and Cross, 2007). The purpose of endotoxemia is to elicit a systemic inflammatory response mimicking a bacterial infection. The endotoxin dose given to humans (≤4 ng/kg) is 2 orders of magnitude lower than the doses tolerated by rodents but is able to induce a variety of flu-like symptoms, such as fever, chills, fatigue, headaches and joint and muscle aches. They start at 1 hr post infusion and normally last 2-4 hr. Increased body temperature (generally raising to 38°C) and heart rate peak at 3-4 hr post injection and last 6-7 hr (Lowry, 2005).

A decreased heart rate may develop, which either resolves spontaneously or can be treated using medications (Bahador and Cross, 2007).

We designed the timing of our experiment considering the above observations. So, participants underwent the 1 hr PET scan just after the symptoms peak (3½ after injection) and were monitored for 7 hr. Then, subjects were able to stay in a more comfortable clinical environment while experiencing the more pronounced effects of LPS and could more easily keep still during the scan; the planned discharge time (~ 7hr after injection) was expected to correspond with a significant improvement of the vital sign values.

LPS activates macrophages in a dose-dependent manner through the Toll-like receptor 4 (TLR4) and induces the release of various proinflammatory cytokines such as IFN-γ, TNF-α, IL-6 and IL-8 (Mukherjee *et al.*, 2009).

The peripheral administration of LPS (i.v. or intraperitoneal) can trigger an immune activity in the brain parenchyma and in the choroid plexus, as well as affect BBB integrity and permeability (Marques *et al.*, 2009; Erickson and Banks, 2018). The effect of LPS within the brain parenchyma is mostly mediated by microglial cells, which release proinflammatory cytokines that propagate the inflammatory reaction (Marin and Kipnis, 2017). The process by which LPS triggers microglia activation *in vivo* is still not fully understood. The circumventricular organs are considered one of the principal mediators of the glial response to LPS. LPS stimulates the release of cytokines by macrophages at the circumventricular organs, which can subsequently penetrate into the brain parenchyma and target microglial cells (Rivest, 2003; Dantzer *et al.*, 2008). An increased level of IL-6 in the CSF has also been reported in healthy humans after a 0.8 ng/kg LPS injection, supporting the active role of CNS cells in propagating the systemic immune response (Engler *et al.*, 2017). In vitro studies have often used LPS to investigate the putative neurotoxic effect of activated microglia (Lively and Schlichter, 2018). However,

the interpretation of such data is complicated by the fact that it is not clear whether LPS can directly target glial cells when injected into the blood stream.

Here I present the physiological response of healthy humans to LPS i.v. administration.

4.2 Methods

4.2.1 Subjects

The vital signs (body temperature, hart rate and blood pressure) include data from the entire study group (N=20) (mean age: 23.7±4.4 (std) years, mean BMI: 24.9 ± 2.2 (std) kg/m^2). White Blood Cells (WBC) and cytokine data refer to participants from the first cohort that completed the two sessions (N=15) (mean age: 24.3±4.8 (std) years, mean BMI: 24.4 ± 1.6 (std) kg/m^2). Eight participants of the first cohort received minocycline (100mg bd for 3½ days before each session), and the other 7 received a placebo.

4.2.2 Vital signs and haematology

Participants had continuous heart rate monitoring (Mindray iMEC10) throughout each 8-hour testing session, with body temperature, systolic and diastolic blood pressure and respiratory rate additionally recorded at 5 min, 15 min, 30 min, 60 min, 90 min, 2 hr, 3 hr, 3.5 hr, 4 hr, 5 hr, 6 hr and 7 hr post LPS/saline injection. A venous cannula was inserted after medical recheck in each session and was removed after the last blood sample. Blood samples were collected at baseline, 3 and 6 hr post injection, to measure the total and differential WBC count and cytokine responses. Venous blood was collected into 4 mL

EDTA tubes, labelled and delivered to the pathology laboratory at Royal Sussex County Hospital.

4.2.3 Cytokine Analyses

Blood was drawn into purple top (EDTA) BD Vacutainer tubes (Becton, Dickson and Company, Franklin Lakes, New Jersey, United States), centrifuged at 2000 rpm for 20 min; then plasma was removed, aliquoted, and frozen at -80 °C. The plasma IL-6, TNF-α, IL-8 and IL-10 were measured using Quantikine® High Sensitivity ELISA kits (R&D Systems inc., Minneapolis, United States). The detection limits were 0.031 pg/mL, 0.022 pg/mL, 0.13 pg/mL and 0.09 pg/mL respectively, and intra- and inter-assay coefficients of variation were 4.1% and 6.5% (IL-6), 2.0% and 6.5% (TNF-α), 5.5% and 5.5% (IL-8) and 6.6 % and 9.8% (IL-10). For the IL-10, ~30% of the saline session and pre-LPS samples measured below the lowest standard. All other samples were in the quantifiable range. IL-10 samples that measured below the lowest standard were assigned a value of half the lower limit of detection (Breen *et al.*, 2011). There were no samples found to be below the lowest standard for the other cytokines. All samples were tested in duplicate.

4.2.4 Statistical Analysis

The effects of LPS were analysed using repeated-measures factorial Analysis of Variance (ANOVA) (factors: condition (Saline/LPS), time (pre injection, post injection as described)) followed by paired-sample t-test at each time point between condition. Analyses were repeated to investigate the potential effect of minocycline using a mixed model repeated measures ANOVA (condition (Saline/LPS) and time as within factors and group (Placebo/Minocycline) as between factor). The correlation between cytokines and

differential cell counts was assessed using Pearson's correlation. Analyses were conducted using SPSS statistics 28.

4.3 Results

4.3.1 Vital signs

LPS induced significant increases in body temperature and heart rate (Figure 4.1): condition (Saline/LPS) × time interactions: ($F_{(4.2,54.7)}$=54.74, $p<0.001$) and ($F_{(4.6,79.3)}$=18.11, $p<0.001$) respectively. Post-hoc paired t-tests demonstrated significant treatment-associated differences in temperature from 30 minutes to 7 hours and in heart rate from 2 hr to 7 hr after drug administration (all $p<0.05$). I observed no significant effects of LPS on systolic or diastolic blood pressure or respiratory rate, and no significant main effect or interactions of minocycline on any physiological measure.

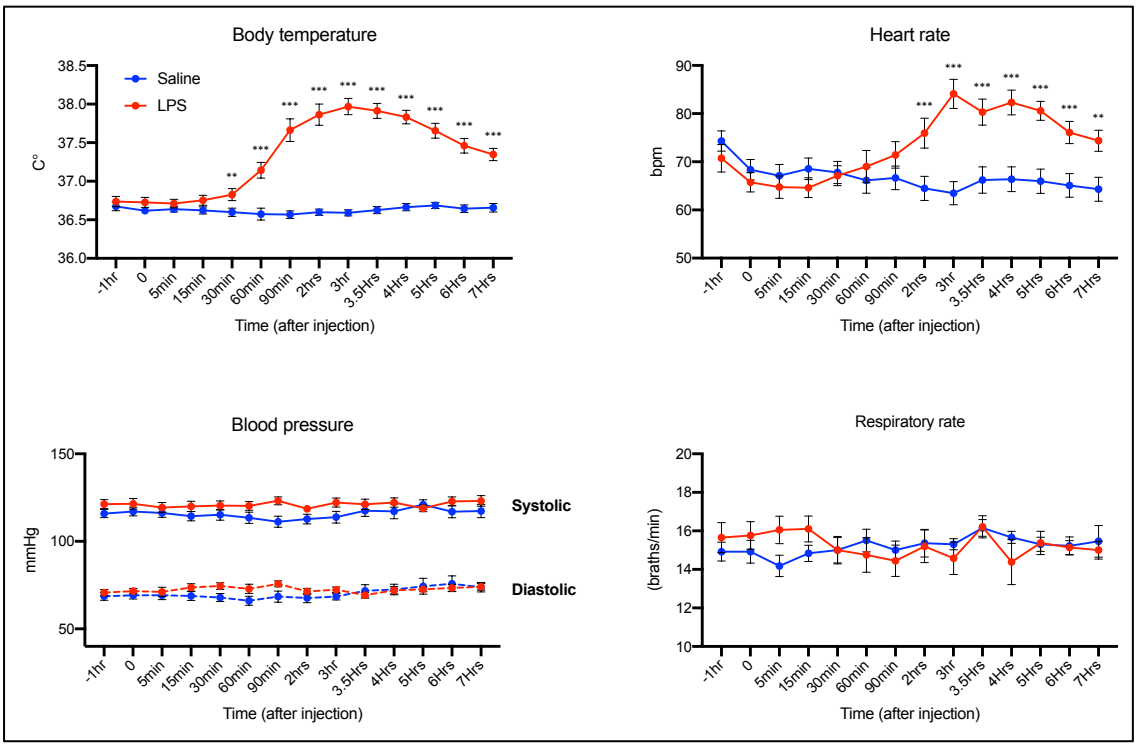

Figure 4.1 LPS effect on vital signs.

Means ± SEM are shown. * p<0.05, ** p<0.01, *** p<0.001 vs. matching time between conditions.

4.3.2 Haematology

LPS induced significant changes in total and differential WBC counts (Figure 4.2 A): condition (Saline/LPS) × time (0/3/6 Hrs) interaction for total WBC: $F_{(2,28)}$=86.34, p<0.001); Neutrophils: $F_{(2,28)}$=68.69, p<0.001; Lymphocytes: $F_{(2,28)}$=73.73, p<0.001; Monocytes: $F_{(2,28)}$=67.21, p<0.001. There was no significant main effect or interaction of minocycline on any of these measures. Data shown in Table 1.

The post-LPS cell count increases at 6 hours (compared to baseline) were: 96.6 ± 11.9% and 196.5 ± 20.6% for Total WBC and Neutrophils respectively. Monocytes displayed a

57.8 ± 5.5% decrease at 3 hr after LPS followed by a 59.2 ± 9.4% increase at 6 hr after LPS (both relative to baseline) consistent with results reported in other LPS challenge studies (Peters van Ton *et al.*, 2021). Lymphocytes showed a decrease at both 3hr (68.9 ± 2.4%) and at 6hr (59.4 ± 4.8%) likely due to cells leaving the circulating pool to migrate into tissues.

4.3.3 Cytokine Analyses

Significant condition (Saline/LPS) × time (0/3/6 Hours) interactions were observed for each cytokine (Figure 4.2 B): IL-6 ($F_{(2,28)}$=109.80, $p<0.001$); TNF-α ($F_{(2,28)}$=120.60, $p<0.001$); IL-8 ($F_{(2,28)}$=32.05, $p<0.001$); IL-10 ($F_{(2,28)}$=44.63, $p<0.001$), with post-hoc paired t-tests confirming significantly higher concentrations of all cytokines at both 3 and 6 hours after LPS, compared to the placebo (data at each time point are shown in Table 2). To test whether the order of Saline/LPS (LPS or saline in Session1) affected the plasma cytokine concentrations, I conducted a condition (Saline/LPS) × time (0/3/6 Hours) (as within-subject factors) × condition sequence (as between-subject factor) mixed model repeated measures ANOVA. The analysis revealed no significant interaction effect between treatment, time, and session order and no significant main effect of session order for all cytokines (all $p>0.05$). Confirming that the order in which participants received the treatments did not have a significant impact on the observed effects of treatment over time. Moreover, the baseline sample in subjects that received LPS in the first session did not significantly differ from the baseline sample in the saline condition (all $p>0.05$), confirming a return to baseline level between the two sessions.

Similar to findings for the physiological and differential white cell counts, there were no significant main effects or interactions with minocycline on any of the cytokines measured (all p>0.05) confirming no effect on systemic immune responses to LPS.

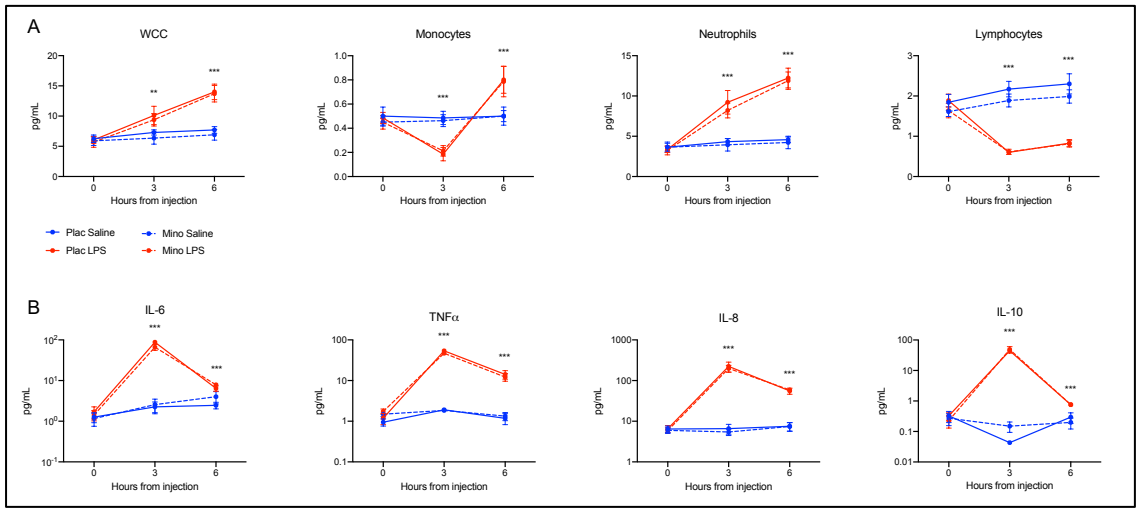

Figure 4.2 Effect of LPS on white blood cells and plasma cytokines

Means ± SEM of total and differential WBC (A) and plasma concentration (natural log transformed) of circulating cytokines (B). Significance values were tested with paired sample t-tests (* p<0.05, ** p<0.01, *** p<0.001).

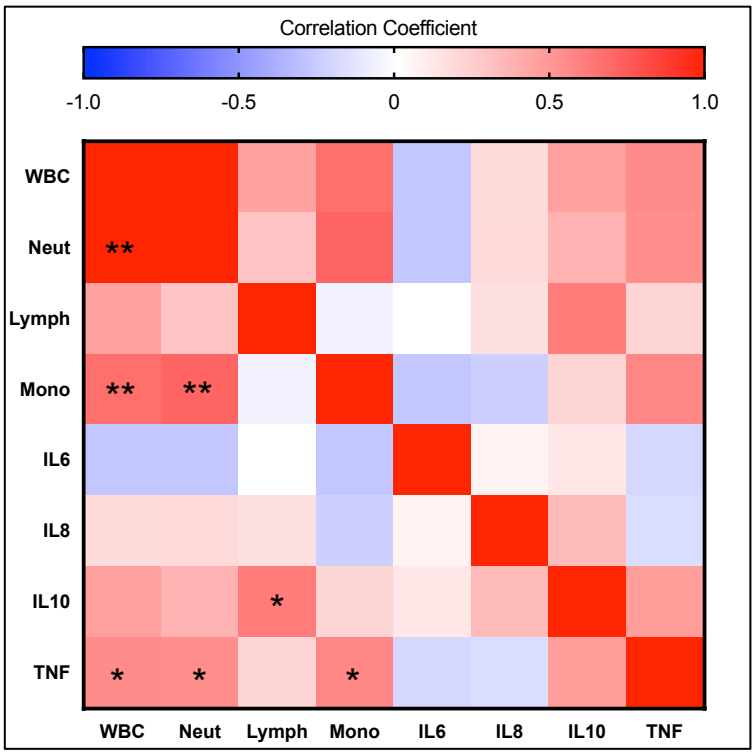

Figure 4.3 Correlations between haematology and cytokines measures

Colour map represents Pearson's correlation coefficients (*p<0.05, **p<0.001).

4.4 Discussion

Making use of endotoxemia to investigate neuroinflammation in healthy individuals relies on the assumption that LPS intravenous injection induces a robust and transient systemic immune response. Here the physiological response to LPS was described.

LPS markedly elicited a systemic inflammatory response, as shown by the vital signs, white blood cells and circulating cytokines. These data are in line with a large body of literature that shows a rapid effect of LPS with the peak of body temperature and cytokines plasma concentration between 2 and 3.5 hr post injection (Sandiego *et al.*, 2015; Lasselin, Treadway, *et al.*, 2016; Peters van Ton *et al.*, 2021).

These data confirm that endotoxemia can be used to induce a transient inflammatory state with progression of symptoms consistent across subjects.

It is worth mentioning that during the acute phase of symptoms it was challenging for most subjects to perform any type of task, such as filling the questionnaires, and they occasionally required extra monitoring and intravenous saline injections to maintain their hydration levels. However, the reliable pattern of symptoms with a substantial improvement after 3 hr allowed keeping the design of the experiment unchanged, even when participants showed a more robust response. Most importantly, the improvement of the symptoms allowed participant to undergo the PET scan at 3½ hr post injection. There were not severe side effects that led to the interruption of the experiment. However, one case of transient bradycardia was observed which quickly resolved without any intervention. In this occasion, the participant was still able to complete the study in all of his parts.

Total WBC and plasma IL-6 concentration were slightly increased during the experiment session after saline solution injection. This might be due to the insertion of the cannula, which can cause minor inflammation. However, the treatment × time interaction and paired contrasts between sessions at matching time showed highly significant differences, demonstrating the robust effect of LPS. Moreover, the order of saline/LPS did not affect the cytokine response to treatment over time, indicating that immune markers were at baseline level at the beginning of each session and that the randomization order of the treatments did not introduce a systematic bias. Hence, endotoxemia is a useful tool in causing transient systemic inflammation, especially in the contest of a study with a slightly invasive design.

The clear physical responses to LPS mean that both the participant and the researcher become aware of allocation to the LPS condition ~1 hour after its administration (though notably not all participants who received saline in the first session realized this until they had completed the second LPS session). However, one participant in the second cohort did not exhibit the typical physiological response to LPS, as shown by the unchanged body temperature and blood pressure during the LPS session. As mentioned above, it was difficult to collect, process and analyse blood samples from subjects of the second cohort because of the overlapping of other procedures and the time limitations of the project. However, given the unexpected reaction of this subject that did not show physiological changes during the LPS session, I undertook to collect at least one plasma sample post LPS and to analyse the cytokines, where possible. Strikingly, while the rest of the participants had a substantial IL-6 increase at 3 hr (~70-fold compared to baseline), this subject had a remarkably smaller change (8.3-fold) at time ~3 hr post LPS. A similar lack of response was also observed for IL-8. This surprising lack of LPS response might be due to technical issues during LPS reconstitution or injection or to biological features. The former was investigated and no clear mistakes during the LPS reconstitution steps or materials flaws could be identified. Biological factors that might affect the LPS response are two SNPs of the TLR4 gene (encoding the receptor known to recognize LPS and initiate the immune response). Each of these two SNPs have been linked with hyporesponsiveness in humans (Arbour *et al.*, 2000). It is possible that the subject that did not respond to LPS carries one or both SNPs. However, the effects of these two SNPs (which imply 4 different haplotypes) on i.v. LPS-induced vital signs and plasma cytokines have not been characterized. The neuroimaging data of this participant were still collected

and analysed. Nevertheless, since this subject could be considered an outlier, in Chapters 5 and 6, I also present sensitivity analyses that exclude him.

In this study minocycline was administered to one half of the participants in the first cohort as a putative inhibitor of microglia. Thus, minocycline was expected to alleviate the LPS effect on the CNS without significantly affect the systemic response. Physiological results did not show any minocycline effect in inhibiting the LPS-induced peripheral immune activity, supporting its use (through a 3-days pre-treatment) as a selective inhibitor of CNS inflammation during endotoxemia. However, it is worth noting that the potential anti-inflammatory effects of minocycline have been investigated in various contexts, and divergent findings have been reported. For instance, a study examining the antidepressant effects of minocycline in humans, with a treatment period of 4 weeks at a dose of 200 mg/day, found no significant effect on the plasma concentrations of IL-1β, IL-2, IL-6, IL-8, IL-10, IL-13, TNF-α and CRP, but reported a reduction of IFN-γ (Nettis *et al.*, 2021). Another clinical study on patients with schizophrenia receiving minocycline treatment for 3 months observed a reduction in serum IL-1β and IL-6, suggesting a potential immunomodulatory role of minocycline (Zhang *et al.*, 2019). Moreover, preclinical studies have also provided evidence on minocycline's role in regulating pro-inflammatory cytokine release. A study conducted on mice demonstrated that minocycline effectively decreased the levels of LPS-induced IL-6 in the plasma, while leaving the IL-1β levels unchanged (Henry *et al.*, 2008). Additionally, an in vitro study reported a dose-dependent effect of minocycline in inhibiting pro-inflammatory cytokine production in LPS-treated humans monocytes cultures (Tai *et al.*, 2013). Taken together, these findings suggest that the immunomodulatory effects of minocycline may be influenced by factors such as dosage,

treatment duration, and experimental settings (in vitro, animal models, or different clinical populations). To my knowledge, the effect of short-term minocycline pre-treatment on acute systemic inflammation in humans has not been previously investigated. It is important to acknowledge that the current study may have lacked sufficient statistical power to detect alterations in the concentration of specific circulating immune markers or immune cells. Hence, future studies including a larger cohort of participants and a broader range of cytokines will be necessary to further explore these aspects.

Minocycline dose and dosing schedule were informed by data from human pharmacokinetic studies and clinical use (e.g. in prophylaxis of meningococcal meningitis), and rodent data on the effects of minocycline in blocking LPS-induced neuroinflammation. In humans, minocycline has a half-life of ~13 hours, readily crosses the blood-brain barrier and is consequently dosed twice daily for clinical indications (Agwuh and MacGowan, 2006). For most indications a dose of 200 mg per day is well-tolerated. In rodents, three days treatment has been shown to be sufficient to block LPS-induced neuroinflammation, more prolonged treatments (4 weeks) affect the microbiome (Yang *et al.*, 2020).

Preclinical studies have shown that minocycline inhibits the brain expression of IDO, an enzyme responsible for TRP metabolism that can cause a reduction of serotonin and higher kynurenine concentration ultimately inducing sickness behaviours (Henry *et al.*, 2008). In mice treated with LPS, minocycline modulated the plasma kynurenine/tryptophane ratio, suggesting that minocycline may exert part of its activity

also in the periphery (O'Connor, Lawson, André, *et al.*, 2009). However, the effect of minocycline on IDO activity in humans has not been characterized.

In this study only male participants were included. Previous data have indicated that there may be sex differences in the response to the injection of low-dose LPS, with women demonstrating a more robust increase in plasma pro-inflammatory cytokine (TNF-α and IL-6) and cortisol compared to men (Wegner *et al.*, 2017). Hence, the present findings may not be directly applicable to the female population. It would be valuable for future investigations to include both male and female participants to better understand and compare potential sex-based differences in the immune response to LPS and the associated effect of an anti-inflammatory agent.

In conclusion, LPS showed the expected robust peripheral inflammatory effect which was not altered by the minocycline treatment. However, in light of the promising results of minocycline as an antidepressant, a more comprehensive characterization of its potential immunomodulatory effect, for example on CSF cytokines concentration, could be beneficial to validate the premise that minocycline exerts its antidepressant activity centrally.

	Time post injection (hr)	Saline	LPS	p-values (Saline vs. LPS)
Total WBC	0	6.43 (0.58)	5.87 (0.50)	.593
	3	6.79 (0.57)	9.72 (0.87)	.002
	6	7.27 (0.5)	13.85 (0.92)	<.001
Monocytes	0	0.47 (0.04)	0.47 (0.03)	.865
	3	0.47 (0.04)	0.21 (0.03)	<.001
	6	0.50 (0.04)	0.79 (9.06)	<.001
Neutrophils	0	3.65 (0.40)	3.38 (0.36)	.392
	3	4.12 (0.45)	8.92 (0.81)	<.001
	6	4.40 (0.43)	12.11 (0.83)	<.001
Lymphocytes	0	1.72 (0.11)	1.75 (0.12)	.591
	3	2.02 (0.13)	0.61 (0.04)	<.001
	6	2.13 (0.15)	0.82 (0.06)	<.001

Table 1 Haematology data

Data express means [10^9/L] ± SEM.

	Time post injection (hr)	Saline	LPS	p-values (Saline vs. LPS)
IL-6	0	1.21 (0.26)	1.56 (0.33)	.331
	3	2.41 (0.53)	76.36 (6.90)	<.001
	6	3.37 (0.81)	7.19 (0.68)	<.001
TNF-α	0	1.23 (0.19)	1.30 (0.24)	.762
	3	1.81 (0.12)	48.62 (4.86)	<.001
	6	1.15 (0.24)	11.62 (2.22)	<.001
IL-8	0	6.19 (0.72)	6.24 (0.67)	.945
	3	5.98 (0.83)	209.88 (33.91)	<.001
	6	7.48 (1.22)	57.44 (5.71)	<.001
IL-10	0	0.30 (0.08)	0.27 (0.07)	.547
	3	0.10 (0.03)	46.80 (6.97)	<.001
	6	0.24 (0.07)	0.76 (0.08)	<.001

Table 2 Cytokine data

Data express means [pg/mL] ± SEM.

Chapter 5: Effect of LPS on mood and behaviour

5.1 Introduction

Inflammation is increasingly implicated in the pathophysiology MDD (Miller, Maletic and Raison, 2009; Fernandes *et al.*, 2015; Michopoulos *et al.*, 2015; Khandaker *et al.*, 2021). Human experimental studies show that diverse immune challenges e.g. vaccines, proinflammatory cytokines and LPS readily induce mood, motivation and cognitive changes that closely resemble clinical features of depression (Dantzer *et al.*, 2008) and modulate many of the same brain networks that are implicated in the pathogenesis of depression (Harrison *et al.*, 2009; Capuron *et al.*, 2012; Kitzbichler *et al.*, 2021). Furthermore, during sustained therapy with IFN-α for hepatitis-C or cancer, acute actions of IFN-α on the amygdala and hypothalamus-pituitary axis (HPA) stress-responses predict the later emergence of true depressive episodes which occur in ~one third of patients (Capuron *et al.*, 2003; Udina *et al.*, 2012; Davies *et al.*, 2020). Together, these data support an etiological role of inflammatory processes in at least some patients with depression and have stimulated the drive to develop and repurpose immunomodulatory therapies for depression (Köhler *et al.*, 2014).

However, systemic inflammation is not present in all patients with depression, but appears to be more prevalent in patients who present with features of anhedonia, and neurovegetative symptoms or who show resistance to conventional treatments

(Chamberlain *et al.*, 2019; Bekhbat *et al.*, 2020; Cattaneo *et al.*, 2020; Milaneschi *et al.*, 2021).

The effect of inflammation on mood and fatigue has largely been studied in healthy humans using immune challenges, such as typhoid vaccination and LPS, coupled with self-rating questionnaires and scales. For example, the fatigue Visual Analog Scale (fVAS) and the Profile Of Mood State (POMS) are two questionnaires that have been used to assess the effect of immune challenges on mood and fatigue. Notably, depressive symptoms and fatigue measured with POMS and fVAS after LPS and typhoid vaccination have been shown to correlate with functional and microstructural outcomes in neuroimaging studies (Eisenberger *et al.*, 2010; Harrison *et al.*, 2015). Moreover, Sickness Questionnaire (SicknessQ), a self-reported questionnaire that specifically indexes sickness behaviours, has recently been developed using endotoxemia in healthy subjects (Andreasson *et al.*, 2018).

Interestingly, disturbances in reward- and punishment- related behaviour are a central feature of both human and rodent studies that investigate the response to inflammation (Dantzer, 2001; Harrison *et al.*, 2016). In humans, acute challenge with lipopolysaccharide (LPS: 0.8 ng/kg) rapidly impairs the responses to reward cues in the dopamine-rich ventral striatum (Eisenberger *et al.*, 2010). A similar reduction in ventral striatal responses to reward outcomes as well as a reduction in dopamine uptake has also been reported after chronic (4 week) treatment with interferon-alpha (Capuron *et al.*, 2012). Further evidence that dopamine rich regions such as the ventral striatum are particularly sensitive to systemic inflammation has also come from a study of mild inflammation induced using typhoid vaccination. Here, inflammation was associated with

an impairment in sensitivity to rewards versus punishments which was associated with a reduction in ventral striatal reward learning signals and a converse increase in encoding of punishment learning signals in the insula (Harrison *et al.*, 2016). These data are consistent with previous evidence implicating ventral striatal and insula neurons in reward- and punishment-reinforcement learning respectively (Pessiglione *et al.*, 2006).

The mechanisms underlying this inflammation-mediated motivational re-orientation remain unclear. However, preclinical studies have demonstrated that in rodents, endotoxin-induced sickness and anhedonia can be mitigated by minocycline (Henry *et al.*, 2008), a centrally penetrant tetracycline which can inhibit the activation of microglia (Soczynska *et al.*, 2012). Furthermore, proinflammatory cytokines released following microglial activation can impair the synthesis of dopamine via inhibition of the essential cofactor tetrahydrobiopterin (BH4) providing a potential mechanistic role for the activation of microglia in inflammation-mediated motivational re-orientation (Neurauter *et al.*, 2008).

In order to address this, I evaluated the effect of experimental endotoxemia on reward versus punishment sensitivity using a repeated-measures within subject study design in healthy subjects. In addition, half of the participants received minocycline, and half an identical looking placebo, before each testing session. We hypothesized that, similar to typhoid vaccination (Harrison *et al.*, 2016), endotoxin would impair the sensitivity to rewards versus punishments and further that minocycline would attenuate this inflammation-induced motivational reorientation.

5.2 Methods

5.2.1 Subjects

Sixteen healthy non-smoking male participants were recruited. One participant failed to complete the experimental sessions and was excluded from the study. Fifteen subjects (mean age: 24.3±4.8 (std) years, mean BMI: 24.4 ± 1.6 (std) kg/m^2) were included in the analysis. All were screened as described in Chapter 3. Physiological measurements (haematology, vital signs and cytokines) were performed on all subjects; results shown in Chapter 4.

5.2.2 Subjective questionnaires

Participants completed POMS, fVAS and SicknessQ at baseline, and 1, 2, 3, 4 and 6 hours after endotoxin administration. The following subscales were derived from the POMS: negative mood, total mood, tension, anger, vigour, confusion, depression and somatic. Appendix A shows the questionnaires administered to the volunteers.

5.2.3 Reinforcement learning task

Six hours after receiving either the LPS or saline injection, the participants completed a probabilistic instrumental learning task previously shown to be sensitive to inflammation-induced changes in sensitivity to rewards versus punishments (Harrison *et al.*, 2016). In this task, participants were shown three pairs of abstract stimuli on a computer screen. Each pair was associated with a different pair of outcomes. In the gain condition (outcomes gain £1 or gain nothing), the participants had a chance to win money, in the lose condition (outcomes lose £1 or lose nothing), a risk of losing money, and in the

neutral condition (outcomes look at £1 or nothing), neither win nor lose money (Figure 5.1). Within each pair, the two stimuli corresponded to reciprocal probabilities (0.8/0.2 and 0.2/0.8) of the associated outcome. One pair of stimuli was randomly presented in each trial. The two stimuli were displayed on the left and right sides of a central fixation cross with their relative positions being randomly assigned for each trial. Participants had to press a button to select the right-sided stimulus (referred to as a "go response") whereas they choose the left-sided stimulus with absence of a response (“no-go response”). Their chosen stimulus was then circled in red and the outcome shown after a 4-second delay. Participants had to use trial and error to learn the stimulus-outcome associations, and to seek to maximize their wins (by selecting the high probability win stimulus) and minimize their losses (by avoiding the high probability lose stimulus). They were told to be compensated for their winnings, but ultimately received the same fixed amount at the conclusion of the study. Each condition (gain, lose, neutral) consisted of 24 trials (presented in a randomized order). Performance was quantified as a proportion of the last 50% of the trials in which the participants had correctly selected the (high probability) gain stimulus in the reward trials and correctly avoided the lose stimulus in the punishment trials. Data were analysed in a 2 (Treatment (Saline/LPS)) × 2 (Valence (Gain/Lose)) repeated measure ANOVA. Analyses were then repeated to investigate the effect of minocycline with a 2 (Group (Mino/PLAC)) × 2 (Treatment (Saline/LPS)) × 2 (Valence (Gain/Lose)) mixed-design repeated measure ANOVA.

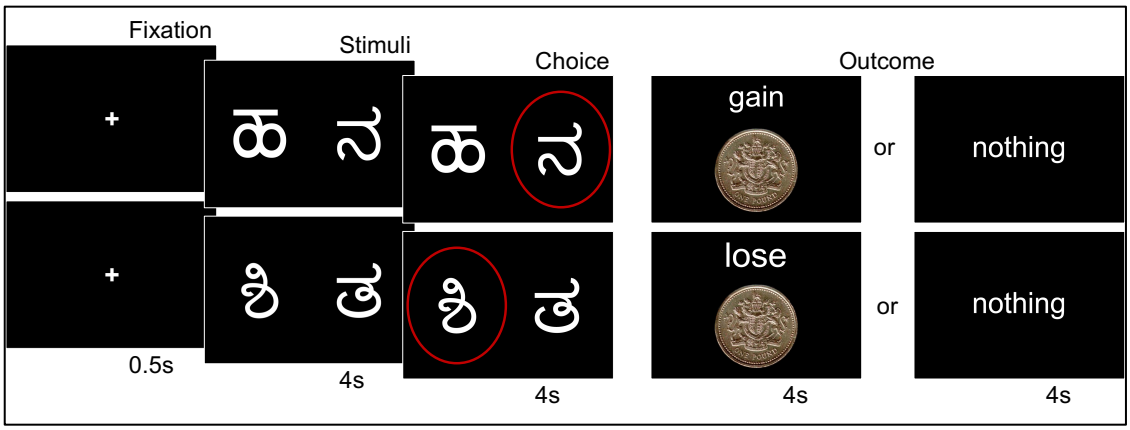

Figure 5.1 Experimental task

In each trial participants selected one visual stimulus of the pair and observed the outcome. In the examples the choices are associated with a probability of 0.8 of receiving a gain outcome ("gain £1") (upper images) and a lose outcome ("lose £1") (lower images) and a probability of 0.2 of obtaining nothing. The neutral pair of stimuli (not shown) was associated with neutral outcomes ("look 1£" or "nothing"). The left/right position of the stimuli was randomized at each trial.

5.3 Results

5.3.1 Subjective responses

Systemic inflammation induced significant mood deterioration, as shown by POMS questionnaire subscales: the total mood score decreased markedly at 1 hr post LPS injection and then showed a trend to return towards baseline values (condition (LPS/Saline) × time $F_{(5,70)}=7.14$, $p<0.001$); negative mood score peaked at 1hr post injection, and slightly improved throughout the session ($F_{(5,70)}=9.64$, $p<0.001$). The other POMS subscales followed a similar trend, with the bigger change at 1 or 2 hr post LPS ((condition (LPS/Saline) × time: Tension: $F_{(5,70)}=21.01$, $p<0.001$; Anger: $F_{(5,70)}=2.61$,

p=0.029; Vigour: $F_{(5,70)}$=1.88, p=0.109; Confusion: $F_{(5,70)}$=4.16 p=0.002; Depression: $F_{(5,70)}$=0.57, p=0.23; Somatic: $F_{(5,70)}$=14.13, p=0.001; a significant LPS main effect was observed in each subscale).

A similar pattern of rapid onset of symptoms which gradually decreased was observed for fatigue (fVAS) ($F_{(5,70)}$=4.05, p=0.003) and sickness (SicknessQ) ($F_{(5,70)}$=12.98, p=<0.001) (Figure 5.2).

Analyses were repeated to investigate the effect of minocycline (condition (LPS/Saline) × time × Group (Placebo/Minocycline). Minocycline was not found to have any effect on total mood, negative mood, fatigue or sickness.

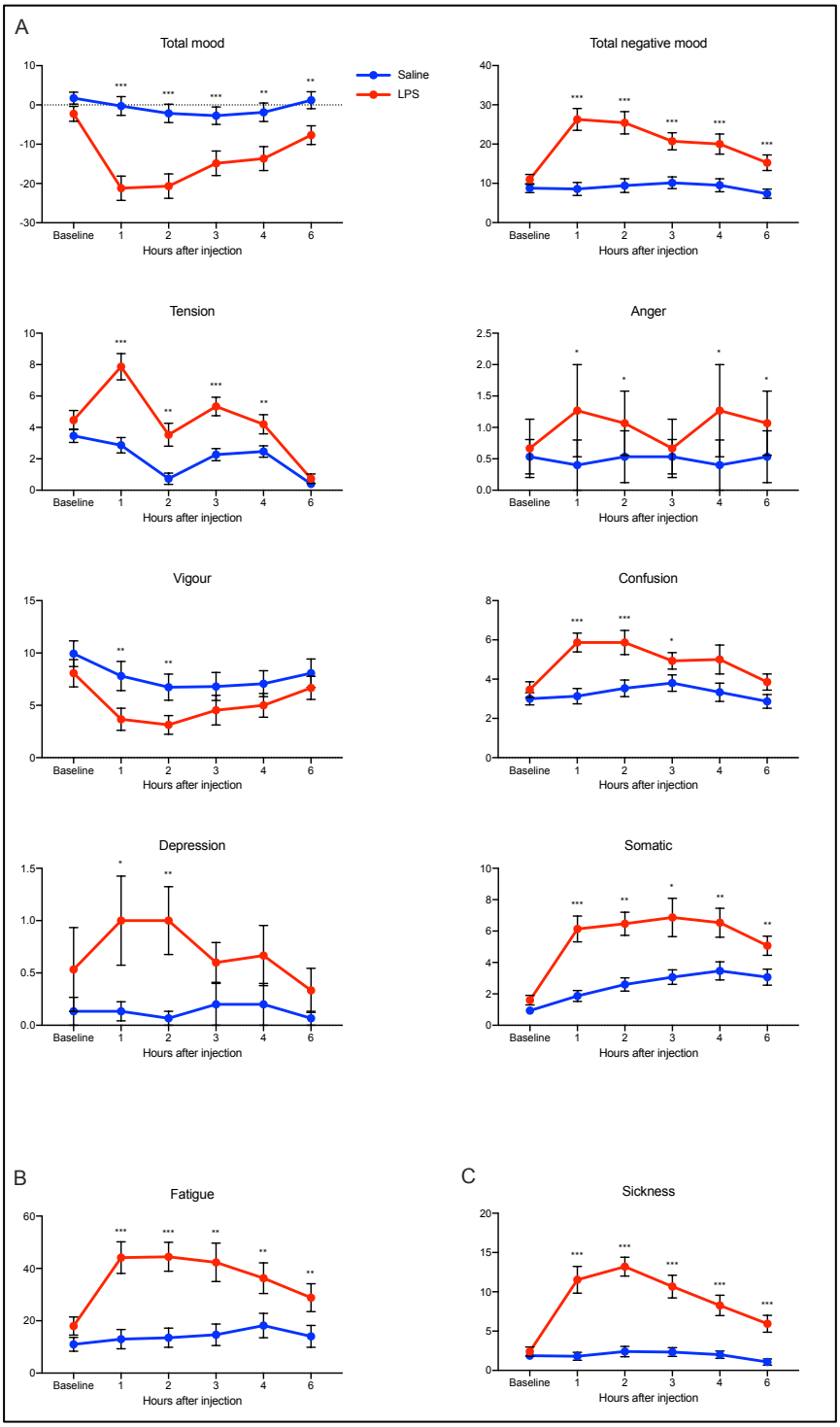

Figure 5.2 Psychological questionnaires

(A) POMS subscales; (B) fVAS; (C) sickness questionnaire. Means ± SEM are shown. * $p<0.05$, ** $p<0.01$, *** $p<0.001$ vs. matching time between conditions.

5.3.2 Reward learning task

Consistent with results previously reported following a milder inflammatory challenge (Typhoid vaccination), LPS was associated with a shift in sensitivity to rewards versus punishments expressed, as a reduced selection of the high probability reward, yet increased avoidance of high probability punishment stimuli in the last 50% of trials (Figure 5.3). This was confirmed by a significant condition (Saline/LPS) × valence (Gain/Lose) interaction: $F_{(1,13)}$=6.10, p=0.028. Post-hoc t-tests for reward and punishment conditions separately were t_{14}=1.48, p=0.161 and t_{14}=-2.03, p=0.062 respectively, indicating that similar to the milder Typhoid vaccination model of inflammation, LPS induced a relative increase in sensitivity to punishments versus rewards. Importantly, there was no significant main effect of inflammation ($F_{(1,14)}$=0.07, p=0.797) nor inflammation by valence interaction ($F_{(1,14)}$=0.45, p=0.513) for go versus no-go responses, confirming equal task engagement across conditions (p=0.972), and no significant time (Session1/Session2) by valence (Gain/Lose) interaction ($F_{(1,14)}$=3.22, p=0.094) indicating that the sessions sequence did not influence the reward/punishment learning.

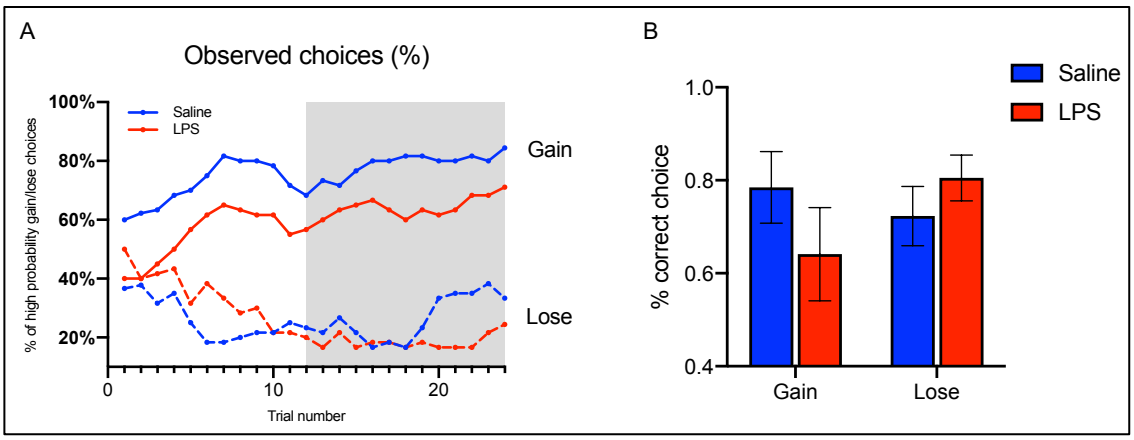

Figure 5.3 LPS effect on experimental task

(A) The learning curves show the percentage of participants that selected the high probability stimulus associated with the gain outcome in the reward trials and avoided the loss outcome in the punishment trials. Given the lack of previous knowledge, the curves start at a value close to 50%. As participants learn the high probability stimuli, they keep selecting the high probability win in the win/nothing trial and keep avoiding the high probability loss in the lose/nothing trial condition. Thus, the learning curve quickly increases in the reward condition and decreases in the punishment condition. The shaded area represents the last 50% of trials which were averaged within subjects and conditions and used for the analysis. (B) Means of the last 50% of trials in which participants chose the high probability gain stimulus and avoided the high probability lose. Means ± SEM are shown.

To investigate the hypothesis that LPS-induced shifts in reward versus punishment sensitivity are driven by activation of (micro)glial (which is hypothesized to be blocked by minocycline) I next performed a Group (Mino/PLAC) × condition (saline/LPS) × Valence (Gain/Lose) interaction analysis. This confirmed that minocycline significantly interacted with the effects of LPS on reward versus punishment sensitivity: $F_{(1,13)}$=4.28, p=0.033 serving to attenuate the inflammation-induced shift in reward versus punishment sensitivity (Figure 5.4). Post-hoc analysis for the reward and punishment conditions separately revealed non-significant trends for Minocycline to simultaneously attenuate both the LPS-induced impairment in reward sensitivity ($F_{(1,13)}$=3.33, p=0.091) and the LPS-induced enhancement of punishment sensitivity ($F_{(1,13)}$=5.29, p=0.095).

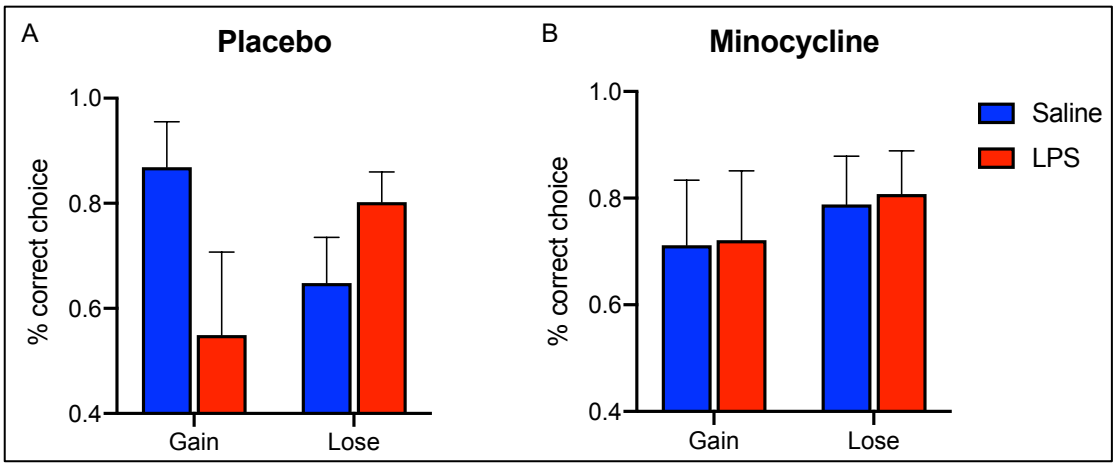

Figure 5.4 Effect of minocycline on observed choice

Proportion of the last 50% of trials in which participants of the placebo (A) and minocycline (B) group chose the high probability gain stimulus and avoided the high probability loss. Means ± SEM are shown.

5.4 Discussion

Consistent with previously reported findings with the Typhoid model of mild systemic inflammation (Harrison *et al.*, 2016), LPS (1 ng/kg) was associated with an acute shift in human reward versus punishment sensitivity, serving to enhance participants' sensitivity to punishments versus rewards. Furthermore, this acute motivational reorientation was attenuated by minocycline, a centrally penetrant tetracycline that has been shown to block inflammation-induced activation of microglia in rodents (Henry *et al.*, 2008).

These data are in line with preclinical results showing that minocycline improves inflammation induced anhedonia and sickness in rodents (Reis, Casteen and Ilardi, 2019). The mechanism by which minocycline exerts these beneficial effects on sickness behaviour is not yet fully understood, although it is believed to relate to inhibition of

inflammation-induced microglial activation (Nettis, 2021). Causally, minocycline inhibits the release of proinflammatory cytokines, such as IL-1β, IL-6, IL-2, TNF-α and IFN-γ, in the brain and promotes the production of the anti-inflammatory cytokines IL-10 (Soczynska *et al.*, 2012). One of the possible mechanisms by which minocycline exerts its anti-inflammatory function is through the inhibition of p38 mitogen-activated protein (MAP) kinase, a key enzyme for the production of inflammatory mediators. Of note, minocycline inhibits the LPS-induced p38 MAP kinase activation (phosphorylation) in microglia cell culture (Nikodemova, Duncan and Watters, 2006). Yet, the specific molecular target has not been characterized.

One of the downstream consequences of this is that minocycline appears to inhibit inflammation-induced upregulation of indolamine 2,3 dioxygenase (IDO) (Henry *et al.*, 2008; O'Connor, Lawson, André, *et al.*, 2009). However, although IDO is central to the regulation of serotoninergic and glutamatergic neurotransmission, which are believed to play a role in mediating LPS-induced mood symptoms, and may relate to alterations in insula-based punishment learning signals, it is less clear how this would modulate dopaminergic pathways which are believed to be central to anhedonia and reward learning (Schultz, Dayan and Montague, 1997; Gorwood, 2008). However, in line with our results, minocycline treatment in a rat model of depression with decreased level of dopamine in the amygdala induced an antidepressant effect and increased dopamine in the amygdala, even though serotonin concentrations remained unchanged (Arakawa *et al.*, 2012). This implicates at least part of the antidepressant properties of minocycline in an action on dopaminergic pathways.

Although I did not directly measure the effects on dopamine turnover in our current study, these results, coupled with evidence from previous imaging studies (Pessiglione *et al.*, 2006; Eisenberger *et al.*, 2010; Capuron *et al.*, 2012; Harrison *et al.*, 2016), suggest an effect of minocycline on dopaminergic activity in humans. In this regard, it is also known that inflammation can lead to a reduction in dopamine by decrease the availability of tetrahydrobiopterin (BH4), a key enzyme co-factor in dopamine synthesis needed for the conversion of phenylalanine to tyrosine and tyrosine to L-DOPA, the precursor of dopamine. BH4 is oxidation-labile, therefore inflammation-induced reactive oxygen species (ROS) can readily reduce the BH4 level and ultimately inhibit dopamine synthesis (Neurauter *et al.*, 2008). Supporting the relevance of inflammation to dopamine levels in humans, chronic IFN-α treatment in hepatitis-C patients has been shown to reduce plasma L-phenylalanine turnover (reflecting a lower BH4 concentration), which negatively correlated with CSF dopamine concentration. Moreover, decreased CSF BH4 concentration correlated with increased CSF IL-6 (Felger, Li, *et al.*, 2013). However, to my knowledge, it has yet to be shown whether minocycline can affect dopamine biosynthesis.

The lack of minocycline effect on self-reported questionnaires for mood, fatigue and sickness might suggest that minocycline specifically ameliorates inflammation-induced motivational reorientation, possibly by acting on dopamine availability. However, dopaminergic imbalances have also been associated with fatigue during inflammation (Capuron and Miller, 2004), whereas here, LPS-induced fatigue (as shown by fVAS) was not affected by minocycline treatment. This experiment might have been underpowered to detect minocycline activity on self-reported fatigue and mood changes. Further studies are needed to investigate minocycline effect subjective symptoms. However, it has been

shown that different drugs targeting monoaminergic systems can selectively modulate anhedonia or fatigue, suggesting that specific molecular pathways can be implicated in distinct symptoms (Billones, Kumar and Saligan, 2020).

Though this study and previous data using the same reinforcement learning task (Harrison *et al.*, 2016) provide further evidence that systemic inflammation can alter reward learning signals and sensitivity to rewards, other studies have reported an effect of inflammation that is mediated by actions on effort sensitivity rather than reward sensitivity per se (Lasselin, Treadway, *et al.*, 2016; Draper *et al.*, 2017). It is worth reflecting on what may underlie these apparent differences. For example, task designs in studies reporting effects on effort sensitivity do not have a learning component during the trial sequence and use two different levels of reward (high vs. low) (Lasselin, Treadway, *et al.*, 2016) or 25 different conditions (combination of 5 effort and 5 stake levels) (Draper *et al.*, 2017), whereas the reinforcement learning task that I used included only a single type of reward (win or nothing). Furthermore, in some studies, LPS-induced somatic symptoms (e.g. aching joints, muscular pain and muscle fatigue) rather than motivation reorientation could, at least in part, account for the decreased willingness to engage in high effort trials. This would be particularly relevant for tasks performed acutely e.g. within 2 hours of LPS injection, when local physical symptoms are at their peak, or using higher doses of LPS (e.g. 2 ng/kg).

To mitigate this, in the current study, participants completed the reinforcement learning task approximately six hours after LPS injection when local physical symptoms, such as muscle aches and pain, had completely resolved, yet symptoms such as raised body temperature and fatigue persisted. Furthermore, the physical effort required to complete

our reinforcement learning task was minimal (button press/no press response) and was not significantly affected by LPS (similar go/no-go responses across conditions p=0.97). Of note, TSPO PET data from other groups confirm substantial glial activation in humans at 3-5 hr post LPS (1 ng/kg) (Sandiego *et al.*, 2015) and at 4-6 hours in baboons (Hannestad *et al.*, 2012), confirming sustained LPS-induced glial activation during this testing time window.

The primary limitation of the present study is the modest sample size. For example, although I detected main effects of inflammation and interactions with minocycline, this study was likely underpowered to detect any potential correlations between peripheral immune markers and psychological changes. Moreover, endotoxemia is a reliable method to induced systemic and central inflammation and has been described as a valuable traslational approach to test the immunomodulating agent for depression (Lasselin, Lekander, *et al.*, 2020). Therefore, the present data might have translational value in disentangling the mechanism of action of anti-inflammatory therapies in depression and can provide a reproducible protocol to screen potential new drugs that act as inhibitors of neuroimmune pathways. It should be noted that minocycline did not alter levels of circulating immune cells or the plasma concentrations of IL-6, TNF-α, IL-8 or IL-10, which is consistent with previous data (Nettis *et al.*, 2021), suggesting that the anti-inflammatory effect is only exerted centrally.

LPS-induced increases in cytokine levels have been reported to be more marked in female versus male participants (Wegner *et al.*, 2017). Further, low-dose LPS has been associated with decreased ventral stiatal activation in anticipation of rewards in female but not male subjects (Moieni *et al.*, 2019). A limitation of the present study is that participants were

only composed of male subjects and future studies will be needed to determine generalization of these results.

Given its proposed neuroprotective action, minocycline has been tested in clinical trials for brain and spinal injuries and neurodegenerative diseases with mixed but generally negative results. A TSPO PET study on humans showed that minocycline treatment decreases microglial activation in traumatic brain injury (Scott et al., 2018). Nevertheless, clinical data relating to the antidepressant effect of minocycline are more controversial. Results from pilot studies with limited patients number gave mixed results. A 12-week pilot study on depressed patients reported beneficial effects of minocycline on secondary outcomes but not on the Montgomery-Åsberg Depression Rating Scale (MADRS) score (Dean *et al.*, 2017). At the same time, another study on treatment-resistant depressed patients showed a beneficial effect of minocycline as an adjunctive therapy on depression symptoms (Husain *et al.*, 2017). However, in the largest clinical trial bipolar depressed patients failed to respond to minocycline treatment (Husain *et al.*, 2020). However, it has been suggested that the lack of efficacy of the immunomodulating agents on depression could be due to the design of the trial, which does not stratify patients for ongoing inflammation and does not include anhedonia as an outcome variable (Miller and Pariante, 2020). In fact, in a separate study, minocycline had a beneficial effect on a subpopulation of depressed patients with low-grade peripheral inflammation (Nettis *et al.*, 2021). In another trial on patients with the HIV infection, minocycline was associated with improved depression symptoms (Emadi-Kouchak *et al.*, 2016).

In conclusion, to my knowledge, this is the first study to assess the effect of minocycline after experimentally-induced inflammation. I provide two key findings: firstly, a

replication of the finding that systemic inflammation can reorient motivation, impairing sensitivity to rewards versus punishments; secondly, that minocycline, a centrally penetrant tetracycline that blocks microglial activation, can abrogate these effects. Together, these findings suggest that using an immune challenge coupled with a cognitive task that assesses reward sensitivity could be a useful strategy for evaluating target engagement of novel centrally penetrant immunomodulatory drugs in human early phase clinical trials. These data also provide evidence that anti-inflammatory agents such as minocycline may be efficacious in the treatment of specific depressive symptoms such as anhedonia in the context of inflammation.

Chapter 6: Diffusion-Weighted Magnetic Resonance Spectroscopy

6.1 Introduction

Effects of systemic inflammation on the brain are implicated in the aetiology of a range of common mental illnesses and neurodegenerative disorders (Khandaker *et al.*, 2021). Multiple parallel neural and humoral immune-brain communicatory pathways have been identified, though the ultimate mediator of central effects is increasingly recognized to be microglia (Critchley and Harrison, 2013), brain specialized macrophages which constitute ~5-12% of all brain parenchymal cells (Dos Santos *et al.*, 2020). In rodents, peripheral immune challenges, typically using LPS, increase blood brain-barrier permeability (Clawson et al., 1966; Varatharaj and Galea, 2017). They also rapidly triggers a shift in microglial morphometry from a 'resting' to an 'activated' phenotype which is accompanied by an increase in proinflammatory cytokine release (Savage *et al.*, 2019). Although, inter-species sensitivity differs markedly (up to many orders of magnitude), LPS-induced changes in microglial morphometry are also observed in rodents at doses that are broadly species equivalent to those used in human studies. In rodents, these inflammation-induced changes in microglial morphology and secretory profile can be quantified ex vivo using microscopy, immunohistochemistry, and single cell transcriptomics, and *in vivo* using multi-photon imaging through a cranial window (Savage *et al.*, 2019).

In humans, *in vivo* methods for imaging microglial activation are currently limited PET using tracers that bind to TSPO, which is overexpressed on the outer mitochondria membrane of activated microglia. TSPO-PET has been used to demonstrate widespread increases in grey matter TSPO binding, 3-5 hours after an inflammatory challenge (using LPS) in humans (Sandiego *et al.*, 2015), and 4-6 hours in nonhuman primates (Hannestad *et al.*, 2012). However, TSPO PET is an invasive procedure, involving exposure to radioactivity, and TSPO is also expressed in other glial cells as well as on vascular endothelium. Furthermore, precise quantification of the TSPO PET signal in the brain is substantially complicated by LPS-induced redistribution of TSPO radiotracers across compartments (Yoder *et al.*, 2015), limiting its more widespread use to research and its potential as a viable clinical tool (J. Schubert *et al.*, 2021). MRI-based approaches have been used to index effects of systemic inflammation on brain functional reactivity (fMRI), functional connectivity (resting state fMRI), neurochemistry (MRS) and microstructure (qMT and DW-MRI). While these approaches have highlighted a matrix of brain regions sensitive to peripheral inflammation (Critchley and Harrison, 2013; Kraynak *et al.*, 2018; Garcia-Hernandez *et al.*, 2020), they cannot provide direct information on the likely cellular substrates that underpin these inflammation-related changes.

Diffusion-Weighted Magnetic Resonance Spectroscopy (DW-MRS) offers the potential to address these shortcomings. Briefly, DW-MRI is highly sensitive to tissue microstructure and water compartmentalization (Pierpaoli and Basser, 1996). However, its cellular specificity is limited, as water diffuses similarly through all cell types as well as the extra-cellular environment. In contrast, MRS probes the signal from metabolites, which are predominantly intra-cellular, and in some cases cell-specific. Of the commonly measured metabolites, N-Acetyl-Aspartate (NAA) is exclusively confined within

neurons, total creatine (creatine + phosphocreatine = tCr) is found in each brain cell type, while choline compounds (Choline, phosphocholine and glycerophosphocholine = tCho) predominantly reside in glial cells (with a ~3-fold higher concentration than in neurons) (Urenjak *et al.*, 1993) (Figure 6.1). The specificity of DW-MRI to different cell types can thus be dramatically improved by combining it with MRS, enabling the morphological properties of specific cell types to be probed by measuring the Apparent Diffusion Coefficient (ADC) of different metabolites (Ingo *et al.*, 2018; Palombo *et al.*, 2018).

In line with this, DW-MRS has been shown to be sensitive to cell-specific metabolite diffusion changes in the brain, in animal models and in patients with chronic inflammatory conditions. For example, in the cuprizone mouse model of Multiple Sclerosis (MS), the ADC of both tCho and myo-inositol was observed after 6 weeks of cuprizone with these changes showing moderate to strong correlations with histological measures of microglial and astrocytic area fractions respectively (Genovese, Palombo, *et al.*, 2021). In humans, patients with Systemic Lupus Erythematosus (SLE) exhibit an increased intracellular diffusion of total creatine and total choline in the white matter, compared with healthy controls (Ercan *et al.*, 2016). The diffusion of tCr and tCho has also been found to increase in the primary motor cortex of patients with Amyotrophic Lateral Sclerosis (ALS), suggesting the presence of reactive glia (Reischauer *et al.*, 2018). Data from the thalamic grey matter of MS patients has shown a decrease in ADC(NAA), which is believed to reflect accompanying neuronal-axonal loss or mitochondrial dysfunction, and a decrease in ADC(tCr), which is thought to reflect an impaired cell energy metabolism (Bodini *et al.*, 2018).

Here I employed DW-MRS to assess the effect of peripherally administered LPS on the ADC of NAA, tCr and tCho within a grey and a white matter region of interest in healthy humans. The thalamus and the corona radiata were selected as regions of interest, as they are homogeneous regions of grey and white matter respectively. Of note, the thalamus is known to be susceptible to peripheral LPS administration (Buttini, Limonta and Boddeke, 1996; Sandiego *et al.*, 2015).

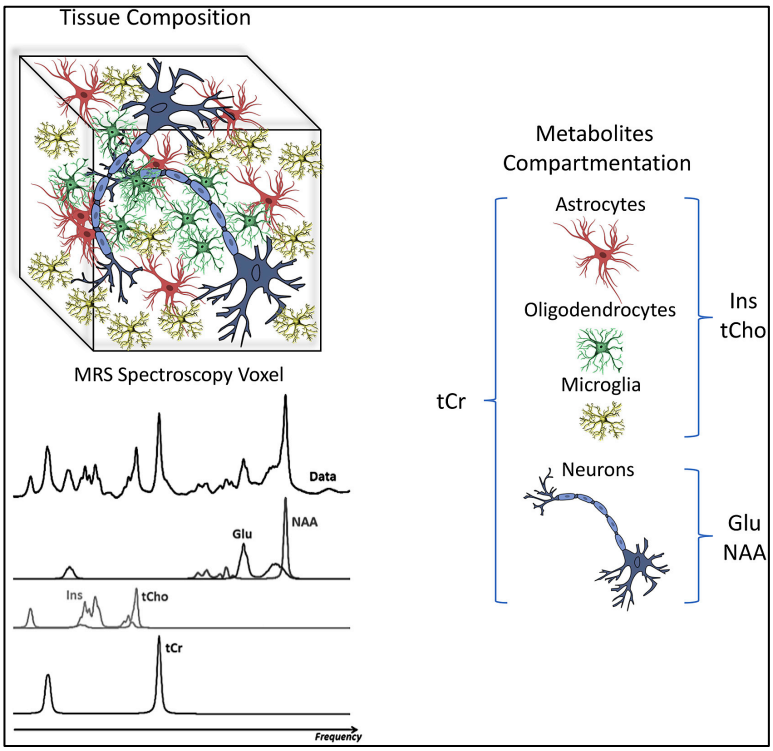

Figure 6.1 Composition of a spectroscopic voxel of the brain parenchyma
DW-MRS can provide cell-specific information on brain microstructural properties by measuring the diffusion of intracellular metabolites that mostly reside in a particular cell type (Figure taken from Palombo et al., 2018).

6.2 Methods

6.2.1 participants and study design

Seven participants were recruited and tested during the first stage of the study, among this subgroup 6 received minocycline as described and 1 the placebo. The new cohort (N=5) recruited for the new study phase also underwent DW-MRS (Figure 3.3 illustrates study subgroups). In total 12 subjects (mean age: 24.38 ± 4.9 (std) years, mean BMI: 24.6 ± 1.7 (std) kg/m^2) were included; 6 were pre-treated with minocycline. All subjects were screened as described in Chapter 3. A DW-MRS scanning session was scheduled for 5-5½ hr after each injection of LPS or saline. This timing was informed by: 1) prior human and baboon TSPO PET studies that report increased TSPO uptake at 3-5 and 4-6 hours post LPS, respectively, as well as sustained subjective sickness and systemic inflammatory responses at these time-points, confirming an ongoing peripheral and central inflammatory response; 2) evidence from prior human studies using 1 ng/kg LPS that show a significant reduction in peripheral limb and joint discomfort, coupled with less pronounced pyrexia, at 5 hr post injection, meaning that the participants would be better able to comply with the requirements to remain very still during the DW-MRS scanning session (which is highly sensitive to motion).

Physiological (vital signs, differential white blood cell counts and cytokines) and psychological data were collected, as described in Chapters 4 and 5.

6.2.2 DW-MRS acquisition and analysis

MRI and MRS were obtained at 3T (Siemens Magnetom Prisma, Siemens Healthineers, Erlangen, Germany). After a standard localizer, a T1-weighted magnetization prepared

rapid acquisition gradient echo (TR=1900 ms; TE=3.97 ms; TI=904 ms, flip angle=8 deg, FOV 220 × 220 mm^2, matrix size 192 × 192) was acquired in sagittal orientation and reconstructed in 3 orthogonal planes. These high-resolution scans were used to position two 4.5 cm^3 DW-MRS Volumes Of Interest (VOIs) on the left thalamus and left corona radiata. The VOIs were chosen mainly based on the need to obtain a signal from homogeneous grey and white matter. The left hemisphere was chosen as it is more commonly implicated in inflammation-induced cognitive changes (Haroon *et al.*, 2014; Harrison *et al.*, 2015). The DW-MRS sequence used was a bipolar sequence based on a semi-Localization by Adiabatic SElective Refocusings (semi-LASER) sequence (Genovese, Marjańska, *et al.*, 2021) with TE=100 ms, TR=5 s, spectral width=2500 kHz, number of complex points=1024. The following diffusion weighting conditions were used: one at b=0 s/mm^2 and three at b=3823 s/mm^2, with diffusion gradients applied in three orthogonal directions ([1, 1, −0.5], [1, −0.5, 1], [−0.5, 1, 1] in the VOI coordinate system, diffusion gradient duration=14 ms, diffusion time=50 ms). The Number of Signals Averages (NSA) was 32 for each condition. A short (NSA=4) scan without water suppression was performed for eddy current correction. B_0 shimming was performed using a fast automatic shimming technique with echo-planar signal trains utilizing mapping along projections, FAST (EST) MAP (Gruetter and Tkáč, 2000).

The spectra were transferred off-line for analysis with customized software implemented in Matlab R2019b (Mathworks, Natick MA, USA). Spectral analyses were performed with linear prediction singular value decomposition (LPSVD), and the peak area estimates for the three orthogonal gradient directions at high b value were averaged and the resulting mean values were used to compute the ADC values for the three metabolites. The spectra at b=0 s/mm^2 were used to estimate relative tCho and tNAA (tNAA = NAA

+ NAAglutamate) concentrations, expressed as the ratio between their peak area to the tCr peak area.

6.2.3 Statistical analysis

The ADC of the three metabolites, as well as the tCho and tNAA concentrations relative to tCr ([tCho]/[tCr] and [tNAA]/[tCr]) were compared between sessions (LPS vs. saline), using a paired-sample t-test. Associations between changes in ADC(tCho) and changes in mood (POMS), temperature and peripheral immune measures (cell counts and cytokines) were assessed using Pearson's correlation. Exploratory analysis of the minocycline effect was conducted using a two-way ANOVA with condition (Saline/LPS) as a within-subject factor and group (Minocycline/Placebo) as a between-subject factor.

6.3 Results

6.3.1 Physiological effects:

The physiological results previously shown include all participants (N=20). Herein the results relative to the DW-MRS subgroup are presented. Significant condition (Saline/LPS) × time interactions were observed for body temperature ($F_{(13,78)}$=21.6, $p<0.001$) and heart rate ($F_{(13,78)}$=8.48, $p<0.001$). LPS significantly increased body temperature, from 60 minutes, peaking at 3 hours post injection, and significantly increased heart rate which peaked between 2 and 4 hours post-injection. Significant condition (Saline/LPS) × time interactions were also observed for total WBC count ($F_{(2,12)}$=30.6, $p<0.001$) as well as for each differential WBC count (Neutrophils:

$F_{(2,12)}$=54.9, p<0.001; lymphocytes: $F_{(2,12)}$=26.2, p<0.001; monocytes: $F_{(2,12)}$=23.7, p<0.001) with the greatest changes observed at 6 hours.

6.3.2 Cytokine levels

LPS induced significant increases in circulating cytokines, as shown by significant condition (Saline/LPS) × time (baseline, 3 hr and 6 hr) interactions for IL-6: $F_{(2,12)}$=49.12, p<0.001; TNF-α: $F_{(2,12)}$=120.60, p<0.001; IL-10: $F_{(2,12)}$=59.75, p<0.001; IL-10: $F_{(2,12)}$=12.05, p=0.001.

6.3.3 Behavioural response

The effect of inflammation on subjective symptoms in the first cohort is shown in the previous chapter. Here, I present the psychological data of the last 7 subjects from the first cohort, who underwent the DW-MRS scans. LPS injection led to significant temporary changes in mood, fatigue, and sickness symptoms, as shown by the POMS questionnaire, fVAS, and sickness questionnaire. Specifically, LPS was associated with a reduction in total mood score: main effect of condition ($F_{(1,6)}$=77.73, p<0.001), condition × time interaction ($F_{(5,30)}$=2.31, p=0.068) and increase in negative mood score: main effect of condition ($F_{(1,6)}$=57.17, p<0.001), condition × time interaction ($F_{(5,30)}$=2.38, p=0.062). LPS-induced changes in both total mood and negative mood scores (compared to saline) peaked at 2 hr post injection (paired-sample t-tests vs. baseline: $t_{(6)}$=3.6, p=0.011; $t_{(6)}$=-3.0, p=0.024 respectively) (Figure 6.2 insets). Moreover, LPS induced a significant increase in both fatigue (significant condition × time interaction for fVAS: $F_{(5,30)}$=4.06, p=0.010) and sickness score ($F_{(5,30)}$=6.34, p=0.001). fVAS showed a rapid increase in fatigue that peaked at 1 hour post LPS injection, compared to the baseline

(paired-sample t-test $t_{(6)}$=-3.6, p=0.011), while the sickness score peaked at 2 hours ($t_{(6)}$=-5.5, p=0.002) followed by a gradual improvement.

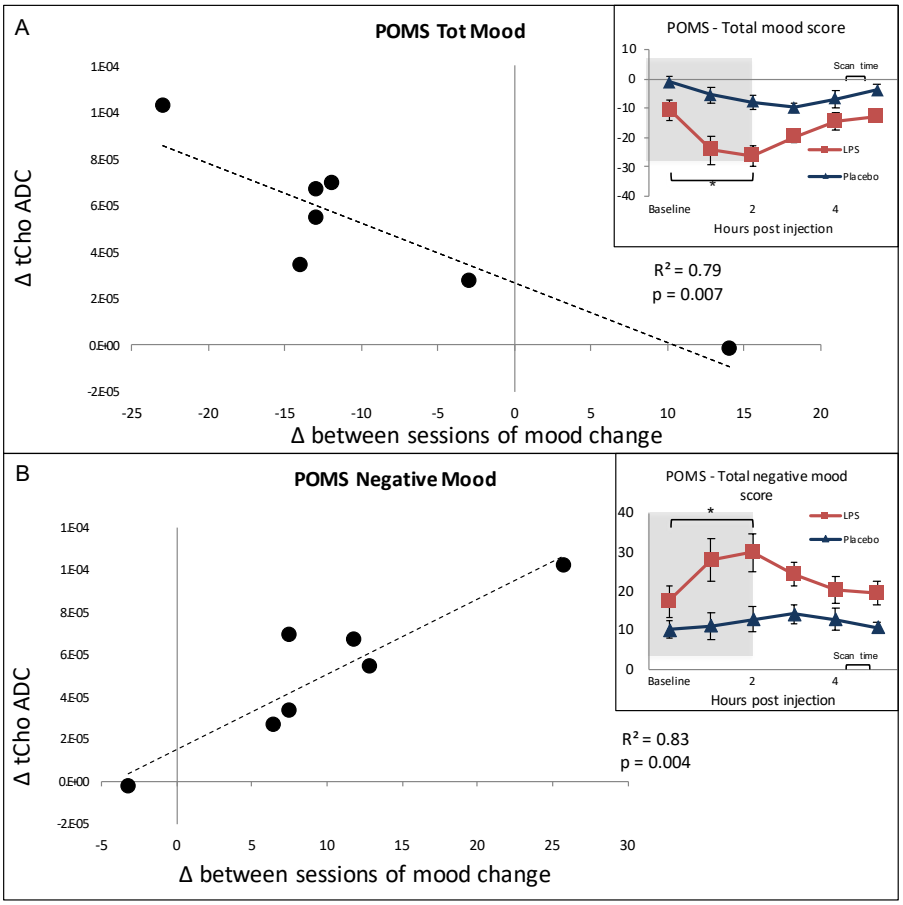

Figure 6.2 Effect of LPS on mood and relationship with tCho ADC change

Correlation between ADC(tCho) change between the two sessions and the difference between mood changes from baseline to 2 hr post injection in the two session. (A) POMS total mood score, (B) POMS negative mood score. Insets show the mood score throughout the two sessions; the grey shaded areas indicate the two timepoints used to obtain the POMS difference correlated with the ADC(tCho) change.

6.3.4 LPS effects on metabolites ADC

The spectra were of good quality for all participants. As an example, Figure 6.3 shows spectra acquired in the thalamus of the same participant in the two conditions (saline and LPS). The average ADCs of tNAA, tCr and tCho are shown in Table 3; The between-condition difference in metabolite ADC is shown in Figure 6.4. Paired t-tests revealed a significant increase in ADC(tCho) in the thalamus for the LPS compared to the saline condition ($t_{(11)}$=-2.74, p=0.019; Cohen's *d*=1.22), (ADC(tCho) (Thalamus): saline (M=0.119 μm^2/ms SD=0.029), LPS (M=0.159 μm^2/ms, SD=0.035)). The significantly increased ADC(tCho) after LPS was still present when the analysis was repeated excluding the outlier that did not show physiological changes post LPS (as discussed in Chapter 4) ($t_{(10)}$=-2.69, p=0.022). The analysis was also repeated excluding the subject that demonstrated a substantial increase (184%), in order to assess the potential influence on the overall results. The ADC(tCho) in the LPS condition remained significantly higher than in the saline condition ($t_{(10)}$=-2.38, p=0.039).

No significant difference was detected in ADC(tCho) in the WM control region between the two conditions. ADC(tNAA) and ADC(tCr) did not differ significantly between conditions in either VOI. No significant differences in the metabolites' relative concentration (expressed as [tCho]/[tCr] and [tNAA]/[tCr]) were observed in either region between conditions (Figure 6.5). There was no significant correlation between LPS-induced changes in body temperature and ADCs for any of the metabolites (all p>0.1). Exploratory analyses investigating associations between ADCs and peripheral immune measures revealed a trend association between LPS-induced changes in thalamic ADC(tCho) and associated change in monocyte count at 6 hours (R^2=0.46; p=0.09). All

other associations were non-significant (p>0.1). Minocycline treatment did not affect the ADC(tCho), as shown by the (LPS/Saline) × group (Minocycline/Placebo) interaction ($F_{(1,10)}$=0.41, p=0.53).

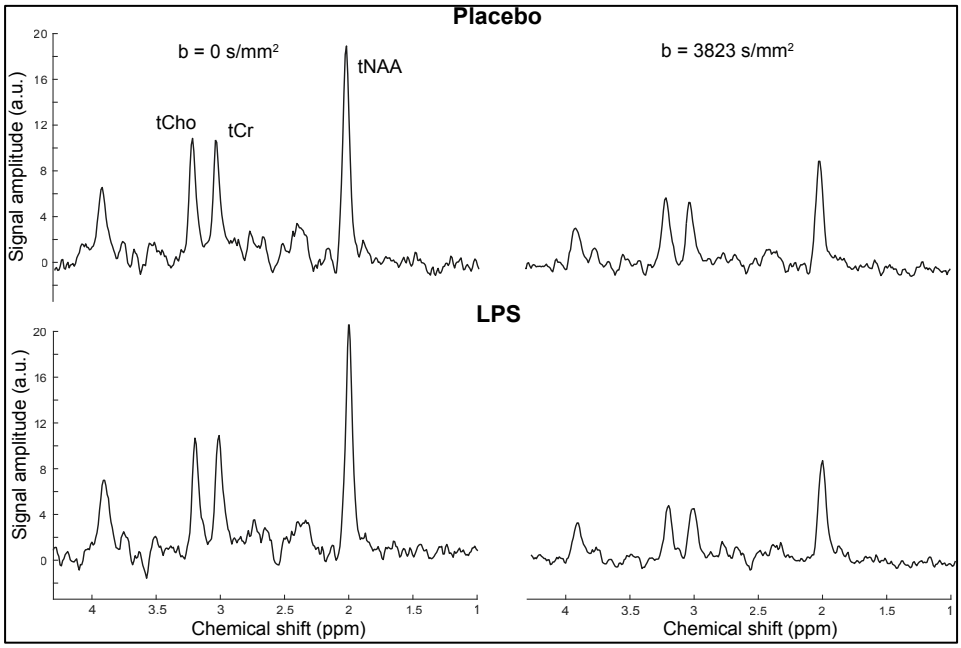

Figure 6.3 MRS Spectra

Example of MR spectra acquired at b=0 s/mm^2 and b=3823 s/mm^2 in the left thalamus of one subject after saline (top) and LPS (bottom) injections**.**

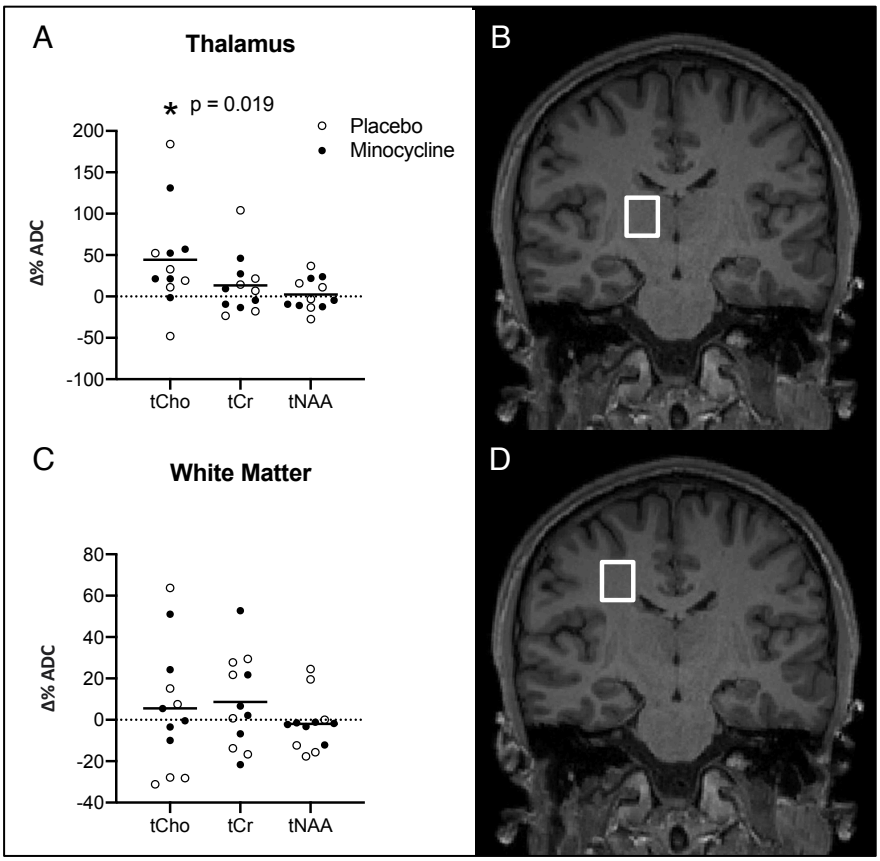

Figure 6.4 Metabolites ADC responses to LPS

tCho, tCr and tNAA ADC % differences (calculated as (ADC_{LPS}-ADC_{saline})/ADC_{saline})*100) between LPS and saline sessions in thalamus (A) and white matter (C). Mean and individual differences are reported. Volumes of interest (VOIs) were located in the thalamus (B) and in the parietal white matter (corona radiata) (D). P-value relates to comparison between LPS and saline session.

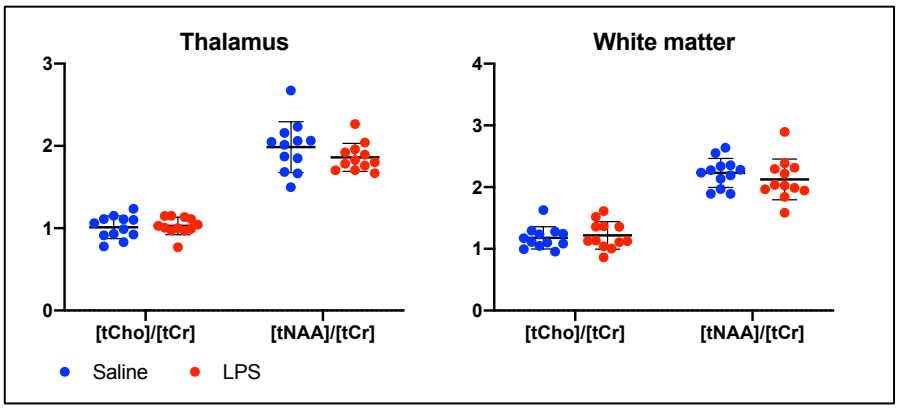

Figure 6.5 Effect of LPS on metabolites concentrations

Bars represent mean ± SEM.

6.3.5 Correlation between mood deterioration and ADC(tCho) change

To investigate potential associations between mood change and putative changes in neuroinflammation I regressed peak change in mood (2 hour post injection minus baseline) for LPS compared to saline, against changes in the ADC(tCho) between conditions. LPS-associated changes in both POMS total and negative mood were significantly associated with changes in the ADC(tCho) of the thalamus (R^2=0.79; p=0.007 and R^2=0.83; p=0.004, respectively) (Figure 6.2**)**.

6.4 Discussion

Glial activation is a hallmark of the neuroinflammatory cascade and a pathological feature of a wide range of severe and disabling central nervous system (CNS) diseases. Increased density, altered morphology, and/or a proinflammatory immune phenotype of microglia and astrocytes are consistent post-mortem findings in autoimmune neuroinflammatory

disorders, such as MS or Neuro SLE, and neurodegenerative diseases such as ALS and Alzheimer's disease (McGeer and McGeer, 2002; Perry and Holmes, 2014; González-Reyes *et al.*, 2017). Furthermore, post-mortem and neuroimaging evidence of alterations in microglia and astrocytes in depression and schizophrenia have implicated glia in the neuropathology of psychiatric disorders that are linked to heightened systemic inflammation (Lanquillon *et al.*, 2000; Dantzer *et al.*, 2008; Najjar *et al.*, 2013; Almeida *et al.*, 2020). Yet, the exact mechanisms that underly the brain response to systemic inflammation remain elusive, as sensitive and viable neuroimaging methods for the *in vivo* assessment of glial response to systemic inflammation are yet to be fully developed.

Here, using DW-MRS, I report results from 12 healthy subjects, which provide preliminary evidence for altered intracellular metabolite diffusion in the context of experimentally-induced systemic inflammation in humans. Changes in metabolite diffusion properties have been considered to mirror the cytomorphological cell rearrangement or, in a pathological framework, the tissue damage. The primary finding of this study is the increased ADC(tCho) in the grey matter after the injection of LPS, compared to saline. This result suggests that cytomorphological changes in glial cells, observed using microscopy, in rodents after systemic inflammation can also be detected *in vivo* in humans using DW-MRS. This finding is also in keeping with recent DW-MRS results in rodents showing an increase in tCho and myo-inositol ADCs, using the Cuprizone model of neuroinflammation, which correspondingly correlate with induced changes in microglial and astrocytic area fraction recorded histologically (Genovese, Palombo, *et al.*, 2021), as well as in human neurological diseases, such as neuropsychiatric systemic lupus erythematosus (Ercan *et al.*, 2016) and ALS (Reischauer

et al., 2018), which are each characterized by glial activation. However, confirmation of our preliminary findings will require future replication in larger studies.

The absence of a significant change in the neuronal marker ADC(tNAA) in our current study is also consistent with histological studies which indicate no effect of LPS on neuronal morphology. However, it is worth stressing that the small sample size may have meant I was under powered to detect diffusion changes in other metabolites. Of note, reductions in ADC(tNAA) have been previously reported in MS, however this finding has been interpreted as reflecting accompanying neuronal damage or cell loss, which is a feature of this model but not systemic LPS (Bodini *et al.*, 2018). A potential bias in our experiment was the effect of LPS on body temperature and, consequently, metabolite diffusion. However, the absence of an effect of LPS on the diffusion of the neuronal marker tNAA in either VOI or on tCho in our white matter region, coupled with an absence of even a trend-level association between changes in body temperature and any of the metabolite ADCs suggests this is an unlikely cause of our findings.

Minocycline pre-treatment did not appear to affect LPS-induced ADC(tCho) changes. The lack of a minocycline effect may be due to the small sample size of the study. However, a study on a mouse model of brain injury showed that minocycline inhibits microglial proinflammatory activity, without significantly affecting cytomorphological properties. Thus it is possible that the neuroprotective effect of minocycline does not alter microglial cytomorphological rearrangements (Blecharz-Lang *et al.*, 2022). One limitation of our study was the unbalance in the randomization placebo/minocycline that occurred due to participant dropouts and sessions cancellation that led to rearrangement of the study calendar with consequent changes of the randomization table (as mention in

section 3.1). Due to changes to the scheduled randomization, 6 out of 7 subjects of the first cohort were in the minocycline arm. The other 5 subjects, of the second cohort (see Figure 3.3), that underwent DW-MRS did not receive minocycline/placebo treatment. Here these subjects were included in the placebo arm. Hence this may constitute a bias for the interpretation of the effect of minocycline on the DW-MRS signals. However, it is important to note that this study was conducted as a preliminary investigation utilizing a novel technique, with the primary focus being the sensitivity to the immune challenge rather than the specific effects of the minocycline treatment, which were considered as a secondary aim. Nevertheless, future studies including a limited number of subjects will have to prevent the randomization unbalance by implementing different type of randomization. For example, a block randomization approach, dividing the study population in two groups might have mitigated the impact of subject dropouts or session cancellations. Another valid approach to cope with the session cancellations could be the adaptive randomization, to dynamically balance the number of subjects in each group throughout the study.

Though tCho has only limited specificity to glial cells, its significant ADC change following LPS, compared to saline, is consistent with previous studies that report microglial and astrocytic neuroinflammatory responses following peripheral LPS exposure in mice (Ryu *et al.*, 2019). Microglia are known to be the principal mediator of innate immune responses within the CNS. In the healthy brain, microglial cells monitor the brain parenchyma and are characterized by a ramified cell shape (Nimmerjahn, Kirchhoff and Helmchen, 2005). Changes in brain homeostasis due to infection, injury or neurodegeneration can alter microglia gene expression, morphology and motility (Helmut *et al.*, 2011). However, during neuroinflammation both microglia and astrocytes undergo

metabolic, functional and morphological changes (Heneka, Kummer and Latz, 2014). In this reactive state glial cells can release neurotoxic factors such as proinflammatory cytokines and reactive nitrogen and oxygen species, ultimately affecting neuronal transmission and neurogenesis (Orihuela, McPherson and Harry, 2016). Once activated, microglia display a thickening and a retraction of their processes and assume an amoeboid spherical shape with increased cell body size (Davis, Foster and Thomas, 1994). In a similar way, reactive astrocytes are characterized by cellular hypertrophy and overlapping processes (Sofroniew and Vinters, 2010). It is therefore uncertain whether the changes in tCho diffusion that I observed stemmed from microglial or astrocytic activation. However, in a mouse model of astrocytic hypertrophy myo-inositol diffusion changes were sensitive to cytomorphological rearrangement, whereas tCho was unaffected (Ligneul *et al.*, 2019). Similarly, in the cuprizone model mentioned earlier, induced changes in tCho scaled with histological changes in microglia and myo-inositol with changes in astrocytes (Genovese, Palombo, *et al.*, 2021).

It is worth noting that I was unable to quantify myo-inositol diffusion using our current method. The quantification of myo-inositol present specific challenges, primarily due to the requirement of a short TE, which is difficult to achieve when applying diffusion weighting. This poses a particular difficulty when measuring a deep brain structure such as the thalamus, leading to potentially noisy acquisitions. Moreover, the myo-inositol concentration is lower than that of tCho and tNAA, resulting in higher estimation errors for its apparent diffusion coefficient (ADC).

The higher diffusivity of tCho I observed is also consistent with the increased intracellular space that characterizes microglia in the activated state (Savage *et al.*, 2019).

Furthermore, although microglial and astrocytic activation are both key components of neuroimmune processes, microglia are thought to initiate the process triggered by LPS and then causally induce astrocytic activation (Liddelow *et al.*, 2017). In line with this finding, a DW-MRI study using a multi-compartment tissue model based on the microglia and astrocyte cell shapes has recently shown typical microglial changes at 8 post LPS injection in rodents with a subsequent astrocytic signal emerging later, at 24 hrs (Garcia-Hernandez *et al.*, 2020). This time-dependent neuroimmune cascade allows us to speculate that the observed increase in ADC(tCho) may selectively reflect microglial activation. In support of this, since the tCho concentration was unchanged between sessions it is unlikely that the observed change in ADC was influenced by infiltrating or perivascular immune cells.

The localized effect in the grey matter is also consistent with in vitro data of the cytomorphological properties of a microglial cell culture. Though no significant differences in cell shape (ramified/amoeboid) were observed, grey matter microglia display increased elasticity and rearrangement of cytoskeleton components following LPS treatment. Despite showing higher elasticity under normal condition, white matter glial cells were not affected by LPS (van Wageningen *et al.*, 2021). Hence, the lack of ADC(tCho) changes in the corona radiata might also be due to the intrinsic properties of white matter glial cells , which are less prone to undergo morphological changes. This is consistent with known intrinsic region-specific microglial diversity (Stratoulias *et al.*, 2019).

A second finding of our study was the correlation between LPS-induced changes in thalamic ADC(tCho) and the severity of induced mood changes. Despite being

characterized by a high density of microglial cells, the thalamus has not previously been reported as a key structure for the psychological and behavioural effects associated with systemic inflammation (Harrison, 2017). Instead, previous fMRI studies have reported functional changes in the subgenual cingulate and amygdala (Harrison *et al.*, 2009; Davies *et al.*, 2020) following immune challenges which correlate with the severity of mood/depressive changes. Decreased global functional connectivity has also emerged as a putative neurobiological underpinning of mood deterioration driven by peripheral inflammation (Dipasquale *et al.*, 2016). This latter finding suggests a potentially widespread effect of systemic inflammation on grey matter which is consistent with the widespread increase in TSPO expression previously reported following LPS injection in both baboons and humans (Hannestad *et al.*, 2012; Sandiego *et al.*, 2015). Hence, the effect that I reported within the thalamus (which was selected based on tissue homogeneity and sensitivity to LPS, rather than a specific role in mood processing) is likely a proxy of more general glial morphological changes in the brain grey matter. However, I did not observed correlations between ADC(tCho) changes and outcomes of the reinforcement learning task reported in Chapter 5. Previous studies using the same reinforcement learning task have related the reward prediction error and the punishment prediction error with the activity of the ventral striatum and the insula respectively (Pessiglione *et al.*, 2006; Harrison *et al.*, 2016). Although the thalamus might represent a proxy of widespread neuroinflammation, it is possible that there might be region specific difference in the magnitude of microglial activation. Given the time implications for acquiring data in multiple VOIs and the limited spatial resolution (4.5 cm^3) of DW-MRS, making it challenging to measure metabolites diffusion in small areas, I restricted this preliminary study to the acquisition of data in a single grey and white matter volume of

interest. Nevertheless, it will be important for future studies to consider data acquisition from a greater range of VOIs to further address the specificity of regional changes to discrete behavioural features.

As discussed above, the main limitation of our study is the relatively modest sample size, and consequently, the need to replicate our findings in future larger studies. Another limitation is that our data were only acquired at a single time-point (5-5½ hours) after saline/LPS injection. Though human LPS studies typically only scan at a single time point, it will be important for future studies to begin to address the temporal evolution of brain changes and their association with the evolution/resolution of specific behavioural and cellular features. Following LPS challenge, changes in physiological e.g. heart-rate, temperature, cytokine and sickness symptoms typically peak 2-3 hours post administration. However, cellular responses e.g. neutrophil and monocyte counts typically continue to increase up until at least 6 hours post injection. TSPO PET studies indicate central (brain) glial activation 3-5 hours after LPS in humans (Sandiego *et al.*, 2015) and from 1-3 hours in baboons, rising further at 4-6 hours before returning to (or below) baseline at 22-24 hours (Hannestad *et al.*, 2012). Thus, though many peripheral immune response indices peak relatively early, central glial responses appear to peak later and remain evident until at least 6 hours post LPS. How and when these initial proinflammatory responses ultimately resolve, and how they relate to acute and potentially more persistent symptoms in some participants, will need to be addressed in future studies. Rodent studies combining longitudinal DW-MRS with histological analyses will also be valuable in clarifying the cell-specific basis of each metabolite.

In conclusion, a novel MR imaging paradigm is presented, that could enable the quantification of glial morphological changes *in vivo* in humans. Although resident immunocompetent cells have emerged as a central component in a wide array of brain disorders, there is still no gold standard method to selectively assess different biological mechanisms *in vivo*. TSPO PET has been widely used to quantify neuroinflammation. However, it is invasive and expensive, requires the use of radioactivity, is difficult to quantify without an arterial input function, particularly under conditions where the inflammation is not restricted to the CNS (Nettis *et al.*, 2020). Unlike PET, DW-MRS has the advantage of being non-invasive and it can be acquired with other routine MRI images. One limitation is that it can currently only be acquired in pre-specified VOIs rather than in the whole brain. Nevertheless, pending further validation in larger studies, DW-MRS could be a valuable tool for investigating neuroinflammatory processes in clinical populations and for providing evidence of target engagement for novel pharmacotherapies being developed to target glial cells.

Mean ADC μm²/ms	Voxel position	Condition			
		Saline	LPS	Δ%	p-values (Saline vs. LPS)
tCho	Thalamus	0.121 (0.009)	0.163 (0.011)	44.46 (19.09)	0.019
	White matter	0.143 (0.006)	0.145 (0.008)	4.65 (9.42)	0.863
tCr	Thalamus	0.156 (0.010)	0.161 (0.009)	5.16 (6.42)	0.653
	White matter	0.165 (0.008)	0.172 (0.007)	6.94 (6.80)	0.481
tNAA	Thalamus	0.156 (0.008)	0.152 (0.006)	-0.80 (4.98)	0.628
	White matter	0.153 (0.005)	0.151 (0.005)	-0.73 (3.83)	0.659

Table 3 effects of LPS on metabolites ADC

Data represent mean ± SEM.

Chapter 7: PET imaging studies

7.1 Introduction

TSPO PET imaging is a widely used method to study neuroinflammation *in vivo*. The rationale supporting the use of TSPO PET imaging for neuroinflammatory imaging applications is based on evidence of TSPO upregulation on neuroinflammatory glia, particularly microglial cells (see Chapter 1 for details). However, the use of TSPO PET imaging to index microglial activation in response to peripheral inflammation is complicated by the expression of TSPO in peripheral tissues, in the endothelium and in blood cells (Rizzo *et al.*, 2019). An accurate assessment of the contribution of the blood compartment to the total PET signal is crucial to obtain a precise quantification of the specific signal within the brain. Hence, full compartmental modelling analysis based on a metabolite-corrected arterial input function (AIF) is deemed the gold standard approach for the quantification of TSPO binding (Wimberley *et al.*, 2021). The quantification of an arterial input function can be achieved by measuring the radioactivity in the arterial blood and in the plasma throughout the PET scan duration. During the first part of the scan (~first 10 min), a continuous whole blood radioactivity quantification should be performed to accurately characterize the rapidly changing concentration of the radiotracer in the blood after a bolus administration. In addition, since only the tracer in the plasma contributes to the brain parenchymal signal (see Chapter 2 for details), drawing of sparse discrete arterial blood samples is required throughout the rest of the scan to assess the relative distribution of the tracer radioactivity across the blood and plasma compartments.

Furthermore, PET radiotracers, including [^{18}F]-DPA-714, undergo extensive metabolism, which can result in radiolabelled metabolites contributing to the total radioactivity measured in the blood. Hence, only the fraction of unchanged radiotracer (parent fraction) obtained after metabolite correction should be considered when estimating the input function. Finally, the variability of plasma protein binding is another factor that can bias the quantification of microglial activity (Nettis *et al.*, 2020). Despite arterial cannulation and measurement of blood radioactivity being crucial to enable a precise assessment of microglial responses to peripheral inflammation using TSPO PET, they are invasive, and necessitate highly specialized tools and personnel, which hinders the widespread clinical use of TSPO PET in non-specialized centres.

The development of alternative non-invasive analysis approaches to quantifying TSPO availability *in vivo* constitute an unmet scientific need and would greatly benefit the field of neuroinflammatory imaging. A number of alternative methods have been tested to measure radioligand binding to TSPO when an arterial input function is not available, including methods based on image-derived input functions (IDIF) and population-based input functions (PBIF) as alternatives to the invasive direct sampling of arterial blood. IDIF approaches aim to derive the AIF from the time activity curve (TAC) of voxels that are likely to be within blood vessels, generally the carotids. These techniques are prone to different types of error and have only been validated with some radiotracers (Zanotti-Fregonara *et al.*, 2011). A method to extract an IDIF with [^{18}F]-DPA-714 has recently been proposed; however, population data had to be used for plasma fraction and metabolite correction (Fang *et al.*, 2022). Therefore, this technique relies on the assumption that the radiotracer metabolism and the plasma to whole blood concentration ratio are not affected by experimental conditions or pathologies. This assumption is likely

to be violated in the context of peripheral inflammation, where rate of the radiotracer metabolism and the free plasma fraction may both be significantly altered. Population-based input function methods use an AIF generated by averaging the AIFs from a different dataset. This approach has yielded results that correlate with standard kinetic modelling analysis. However, one or two late blood samples obtained by arterial puncture are still needed in order to scale the PBIF into a subject-specific input function (Mabrouk *et al.*, 2017; Akerele *et al.*, 2021). As a result, despite these being valid methods in specific TSPO PET applications, they might not be sufficiently accurate when the physiological changes induced by peripheral inflammation, such as that acutely induced by my experimental challenge, alter key factors such as total blood radiotracer concentration, radiotracer' kinetic behaviour, plasma over blood ratio and the metabolite profile.

Certain PET radiotracers benefit from a selective distribution of their targets in specific brain regions; this is the case, for example, for tracers that target dopamine transporter or receptors which are only localised in dopamine rich regions. In these circumstances, an alternative and optimal non-invasive approach to PET quantification is possible by using a reference region, which enables to separate the specific signal from signals derived from non-specific and vascular compartments (see Chapter 2 for details). Reference region approaches are critical where an arterial cannulation cannot be performed, for example in clinical populations.

However, there is no region in the brain that is completely devoid of TSPO, thus every region of the brain contains specific (tracer bound to TSPO) and non-specific (free tracer or tracer bound to other macromolecules) signals (Fujita *et al.*, 2008). This prevents the

use of a reference region anatomically informed to correct for the non-specific signals. Reliable pseudo-reference regions (brain regions with negligible TSPO expression used to correct for non-specific signals) have only been validated in pathological contexts where a brain region is thought to be spared by the neuroinflammatory process (Lyoo *et al.*, 2015; Albrecht *et al.*, 2018). The normalization of brain areas for the whole-brain signal has also been used (Loggia *et al.*, 2015; Zürcher *et al.*, 2020). However, this approach may fail to detect TSPO level changes in contexts of widespread neuroinflammation such as that which follows acute peripheral inflammation.

The Supervised Clustering Algorithm (SVCA) enables defining a pseudo-reference region without an a priori identification of an anatomical brain region devoid of neuroinflammation (Yaqub *et al.*, 2012). The SVCA uses a set of kinetic classes that correspond to different tissue types. The algorithm computes the contribution of each class in every voxel. This approach aims to locate the voxels that display a kinetics similar to that of the low-binding grey matter. These voxels can then be considered as representative of a pseudo-reference region since they have a minimal TSPO expression and are less likely to be affected by inflammatory processes. The pseudo-reference region resulting from SVCA, therefore, does not have a localization that corresponds to an anatomically defined brain region, but rather is formed by sparse voxels in the cerebral and cerebellar cortexes. The kinetic classes are created by extracting and averaging the TACs of the white matter, low binding (cortical) grey matter, high binding (thalamus) grey matter and blood vessels.

Importantly, the SVCA method needs to be validated for each pathological or experimental conditions and for each radiotracer. It was initially developed for [^{11}C]-

PK11195 and it has been recently validated for second-generations radiotracers, including [^{18}F]-DPA-714 (García-Lorenzo *et al.*, 2018); however, no study using a TSPO radiotracers has assessed SVCA use during an acute inflammatory challenge.

Prior studies using TSPO radiotracers and gold standard invasive input functions, have assessed the ability of TSPO PET to detect the neuroinflammatory response to an LPS challenge in mice, nonhuman primates (Hannestad *et al.*, 2012; Hillmer *et al.*, 2017; Vignal *et al.*, 2018) and more recently in healthy human subjects: an initial PET study, using [^{11}C]-PBR28, was conducted on 8 healthy humans following an LPS challenge (1.0 ng/kg). The [^{11}C]-PBR28 binding was calculated using a two-tissue compartmental model (2TCM) to estimate the volume of distribution (V_T). A mean increase across brain regions of 46% of [^{11}C]-PBR28 V_T was reported following LPS injection (Sandiego *et al.*, 2015). A follow up study on 10 additional subjects confirmed an increased widespread TSPO availability 3-5 hours post LPS challenge, indicating microglial proinflammatory activation or proliferation induced by acute peripheral inflammation (Woodcock *et al.*, 2021). In this experiment, participants underwent pre and post LPS scans on the same day. Another study assessed TSPO density in humans 5 hours after LPS administration (2.0 ng/kg) using [^{18}F]-DPA-714. A 53% increase in the whole brain Binding Potential BP_{ND} was reported (Peters van Ton *et al.*, 2021). It should be noted that in both studies, a more pronounced effect of inflammation was observed in the cortical regions compared to subcortical areas.

The primary aim of this study was to test whether the SVCA method applied to [^{18}F]-DPA-714 is a sensitive tool that enables the *in vivo* assessment of neuroinflammation induced by LPS, without the need for the AIF for TSPO PET quantification. The SVCA

method was tested against a smaller dataset from a subgroup of volunteers (N=5), based on full AIF quantification.

The exploratory aim was to test whether this experimental paradigm of integrating the non-invasive measurement of the TSPO PET signal with an LPS endotoxin challenge could be used to assess the effect of a short course of a mild anti-inflammatory treatment (i.e. minocycline). Another exploratory aim was to investigate the effect of LPS on the tracer distribution within the blood compartment and on its metabolism rate.

7.2 Methods

7.2.1 Study participants

Two cohorts were studied using [^{18}F]-DPA-714 PET in different phases of my project.

The first cohort comprised 14 male subjects (mean age: 24.3 ± 4.9 (std) years, mean BMI: 24.3 ± 2.4 (std) kg/m^2) and corresponded to the cohort (N=15) previously described in the behavioural analysis (Figure 3.3). These subjects (from cohort 1) received pre-treatment with either minocycline or placebo, as previously described (see Chapter 3). One subject had to be excluded following a failure to complete the second PET scan, this subject was in the minocycline group. Thus, both the minocycline and the placebo arms included in the PET study consisted of 7 subjects. The inclusion criteria are listed in Chapter 3.

The second cohort consisted of a separate subgroup of male subjects (N=5, mean age: 24.36 ± 4.9 (std) years), mean BMI: 25.6 ± 2.3 (std) kg/m^2) who underwent the same

experimental sessions, but with additional arterial blood sampling during the PET scan (Figure 3.3). Additional inclusion criteria were a negative Allen test on both hands, to ensure adequate perfusion to the hands, and clotting parameters (INR, APTT, APTT ratio, prothrombin time and fibrinogen) within normal ranges. For this cohort, 16 subjects were screened; 10 met the eligibility criteria; 5 completed the study, by taking part in both experimental sessions.

All participants were genotyped for the rs6971 SNP. High and mixed affinity binders (HABs/MABs) were included in the study, whereas low affinity binders (LABs) were excluded as they have a substantially lower affinity for second generation radiotracers (see Chapter 2 for details). When possible, a balanced of HAB vs. MAB ratio was prioritize during recruiting. The first cohort was made up of 6 HABs and 8 MABs, the second, of 3 MABs and 2 HABs.

7.2.2 Study design and procedure

Nineteen participants (N=14 from 1st cohort and N=5 from 2nd cohort) completed the PET imaging during both sessions, 3½ hours after receiving the LPS or saline with the TSPO-binding radiotracer [^{18}F]-DPA-714. Sessions were separated by a minimum of 1 week (mean: 3.7±3.3 (±std) weeks).

Five participants (from the 1st cohort) completed identical experimental PET imaging sessions with additional arterial blood measurements. An arterial cannula was inserted by an experienced senior intensive care medicine consultant before the LPS or saline administration, approximately 4 hours prior to the PET scan, and remained in situ until

the end of the PET scan. This was used to collect continuous and discrete blood samples for estimation of the metabolite corrected input function.

None of the 2nd cohort subjects received minocycline/placebo pre-treatment.

The second phase of the study to implement the new protocol was reviewed and approved by the London Queen Square Research Ethics Committee (REF 17/LO/0936, amendment number: BSMS 17 003).

7.2.3 Radioligand synthesis

[^{18}F]-DPA-714 synthesis took place in Centre for Radiopharmaceutical Chemistry, University College London, UK, in accordance with current Good Manufacturing Practice (cGMP) standards as defined and enforced by the Medicine and Healthcare Products Regulatory Agency (MHRA). Quality Control analysis of [^{18}F]-DPA-714 was performed according to European Pharmacopoeia standards. [^{18}F]-DPA-714 was synthesized as described in details by Vicente-Rodríguez *et al.* (Vicente-Rodríguez *et al.*, 2021).

7.2.4 PET protocol

[^{18}F]-DPA-714 was administered as a quick intravenous bolus, followed by a flushing with saline solution (10 mL) (total injection time <10 seconds). Mean injected activity was 155±22.3 (std) MBq.

All PET scans were acquired for 60 min on a Siemens Biograph-64 PET-CT scanner. The iterative reconstruction method was applied in the raw data reconstruction process (this step was carried out by a radiographer using the PET scanner reconstruction software).

Dynamic data were binned into 66 frames (durations: 8 x 15 s, 58 x 60 s) (matrix 256 x 256).

7.2.5 Images pre-processing

DICOM format data were converted into 3D NIfTI (.nii) data, using MRIcron. The image origin was set on a PET mean image and applied to each frame. Dynamic PET data were corrected for motion by frame-to-frame image realignment, using Statistical Parametric Mapping-12 (SPM12). In the realignment process, 7-mm kernel smoothing and 7^{th} degree B-Spline interpolation were used. A remarkable movement was observed in the first 4 frames (corresponding to the first minute of the scan), which was likely due to the low signal present in the images and probable movement of the head at the beginning of the scan. Since this issue affected the quality of the co-registration across sessions, the first 4 frames were initially excluded from the realignment process. They were then moved by applying the transformation matrix obtained by the realignment of the next (5^{th}) frame. A visual inspection for quality control was made on each participant by checking the co-registration of a mean PET image between the two sessions. Realigned images of both sessions were then coregistered to the subject's T-1 weighted structural MRI image. Coregistered 4D data were rebinned into 23 frames (durations: 8 x 15 s, 3 x 1 min, 5 x 2 min, 5 x 5 min and 2 x 10 min), and the radioactivity unit was converted from Bq to kBq. Figure 7.1 shows a diagram of images pre-processing.

7.2.6 ROIs definition

Regions Of Interest (ROIs) definition and relative Time Activity Curves (TACs) extraction were performed using MIAKAT^{TM}, a PET data analysis toolbox implemented

in Matlab R2019b, that incorporates functions from SPM and FSL (FMRIB, University of Oxford) (Gunn, Coello and Searle, 2016). To define the ROI in the subject's space, in order to avoid warping the PET data, the MRI anatomical image was first rigidly registered to the template MRI (brain MRI in MNI space). The MNI template is subsequently nonlinearly registered to the subject's MRI. The deformation field is applied to the atlas, the Clinical Imaging Center neuroanatomical atlas (Tziortzi *et al.*, 2011), for ROIs definition in individual (pseudo MNI) space (brain atlas warped to the brain MRI in MNI space).

The key regions of interest were:

- total brain, as the widespread effect of LPS has previously been reported;
- cortical regions, including frontal, parietal, temporal and occipital cortex, and subcortical regions (basal ganglia, thalamus, amygdala, cerebellum and brainstem) since previous studies have shown a more pronounced effect of LPS on cortical regions (measurements of single ROIs were averaged and presented as cortical and subcortical regions);
- total Grey and White matter (GM/WM) were chosen because a differential effect of LPS on grey versus white matter was observed in my DW-MRS study and the effect on LPS specifically on white matter has not been reported in previous studies;
- the thalamus was also included for comparison with the DW-MRS ADC(tCho) results reported in the previous chapter.

To assess the relationship between the two quantification methods (SVCA approach and full kinetic modelling with an AIF) twelve ROIs were included: total brain, GM, WM,

occipital, temporal, parietal, frontal and insular cortex, amygdala, hippocampus, putamen and cerebellum.

Standardized Uptake Value (SUV) quantification was performed by normalizing the average amount of radioactivity measured in a ROI in the last 20 min of the scan to the total injected activity and subject's body weight.

7.2.7 Supervised clustering algorithm

After assessing tracer uptake and signal specificity by means of semi-quantitative analysis, the SVCA was implemented as described by Schubert et al (J. Schubert *et al.*, 2021) to estimate the LPS effect on TSPO binding.

The SVCA-based approach for defining a reference region requires a set of kinetic classes, which correspond to WM, low binding GM (cortical), high binding GM (thalamus) and blood vessels. I used a set of kinetic classes from an historical dataset of 23 heathy volunteers. The top-right panel in Figure 7.1 shows the set of kinetic classes that was made available from another group. To compute these kinetic classes, each 4D dynamic PET image was normalized by subtracting the mean of all brain voxel and dividing by the standard deviation in each frame. The median TACs of each class across the volunteers form the kinetic classes.

For each subject a set of ROI binary masks was defined from the MRI anatomical image.

The ROI binary masks for each subject were: total brain, total GM and cortical and cerebellar GM. The SPM segmentation function was applied to the MRI anatomical image in MNI space, to obtain a tissue probability map for GM, WM and CSF. The total brain mask was defined by merging the three masks.

A total GM mask was also defined using voxels >0.9 in the GM probability map to minimize signal contamination from other tissues. The cortical and cerebellar grey matter mask was defined using the brain atlas (which had been warped in subject's space as described): left and right cortex and cerebellum were masked over the total GM to exclude non-grey matter voxels. This mask represents the 3D matrix that specifies prospective voxels that will be used to identify the pseudo-reference region. Figure 7.1 shows a schematic version of the segmentation process.

The 4D dynamic PET data of each subject were normalized in the same way described for generating the kinetic classes.

The SVCA-derived pseudo-reference region was extracted with an open-source code implemented in Matlab R2019b (https://github.com/molecular-neuroimaging/svca). The outcome of the SVCA consisted of a 3D binary matrix and respective TAC of voxels whose kinetics resembled low binding grey matter kinetics. A reference region was extracted from each scan (saline/LPS condition) for each subject.

The distribution volume ratio (DVR), was estimated in each ROI using the Logan graphical method, with a linear start time at 35 minutes (Logan *et al.*, 1996), which had previously been shown to be suitable for the SVCA approach using [^{18}F]-DPA-714 (García-Lorenzo *et al.*, 2018).

The modelling for estimating the parameters was carried out using in-house programs implemented in Matlab R2019b. The DVR (defined as BP_{ND} + 1), was used as the main outcome for the TSPO density.

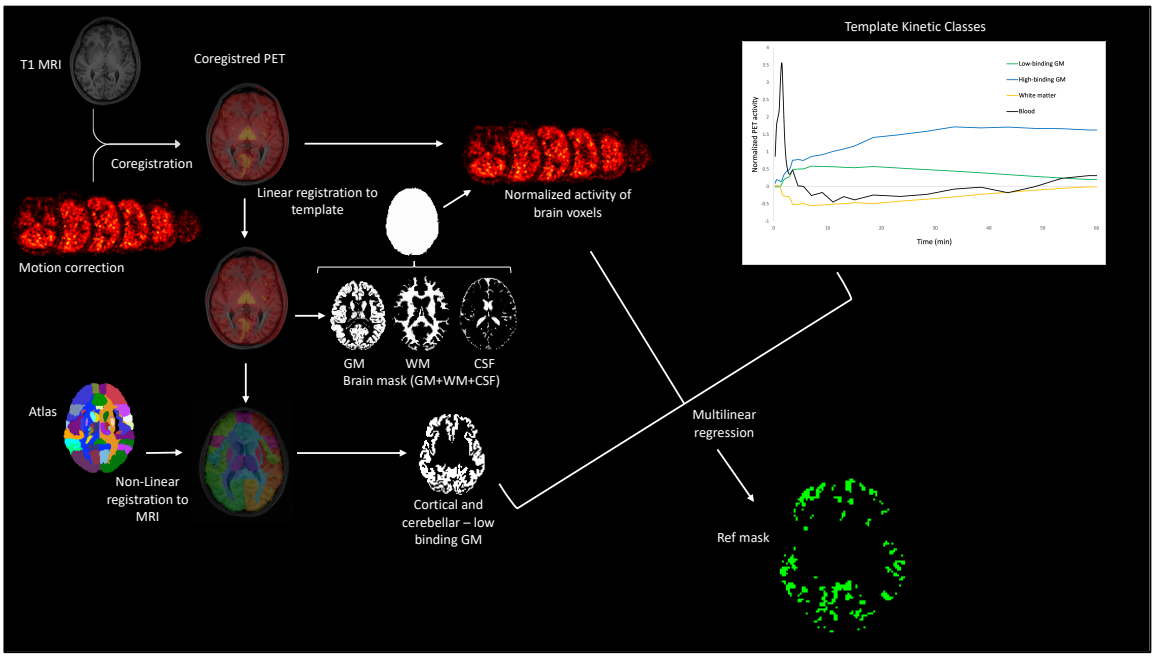

Figure 7.1 Pre-processing and reference mask extraction

7.2.8 Arterial blood data acquisition

Quantitative TSPO PET with arterial sampling was setup for the first time in my institute, in the context of this specific study. Routine clinical PET scanning and prior PET research studies conducted in our centre had not required full AIF quantification. The quantification of radioactivity in arterial blood is a complex procedure that requires the involvement of dedicated personnel and equipment for blood sampling, and the implementation of a radioactivity chemistry laboratory. In the following paragraphs, I describe the steps I followed to set up the laboratory and start blood radioactivity measurements. The necessary equipment for blood radioactivity quantification includes systems for continuous whole blood sampling and measurement, discrete blood and plasma measurement and a filtration system to separate the [^{18}F]-DPA-714 parent fraction from its metabolites. Designing an experimental protocol that implements these parts during the PET scan requires testing different radioactivity counters and cross-calibrating

continuous and discrete sampling system. I initially aimed to measure the blood continuously for the first 10 to 12 minutes and to take at least 2 discrete blood samples (at 12 and 40 minutes after the start of the scan).

[^{18}F]-DPA-714 was only available during the experiment sessions. Consequently, the continuous and discrete measurement systems were tested using H_2O samples containing [^{18}F]-fluorodeoxyglucose ([^{18}F]-FDG), which was delivered in our centre every day for clinical use. [^{18}F]-FDG has the same radioisotope ([^{18}F]) that is present in [^{18}F]-DPA-714. Each system was calibrated against the PET dosimeter of the CISC hot laboratory, which is the detector also used to calibrate the PET scanner. The aim was to calculate the Calibration Factors (CF) that describe the relationship between the counting efficiency of the dosimeter (which is equal to the efficiency of the PET scanner, i.e. 100% efficiency) and those of the two (continuous and discrete) counters.

7.2.8.1 Continuous whole blood sampling system test

The whole blood radioactivity was measured using a continuous automatic blood sampling system (ABSS Allogg, Mariefred, Sweden). The Allogg system consists of a detector (a gamma counter) that continuously measures radioactivity (kBq/mL) and a peristaltic pump that creates a constant flow of blood (or radioactive sample) within a tube that pass through the detector. The system was first tested using radioactive samples made by diluting [^{18}F]-FDG in H_2O. The [^{18}F]-FDG was received in a vial or syringe from stock left over from clinical scanning the previous day and was diluted to reach a radioactivity concentration in the order of the expected arterial blood radioactivity range of values observed in the literature (Arlicot *et al.*, 2012).

In order to simulate the scanning protocol, the measurement lasted 60 min and the peristaltic pump that conveyed the blood to the detector was switched on and off at intervals that reflected a possible blood sampling protocol.

The peristaltic pump was switched off 15 minutes after the start of the measurement. It was switched back on at minutes 30' and 40'. The recording was set as 1 measurement (kBq/mL) per second. Before switching off the pump, the tube was washed with non-radioactive H_2O. Thus, the activity registered when the pump was off corresponded to the background radiation. The 1 hr test recoding is shown in Figure 7.2.

The ratio between the expected (decay-corrected) radioactivity and the recorded radioactivity (as an average of each single value when the pump was on) was 0.98.

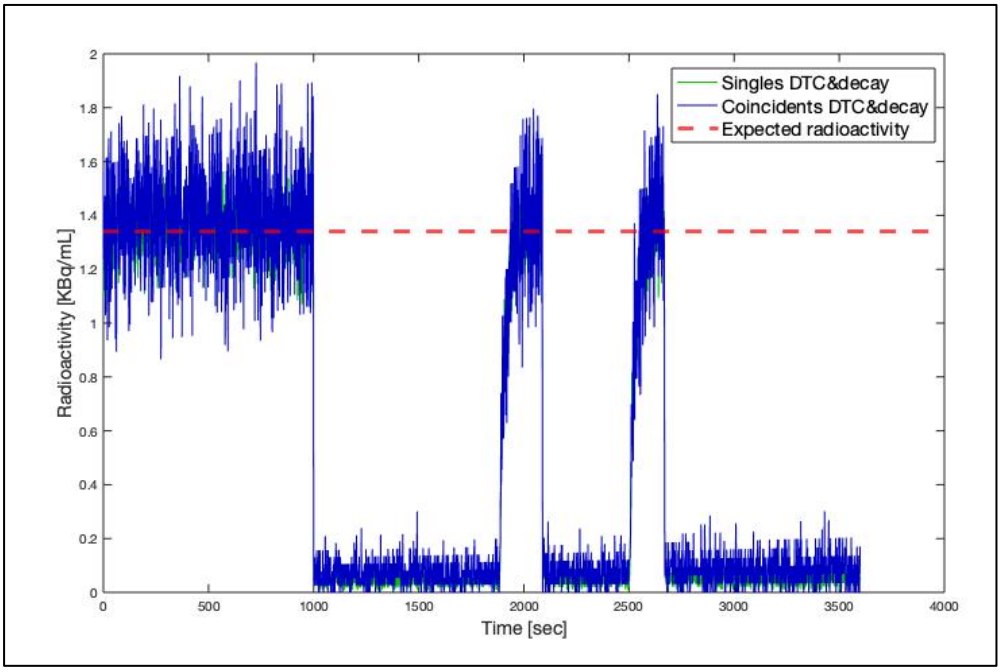

Figure 7.2 Allogg test and calibration

Allogg test simulating a blood sampling protocol with an initial 15 min continuous sampling followed by two discrete samples. Expected activity is based on the sample measured by the PET dosimeter.

7.2.8.2 Discrete blood samples radioactivity measurements

A gamma counter is required to measure radioactivity of small volumes of plasma and blood.

Considering the blood and plasma radioactivity concentration values and metabolism rate reported in the literature (Arlicot *et al.*, 2012), adjusted for the target injected activity (160 MBq) of this study, I expected the blood and plasma samples radioactivity to be in the order of 10^0 kBq/mL in the early phase of the scan and 10^{-1} kBq/mL toward the end of the scan. I prepared the serial dilutions until I reached an expected radioactivity concentration in the order of 10^{-2} kBq/mL to test the sensitivity of the counters.

I first assessed the suitability of a Hidex-Triathler multilabel tester, which was available in my institute. The Triathler requires a solid or liquid scintillator, which absorbs the gamma ray produced by the annihilation of a positron and an electron and emits light. I conducted different tests using a plastic scintillator or a liquid scintillator. 1 or 2 mL of H_2O samples containing known amounts of [^{18}F]-FDG were used. The Triathler was not able to distinguish between background count and samples count when using either a solid or liquid scintillator at various volumes and radioactivity concentrations similar to those found in plasma and blood samples. As a result, the Triathler was deemed not suitable for my intended purpose due to its lack of sensitivity in this range of radioactivity concentration.

Then a CAPRAC® -t well gamma counter (Capintec) was tested and calibrated against the PET dosimeter to assess its suitability for measuring the radioactivity in blood and plasma samples collected during the PET scan.

To prepare radioactive samples, an [^{18}F]-FDG sample was made up to a final volume of 1 mL solution using H_2O. This sample was denoted sample No.1 (Dilution 10^0 in Figure 7.3). The other samples were prepared using serial two-fold dilutions. After quantifying the radioactivity of a sample, half of its volume was collected and mixed in a vial containing the same volume of H_2O, so that each sample had the same volume, decreasing (by a factor of 2) concentration of [^{18}F]-FDG (radioactivity of each sample are shown in Figure 7.3). Each sample was measured for 60 seconds.

The CAPRAC-t reports radioactivity in count per seconds (cps). The radioactivity from the PET dosimeter was given in Bq.

The conversion between Bq and cps depends on the efficiency of the detector. 1 Bq would be equal to 1 cps if the counter is 100% efficient. Here the calibration factor (CF) was calculated for each sample (dilution) as the ratio between the expected (decay-corrected) radioactivity, given in Bq, and the measured value, in cps.

The radioactivity decay formula was applied to obtain the true expected radioactivity value by correcting for the time between the stock (reference) sample measurement and each diluted sample measurement:

$$N_t = N_0 / e^{-\lambda t}$$

Where N_0 = total amount of isotopes at t_0 (stock sample)

λ is the decay constant = ln 2 / half-life = 0.0063 min^{-1}

t: time between measurement of the stock sample and that of each of the other samples.

The CF was calculated as the mean of the CF of each sample.

CF = 0.53 ± 0.006 (mean ± SEM).

The CAPRAC-t was able to measure samples in the expected radioactivity range with a consistent CF across the different samples. The CF was used to correct measured blood and plasma samples collected during the PET experiment sessions.

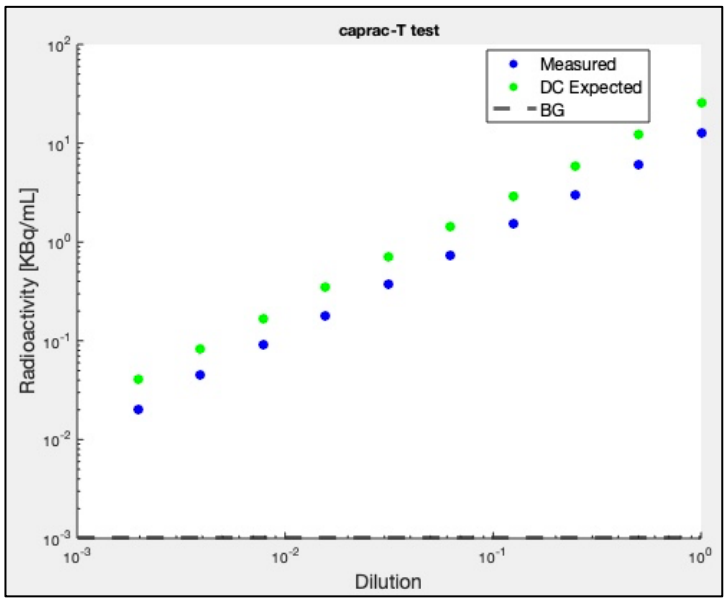

Figure 7.3 CAPRAC-t linearity test

The X axis represents the number of serial dilutions. R^2=0.99; p<0.001. Background (BG) was measured with 1 mL of H_2O.

As I observed a reliable counting efficiency using 1 mL of sample, I aimed to use the same volume for blood and plasma radioactivity quantification during the scan sessions. However, the blood volume collected during the experiment may vary. Since the counting efficiency of a radioactivity detector may be affected by the sample geometry (e.g. sample volume and vial shape), I conducted another linearity test to compare the CF of samples with the same amount of radioactivity in different volumes (1 mL and 0.5 mL).

The samples were made up using two-fold serial dilutions as described above. After half of the volume (0.5 mL) had been removed, each sample was measured again. Then 0.5 mL of H_2O were added so that the total radioactivity was the same, but the volume had doubled.

As shown in Figure 7.4, there was no significant difference between the CF of the 1 mL samples and 0.5 mL samples ($t_{(5)}$=-0.98, p=0.37). Therefore, the same CF was used to calculate the final radioactivity concentration even when only 0.5 mL of blood or plasma was available during the scan sessions.

During the scan sessions, at least 2 samples of arterial blood were collected. Each sample was collected with a syringe and put into EDTA vacutainer tubes. Each sample was taken to the radiochemistry lab, where 1 mL of blood was measured for 60 seconds in a CAPRAC-t glass tube. The blood was then pipetted back into the EDTA vacutainer and centrifuged at 4000 rpm for 5 minutes. 1 or 0.5 mL of plasma were collected and measured using the CAPRAC-t.

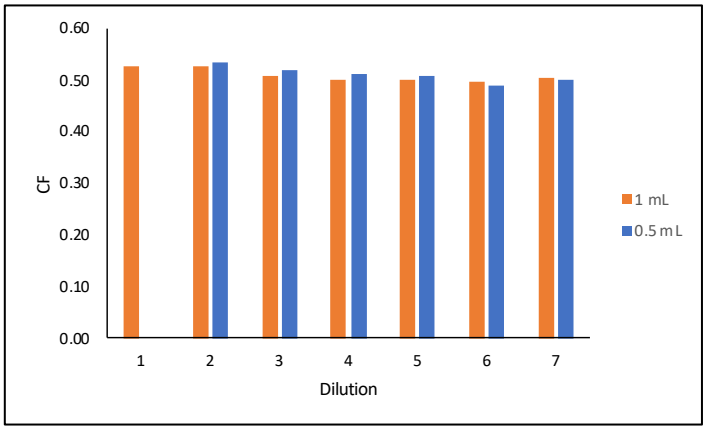

Figure 7.4 CAPRAC-t samples volume effect

Each dilution contains the same concentration of [^{18}F]-FDG but has a different volume (1mL and 0.5 mL).

7.2.8.3 Radiotracer metabolites analyses

As previously explained, radiotracers are broken down into radiometabolites. In order to account for the non-specific signal given by the radiometabolites, the parent fraction has to be measured.

In this experiment the parent fraction was determined using a solid phase extraction (SPE) (Peyronneau *et al.*, 2013). This technique takes advantage of the different polarity of [^{18}F]-DPA-714 and its radiometabolties, with [^{18}F]-DPA-714 being more lipophilic than the metabolites.

60-mg HLB Oasis SPE cartridges were conditioned with 1 mL of methanol (CH_3OH) and equilibrated with 5 ml of H_2O. 200µL of plasma was diluted to 400µL with 4% hydrochloric acid (HCl) H_2O. The resulting solution (F1) was measured using the CAPRAC-t and applied to the cartridge. The cartridge was then washed with 1 mL of H_2O (F2), 1mL of a H_2O solution with 35% of acetonitrile (CH_3CN) (F3), and finally with CH_3CN (F4). The radioactivity of each eluted fraction was measured. The parent fraction (the unchanged [^{18}F]-DPA-714) was calculated as the ratio between the F4 (unchanged [^{18}F]-DPA-714) and the F1 (total plasma).

7.2.9 Arterial input function and kinetic analysis

Kinetic analysis and blood data processing were performed using MIAKAT^{TM}.

The continuous and discrete blood data were integrated to form a whole blood curve for the full duration of the PET scan. A constant plasma-over-blood (POB) model was fitted to the ratio of plasma samples and matching blood samples to generate a continuous plasma activity curve. A single exponential plus a constant parent fraction model was

fitted to sparse parent fraction data and then applied to the total plasma curve to obtain a metabolite-corrected input function.

To account for time delay between the tracer passage in the brain and the radioactivity measurement, both continuous and discrete blood sampling times were shifted by 10s, based on the time that the blood takes to reach the detector (and the syringe for sampling) from the cannulation site.

The TSPO density was estimated in each ROI using the Two-Tissue Compartment Model (2TCM), with a metabolite-corrected arterial input function and a fixed blood volume fraction set at 5%. The 2TCM uses 4 rate constants (K_1, k_2, k_3 and k_4) to describe the radiotracer exchange rate between three compartments: blood, non-specific compartment and specific compartment (Figure 7.5). The V_T was the principal outcome.

$$V_T = \frac{K_1}{k_2} \times \left(1 + \frac{k_3}{k_4}\right)$$

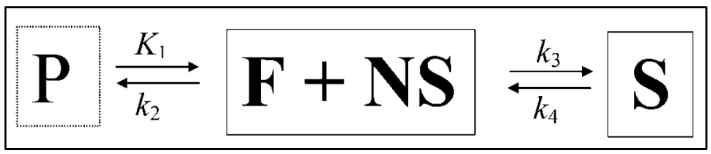

Figure 7.5 Two-tissue compartment model

The tracer enters into the brain parenchyma from the plasma (P) compartment. The tracer concentration within the brain is attributed to the non-displaceable (free (F) and non-specifically bound (NS) tracer) and specific (S) (tracer bound to its molecular target) compartments (Innis *et al.*, 2007).

7.2.10 Statistical analysis

Repeated measure ANOVAs with saline and LPS PET outcomes (SUV or DVR) as dependent variables were conducted in each ROI. To test the effect of the pre-treatment in the two groups, minocycline and placebo were included in the model as a between-subject factor. The p-values were adjusted with a false discovery rate for multiple comparison. Pearson's correlation was used to evaluate the correlation between the outcomes of the SVCA analysis and the results from the TSPO quantification with kinetic modelling. The correlation between the brain DVR and V_T across subjects, and correlation between regions within each subject were investigated. Percentage changes are calculated as (LPS-Saline)/Saline×100 and are reported as mean ± SEM. The normality of the data was assessed using the Shapiro-Wilk test. Sensitivity analyses were conducted excluding the outlying participant (discussed in Chapter 4).

7.3 Results

7.3.1 SUV

There was no significant difference in [^{18}F]-DPA-714 injected activity between the saline (150.93±4.44 (SEM) MBq) and LPS (152.17±5.83 (SEM) MBq) sessions (p=0.77).

HABs (N=8) displayed higher SUV_{40_60} compared to MABs (N=11) at baseline (saline condition) (multivariate ANOVA in all ROIs: $F_{(6,12}$=8.41, p<0.001). A significant difference between genotypes was observed for the whole brain ($F_{(1,18)}$=5.23, p=0.035),

subcortical regions ($F_{(1,18)}$=10.19, p=0.006), GM ($F_{(1,18)}$=5.23 p=0.032) and Thalamus ($F_{(1,18)}$=20.71, p<0.001) (Figure 7.6).

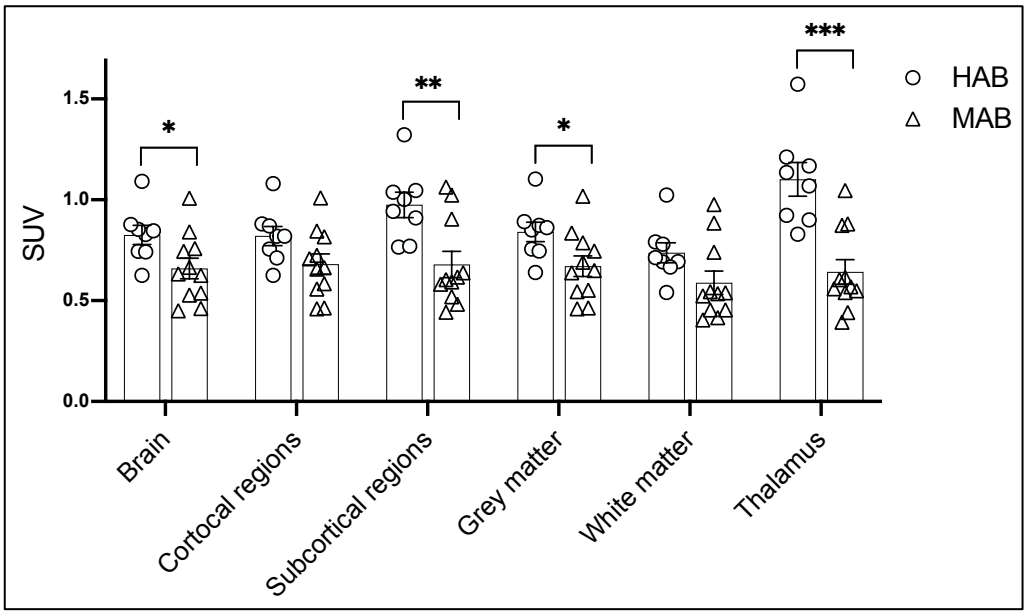

Figure 7.6 TSPO gene rs6971 polymorphism effect on baseline signal
Effect of rs6971 polymorphism on [^{18}F]-DPA-714 baseline SUV values. Means ± SEM are shown. * p<0.05, ** p<0.01, *** p<0.001.

7.3.2 SUVs were reduced by LPS

LPS administration resulted in a decrease in $SUVs_{40\_60}$ (brain: $F_{(1,18)}$=6.32, p=0.022; cortical regions: $F_{(1,18)}$=3.64, p=0.072; subcortical regions: $F_{(1,18)}$11.92, p=0.003; GM: $F_{(1,18)}$=5.51, p=0.031; WM: $F_{(1,18)}$=12.73, p=0.002; thalamus: $F_{(1,18)}$=10.11, p=0.005. The mean % LPS induced SUV decrease across regions was 16.80±2.83 for HABs and 9.56±0.64 for MABs (Figure 7.7). The mean brain TACs across subjects indicates lower TAC peak and tracer uptake after LPS administration, as illustrated in Figure 7.8.

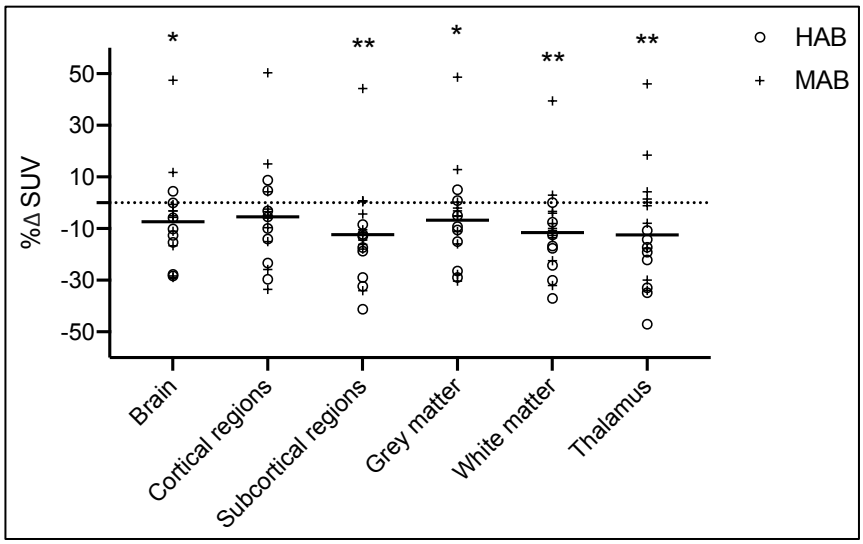

Figure 7.7 LPS effect on SUV

The data points indicate the SUV_{40_60} % changes post LPS. The bars indicate the means. * $p<0.05$, ** $p<0.01$, *** $p<0.001$.

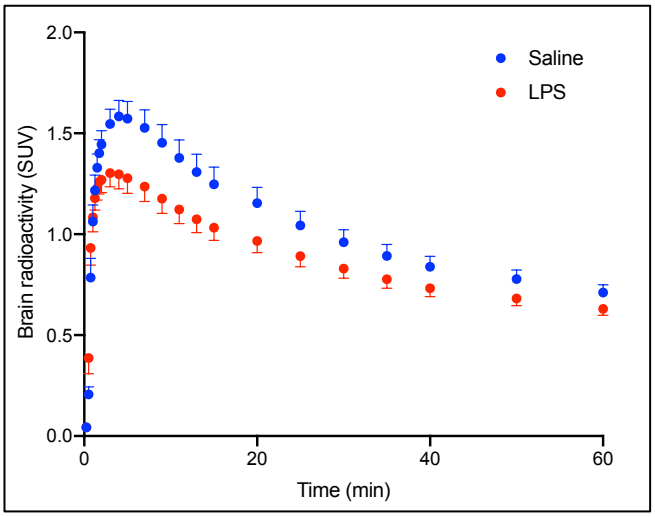

Figure 7.8 Brain TACs

Brain SUV Time Activity Curves show the mean across all subjects at each frame. The error bars are SEM. LPS induced a 7.03±4.05 (mean ± SEM) % reduction in whole brain SUV_{40_60} ($F_{(1,19)}$=6.32, p=0.022).

7.3.3 SVCA Results

The TAC of the SVCA-extracted pseudo-reference region showed higher peak and faster washout compared to the grey map (cortical and cerebellar GM) TAC (Figure 7.9). SUV analysis of the pseudo-reference region showed a lower SUV_{40_60} in the MABs compared to HABs after saline (independent sample t-test: $t_{(18)}$=-2.79, p=0.012). Mean SUV TACs are shown in Figure 7.10.

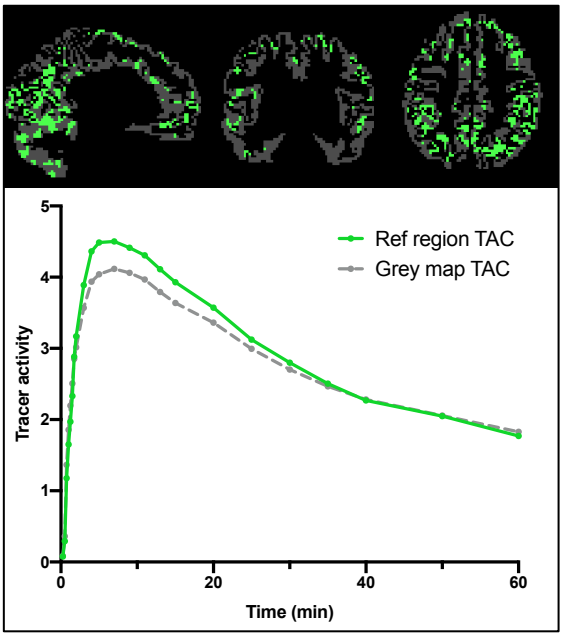

Figure 7.9 Example of SVCA-derived pseudo-reference region and relative TAC
Top panel shows an example of a reference region mask (green) overlapped to the total low binding GM mask (grey). Bottom panel shows an example of non-normalized (kBq/mL) TAC of the two masks.

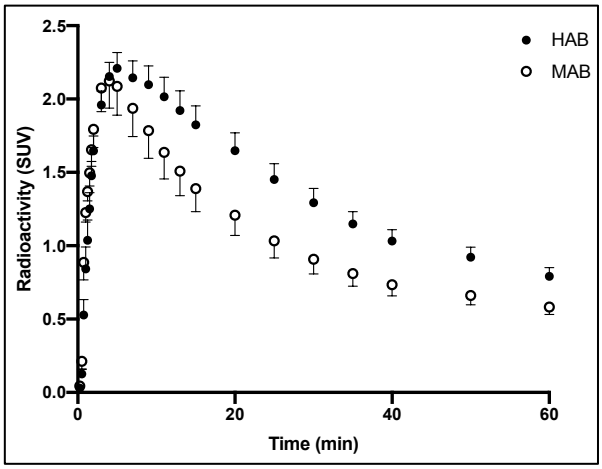

Figure 7.10 Comparison between HABs and MABs SVCA-derived pseudo reference region TAC after saline injection

HABs showed higher tracer uptake in the pseudo-reference region compared to MABs at baseline (higher SUV_{40_60}: $t_{(18)}$=-2.79, p=0.012), likely indicating the presence of specific signal contamination. Data points show mean at each frame ± SEM.

The effect of LPS was first assessed in the whole brain ROI. This showed that LPS induced a 3.78±1.65% DVR increase ($F_{(1,18)}$=9.46, p=0.007; Cohen's *d*=0.56) (Figure 7.11). To determine whether this effect was influenced by the outlying participant, this analysis was repeated after excluding him. The findings after excluding this participant showed a more pronounced effect: 4.58±1.65% DVR increase ($F_{(1,17)}$=26.37, p<0.001). To investigate this further I next investigated the effects in the grey and white matter separately, and in the cortical and subcortical subregions. In the GM, I observed a significant 4.18±0.94% DVR increase after LPS vs. saline ($F_{(1,18)}$=9.43, p=0.007) (DVR% increased to 5.07±1.80 after excluding the outlier, $F_{(1,17)}$=27.11, p<0.001). A significant 5.16±2.66% DVR increase was observed in the cortical regions ($F_{(1,18)}$=6.48, p=0.020)

(sensitivity analysis showed 6.41±1.62% DVR increase, $F_{(1,17)}$=21.05, p<0.001). The subcortical regions, total white matter and thalamus appeared not be affected by LPS administration (p>0.05) (Figure 7.12). There was no effect of treatment order (saline first vs. LPS first) on Brain DVR $F_{(1,17)}$=0.54, p=0.471).

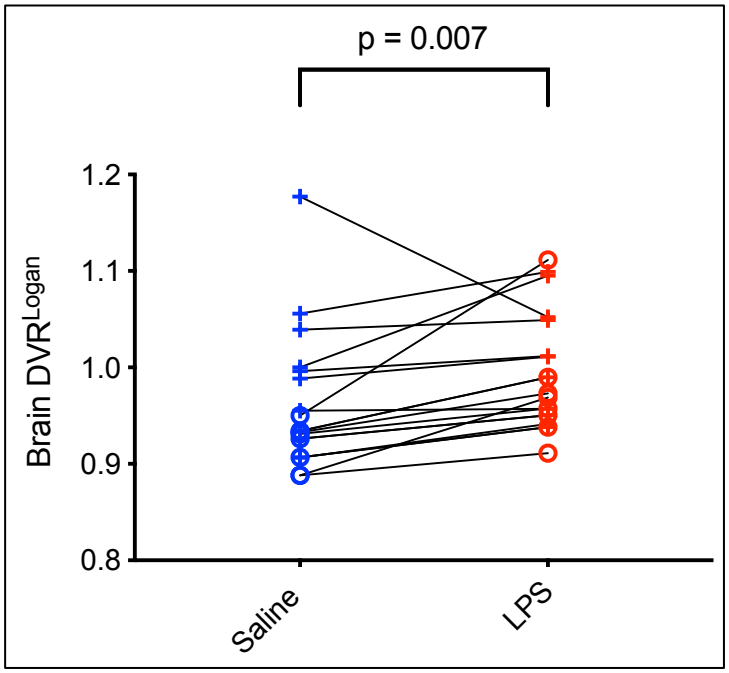

Figure 7.11 LPS effect on brain DVR Logan

Change in whole brain DVR. The shape of symbols indicates the genotype: circles for HABs and crosses for MABs.

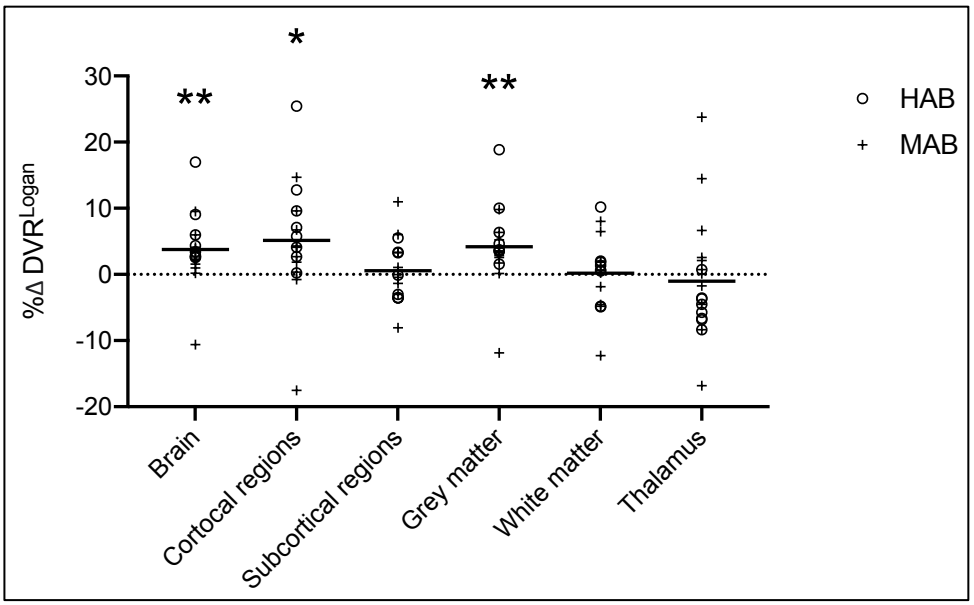

Figure 7.12 LPS effect on brain ROIs DVR Logan

LPS induced a significant DVR increase in the total brain, cortical regions and grey matter. Subcortical regions and total white matter were not affected by LPS administration. * $p<0.05$, ** $p<0.01$, *** $p<0.001$.

7.3.4 Kinetic analysis and blood data results

Results from compartmental analysis using metabolite-corrected AIF are presented in Figures 6.13-6.18.

In the first (saline condition) session of the first subject, for feasibility reasons, I collect and processed only 2 blood samples (at 12 and 40 min). The shape of the metabolite-corrected AIF, which did not reach the equilibrium phase, (Figure 7.13, top panel) and the results of kinetic analysis suggested that two time points are not sufficient for generating of a reliable AIF and for the kinetic modelling analysis. In particular, the 2TCM provided a k_4 parameter value that was noticeably outside the normal range (one order of magnitude lower than the expected range), yielding a V_T that might not represent

the true TSPO density. In the second (LPS condition) scan on the same subject I sought to collect 4 blood samples (at 12, 25, 40 and 50 min). Even though the blood samples were processed within ~2 minutes, some of them quickly coagulated within the syringes. This was not observed in the saline condition. This coagulating effect of LPS could be mediated by caspase-11 (Yang *et al.*, 2019). Given this very rapid effect of LPS, I modify the blood sampling protocol to move the blood from the syringe into an EDTA tube within less than 1 min from drawing the sample. During this session it was still possible to pipette 1 or 0.5 mL of 3 blood samples but not for the one collected at 25 min. It was still possible to separate the plasma in each sample.

Twelve minutes of continuous whole blood sampling followed by 4 discrete samples generated an input function with an equilibrium phase (Figure 7.13). However, given the paucity of blood data in the saline scan it was not possible to compare the AIF and the V_T between conditions.

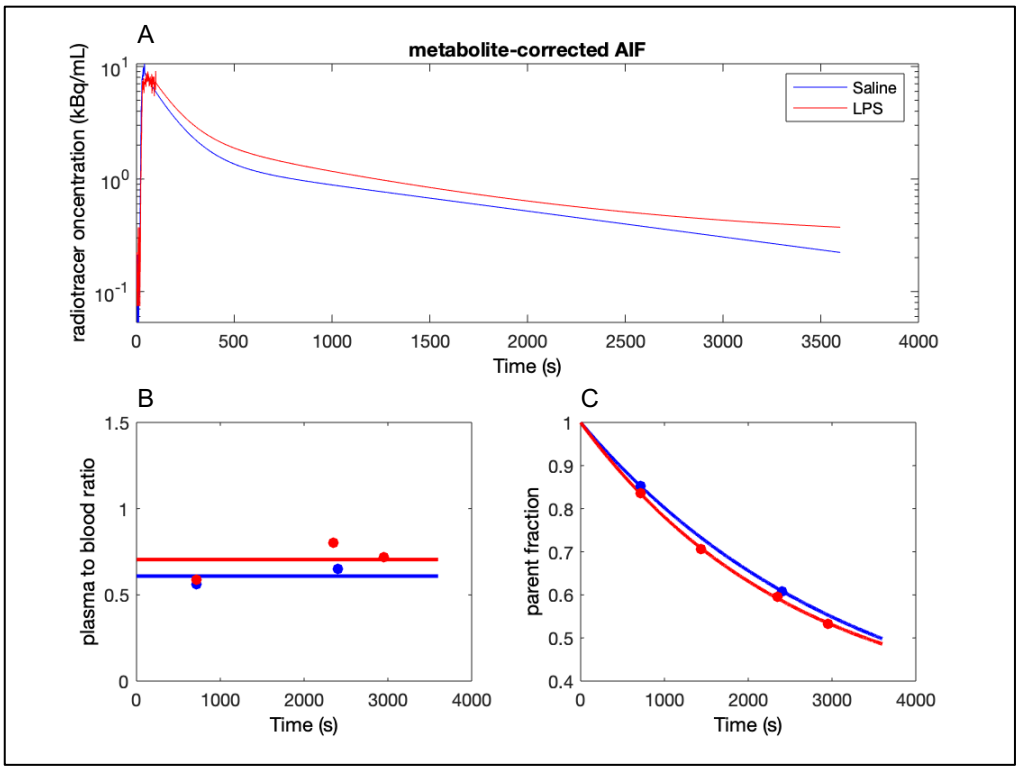

Figure 7.13 Blood data of Subject 1

(A) Metabolite-corrected AIF; (B) Plasma-Over-Blood (POB) fitted to a linear model; (C) parent fraction fitted with a single exponential plus a constant model.

The coagulating effect of LPS had more severe impact during the blood sampling of the second subject. On this occasion the blood coagulated inside the 1.5m (1mm diameter) tube that conveyed the blood from the cannulation site to the Allogg radioactivity detector and to the discrete blood sampling site. It was only possible to draw samples at 12 and 25 min, with substantial consequences on the AIF quality and modelling analysis (Figure 7.14). During the saline scan I collected discrete samples at 12, 25, 40 and 55 min.

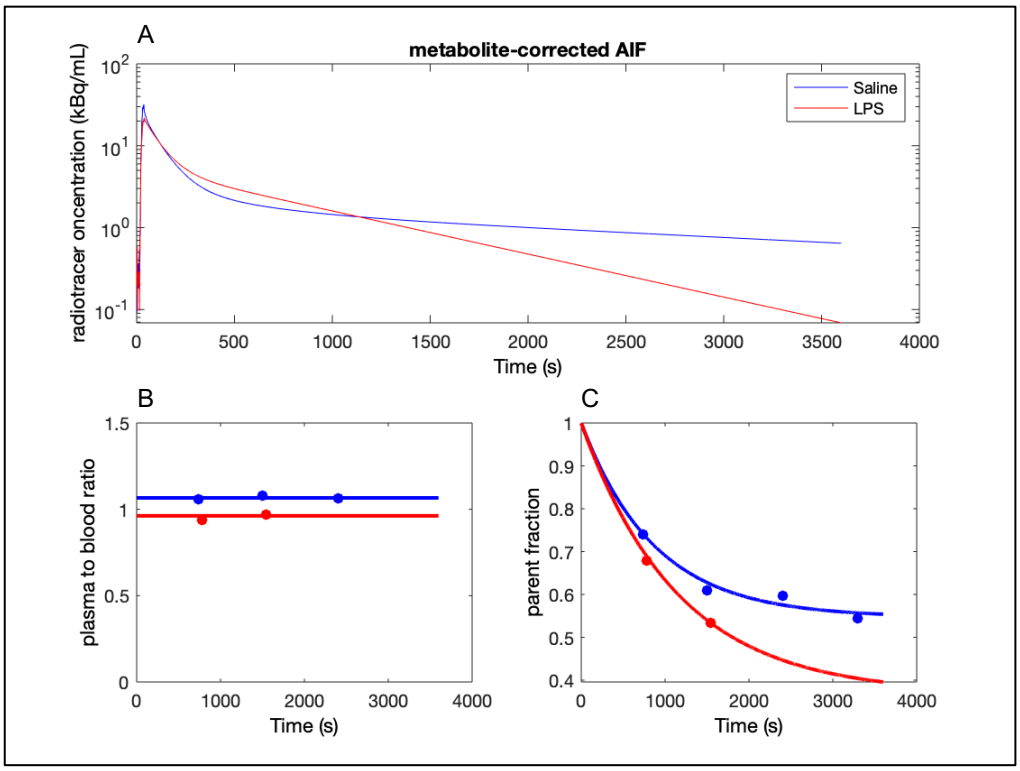

Figure 7.14 Blood data of Subject 2

(A) Metabolite-corrected AIF; (B) POB fitted to a linear model; (C) parent fraction fitted with a single exponential plus a constant model.

To improve the AIF fitting and obtain a more reliable V_T quantification in the LPS condition where only two early samples were present, I added a blood and plasma value at 40 min. The blood value at this time point was calculated by applying to the 25 min sample the decrease rate observed between 25 and 40 min in the saline condition; assuming that the decrease rate between 25 and 40 min was the same in the two conditions. Since the POB ratio was assumed to be constant throughout the scan, I applied the mean of the POB of the 12 and 25 min samples (Figure 7.14 B) to the blood value to obtain a plasma value at 40 min. The resulting AIF was used in the kinetic analysis to obtain the V_T (Figure 7.15).

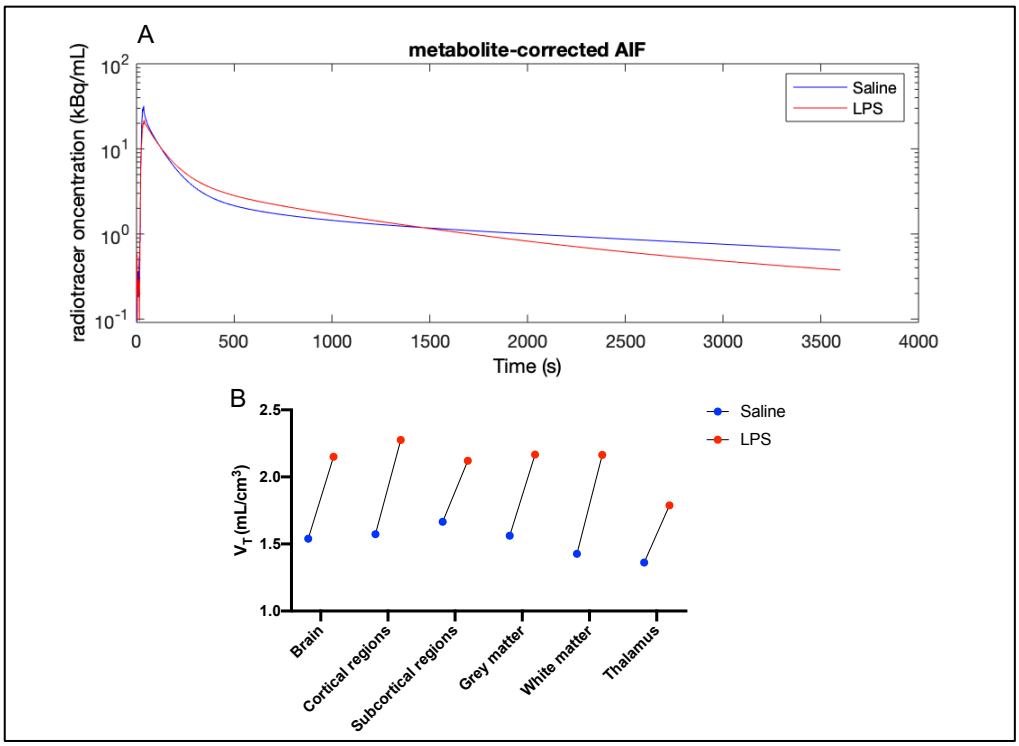

Figure 7.15 AIF and V_T change in Subject 2

(A) Metabolite-corrected AIF generated by adding a time point at 40 min in the LPS scan; (B) V_T change between conditions across ROIs.

During the next experiment sessions on the third subject, I collected discrete blood samples at ~12, ~25, ~40, ~50 and ~60 min (Figure 7.16). However, this was the subject previously described who did not show any physiological response to LPS.

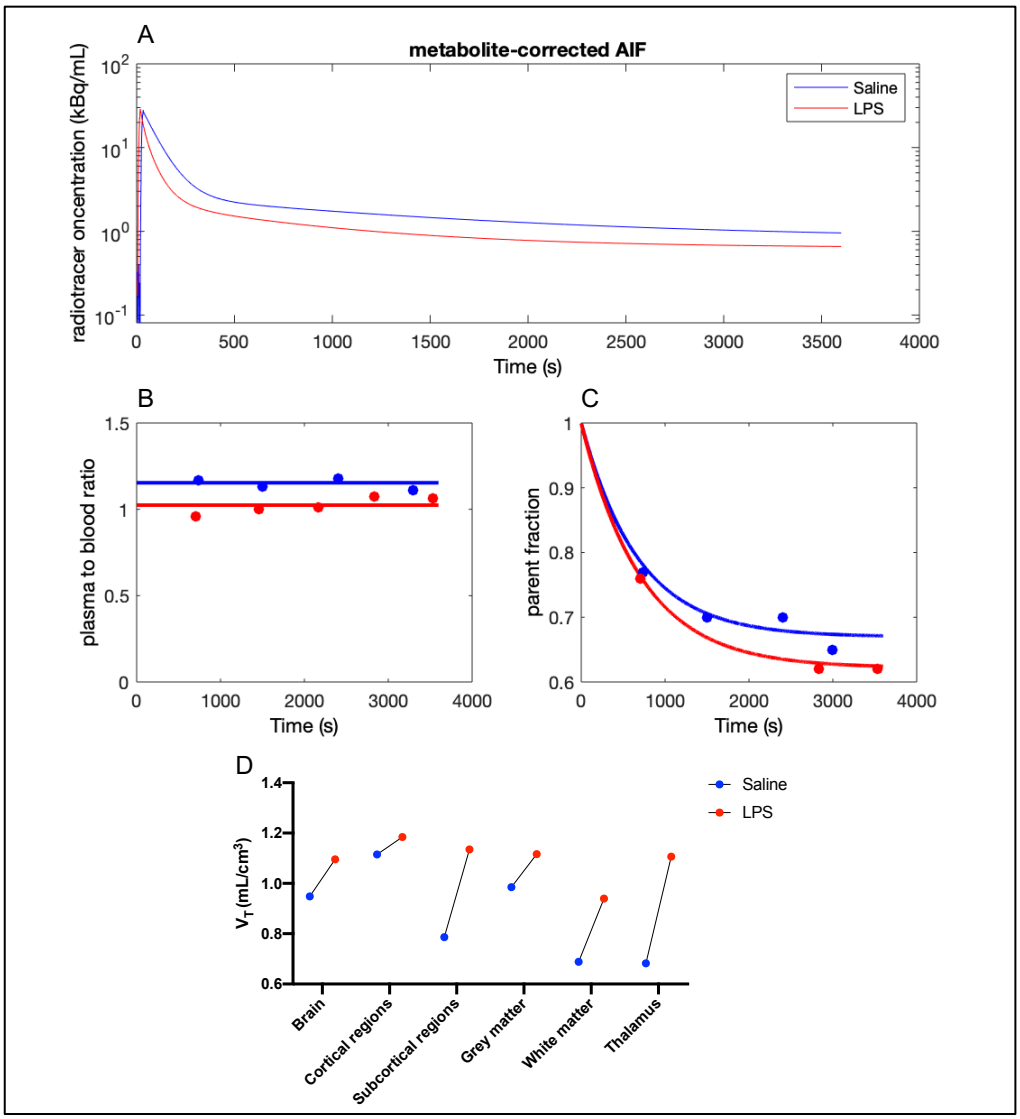

Figure 7.16 Blood data and V_T change in Subject 3

(A) Metabolite-corrected AIF; (B) POB; (C) parent fraction; (D) V_T change between conditions across ROIs.

For the last subject tested with full blood quantification, I processed 3 samples (~15, ~35 and ~50 min) in the saline scan and 4 samples (~12, ~30, ~45 and ~60 min) in the LPS condition (Figure 7.17).

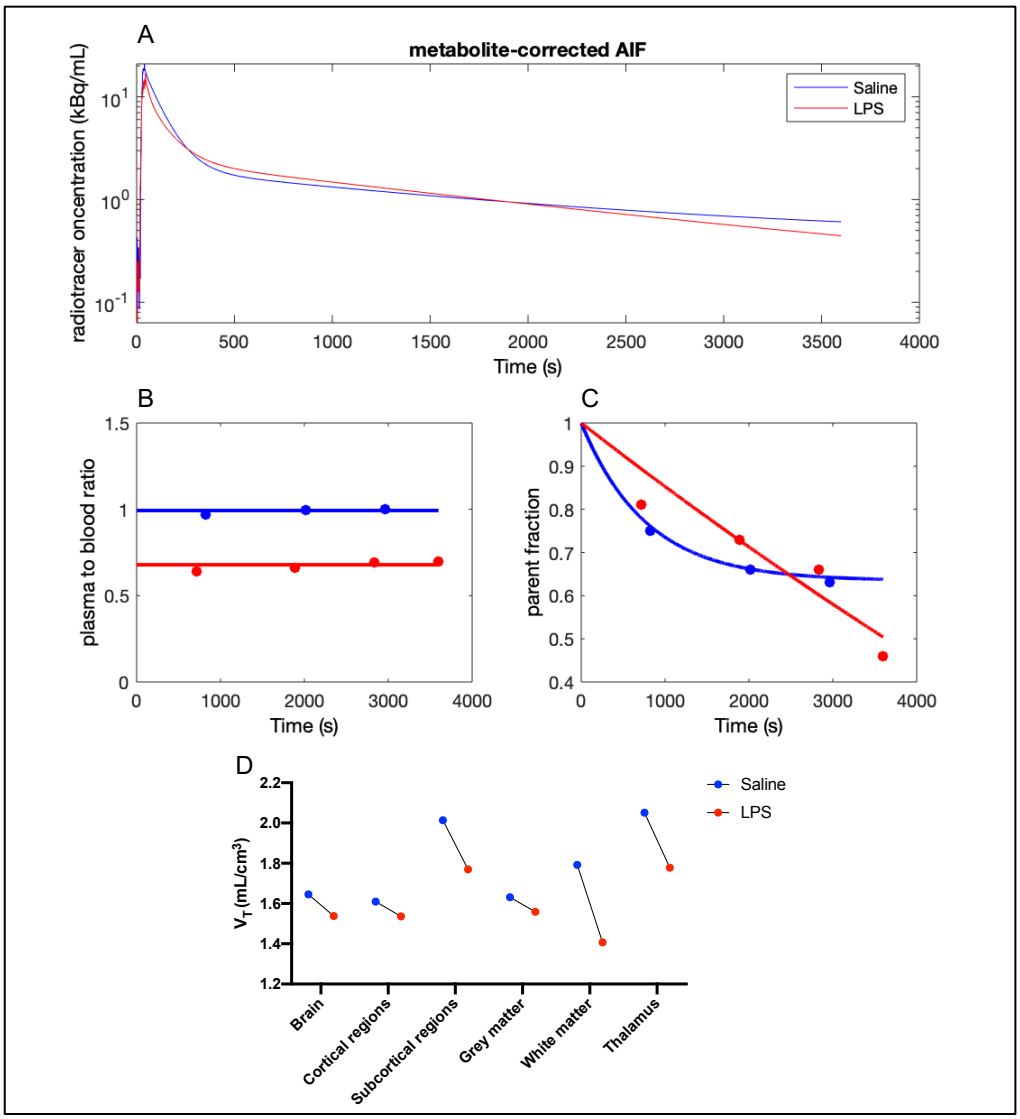

Figure 7.17 Blood data and V_T change in Subject 4

(A) Metabolite-corrected AIF; (B) POB; (C) parent fraction; (D) V_T change between conditions across ROIs.

Another subject was recruited and included in this cohort to be tested with full blood sampling. However, due to a fault in the peristaltic pump that prevented the use of the Allogg system, it was not possible to perform continuous blood radioactivity quantification and kinetic analysis. Discrete sampling throughout the scan duration was

performed on both sessions to assess the LPS effect on the radiotracer plasma to blood ratio and metabolism rate (data included in Figure 7.18 C).

Among participants with available continuous and discrete blood sampling (N=4), the mean LPS-induced % decrease in AIF Area Under the Curve (AUC) was 5.03±12.32% (the decrease was 14.92±10.42% excluding the subject in which the AIF was calculated with only two discrete blood samples). LPS was associated with a 15.70±7.15% reduction in the AIF peak. There were reductions of 11.88±7.67% and 3.97±4.11% in POB and parent fraction AUC respectively in the LPS condition compared to the saline one (Figure 7.18). A 10% reduction of the parent fraction at 50 min was also observed in the subject for which kinetic modelling was not performed. Blood data including all subjects are presented in Figure 7.18.

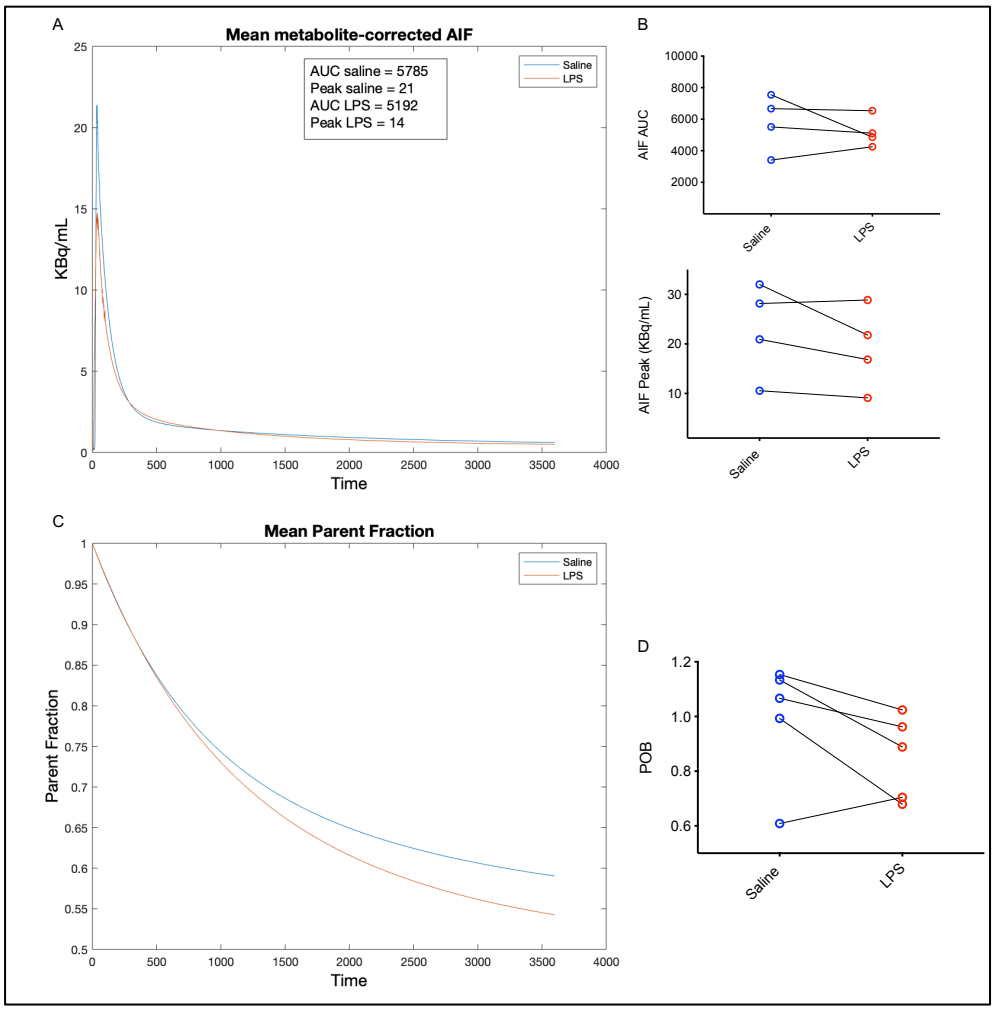

Figure 7.18 Mean AIF and parent fraction

(A) Mean metabolite-corrected plasma AIF across subjects; (B) AIF area under the curve (AUC) and peak changes; (C) Mean parent fraction across subjects; (D) POB changes (including the subject that was tested without continuous sampling), each value represents the mean between the POB ratio of all samples available for each scan.

7.3.5 Relationship between SVCA-DVR change and peripheral inflammation, mood deterioration and DW-MRS measurement change

Correlation analyses between change in brain SVCA-DVR and change in peripheral inflammatory markers (i.e. cytokines, body temperature, and differential blood counts),

mood scores and ADC(tCho) were conducted including all subjects of the first cohort that underwent TSPO PET (N=14). The changes in physiological measurements were calculated as the between sessions change from baseline to 3 hr: [(LPS_{3hr}-$LPS_{Baseline}$)-($Saline_{3hr}$-$Saline_{Baseline}$)]. The same was repeated for measurements at 6hr. The correlations with the total and negative POMS score were assessed using the peak of mood change (2hr) (as explained in Chapter 6). I did not find any significant correlation between the brain DVR increase and any physiological or psychological change. I observed a trend association between LPS-induced changes in the brain DVR and changes in the lymphocytes count at 3 hours (r=-0.518; p=0.058). Analyses on 12 subjects that underwent DW-MRS scan showed no significant correlation between ADC(tCho) increase in the thalamus and DVR changes. Correlations were examined between DW-MRS ADC(tCho) change in the thalamus and changes and in DVR in the thalamus, in the total brain as ROI and in the total GM.

7.3.6 Relationship between SVCA-DVR and 2TCM V_T

Correlation analyses were conducted including the datasets in which at least 3 discrete blood samples were available (N=7). There was no correlation between total brain V_T and total brain SVCA-DVR (Figure 7.19 A). Likewise, no correlations were observed for total GM and WM. However, by including 12 different ROIs, I observed a good correlation between the V_T and SVCA-DVR within datasets. Regional 2TCM V_T were highly correlated with regional SVCA-DVR in five imaging datasets (all $p<0.001$). R^2 values are shown in Figure 7.19 B.

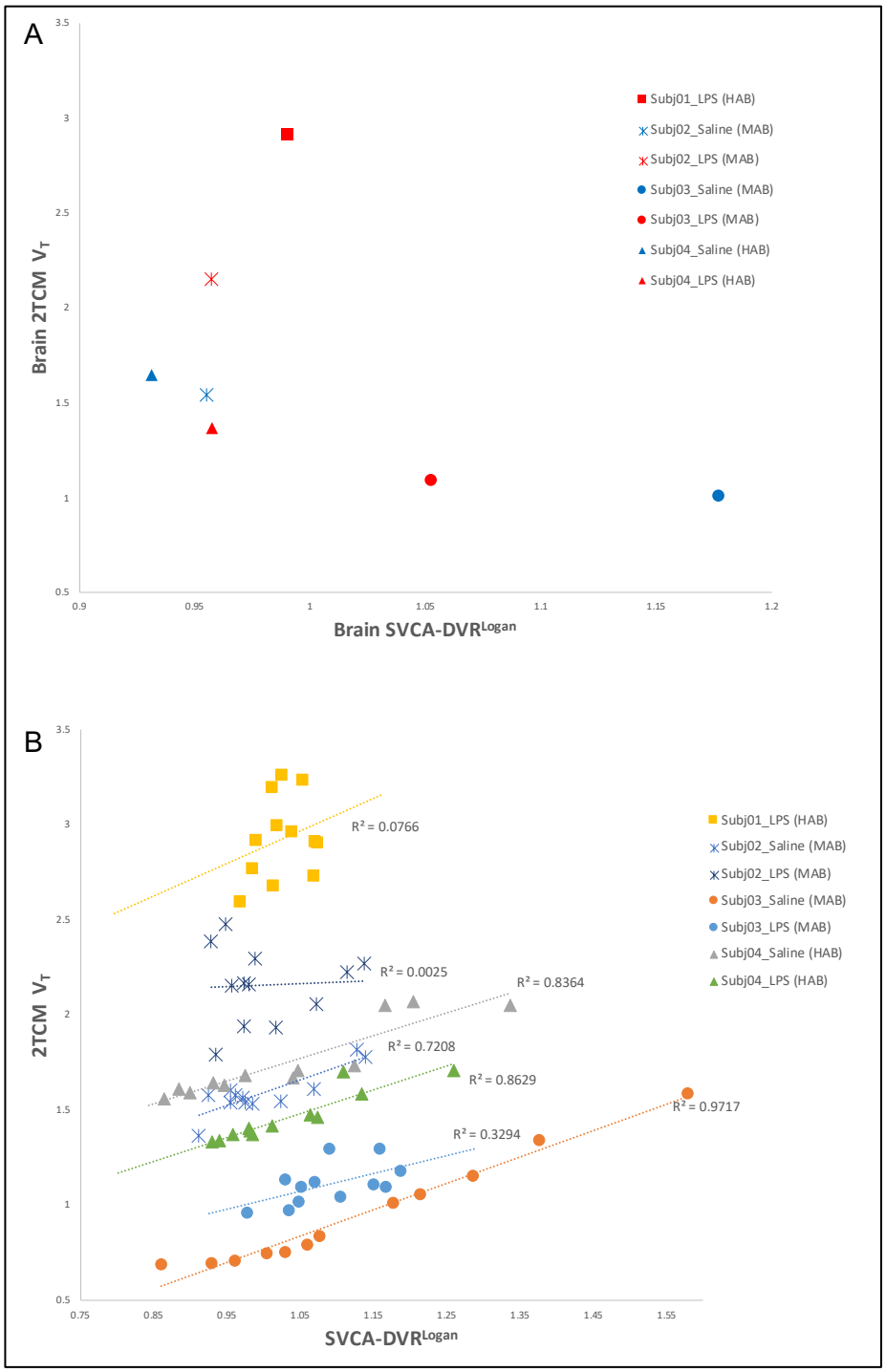

Figure 7.19 Correlation between 2TCM V_T and SVCA-DVR.

(A) The scatterplot shows the correlation between total brain VT and total brain SVCA-DVR. Each point represents a measurement from one study. Each symbol represents a different subject, colours represent the condition (blue for saline and red for LPS). (B)

Correlation between V_T and DVR was assessed within each dataset, considering 12 different ROIs.

7.3.7 Effect of minocycline

The baseline SUVs were not affected by minocycline pre-treatment, as shown by no significant group (Placebo/Minocycline) × ROIs interaction ($F_{(1,17)}$=1.19, p=0.29) and no significant difference between groups in every ROIs (all p>0.05).

To test the hypothesis that minocycline inhibits widespread LPS-induced microglial activation (indexed by TSPO expression), I conducted a group (Placebo/Minocycline) × condition (Saline/LPS) mixed rmANOVA (saline and LPS brain DVR were repeated dependent variables). This did not show significant interactions between condition (Saline/LPS) and group (Placebo/Minocycline) ($F_{(1,17)}$=1.19, p=0.29). Then, the DVR change was assessed between groups (Placebo/Minocycline) within individual regions. There was not significant interaction within each brain area, cortical regions: $F_{(1,17)}$=0.03, p=0.95; subcortical regions: $F_{(1,17)}$=0.10, p=0.92; grey matter: $F_{(1,17)}$=0.01, p=0.97; white matter; $F_{(1,17)}$=1.71, p=0.20; thalamus: $F_{(1,17)}$=0.41, p=0.53.

7.4 Discussion

I presented [^{18}F]-DPA-714 PET imaging results from 19 subjects tested after LPS and saline treatment, to investigate the effect of inflammation on brain TSPO density.

I observed a 4.18% and 5.16% increase of [^{18}F]-DPA-714 TSPO binding after LPS administration in the total GM and cortical regions respectively, measured using a SVCA approach. In a small subgroup that underwent PET imaging scans with full arterial blood sampling, I did not observe any significant correlation between kinetic modelling and SVCA analysis outcomes. Analyses of the [^{18}F]-DPA-714 concentration in the blood compartment suggested an LPS effect on radiotracer distribution and metabolism.

SUVs were initially studied to assess radiotracer uptake in the brain. HABs showed higher SUV compared to MABs in each ROI. The thalamus was the region that displayed the highest [^{18}F]-DPA-714 uptake. These observations confirmed the specificity of the [^{18}F]-DPA-714 signal to TSPO and appear consistent with data indicating increased SUV in HAB subjects compared to MAB and the highest TSPO density in the thalamus (Lavisse *et al.*, 2015).

The SUVs were significantly reduced after LPS in all ROIs, in line with previous observations from animal and human studies with smaller sample sizes, which reported a decreasing trend in SUVs post-LPS (Yoder *et al.*, 2015; Woodcock *et al.*, 2020). This effect may be due to a change in the biodistribution of [^{18}F]-DPA-714 during systemic inflammation. The effect of LPS on TSPO peripheral expression in humans is not known. However, many tissues that express TSPO constitutively might overexpress it under an acute inflammatory condition. Increased widespread peripheral specific binding might cause a decreased tracer uptake into the brain, as a fraction of the injected radiotracer may be bound to TSPO in peripheral tissues. Interestingly, brain SUV TACs showed lower peaks in the LPS condition. Since the TAC peak almost exclusively represents unbound tracer in the blood (non-specific signal), this observation suggests that systemic

inflammation may cause a rapid decrease in the free tracer delivered to the brain. Putative causes of this phenomenon could be specific binding to endothelium cells and pulmonary first-pass specific uptake. The lungs are characterized by a large surface area and receive the entire cardiac output before the intravenously injected tracer is distributed into the body. In humans, TSPO is highly expressed in the lungs (Mak and Barnes, 1990). Thus, an increased TSPO expression might affect the amount of radiotracer left in the blood after the first pulmonary passage and, therefore, be delivered to the brain. These data corroborate the hypothesis that semi-quantitative analyses (SUV) do not provide reliable measurements of the LPS effect on brain TSPO density, as they do not account for differences in tracer delivery to the brain.

In this study I adopted a SVCA approach to define a pseudo-reference region for the estimation of TSPO density. The primary finding of this analysis was a small but significant increase of brain DVR following LPS administration. The first quality control step after the definition of the reference region consisted of visually inspecting of each reference region mask and its TAC. Each reference region extracted by the SVCA was made up of sparse voxels within the low binding (cerebellar and cortical GM) mask. No large clusters of adjacent voxels were observed. The kinetics of the reference regions were characterized by a sharp peak and a fast washout when compared to the cerebellar and cortical GM. The cerebellar and cortical GM (SVCA Grey map) signal is likely to be contaminated by the surrounding WM signal, which is characterized by a slow kinetics (low peak), and by a high-binding GM. This results in a kinetic profile with low peak and high tail. On the other hand, the SVCA reference region only includes voxels that closely correspond to low-binding GM, resulting in a kinetic profile that is characteristic of healthy grey matter and, therefore, is considered suitable as a pseudo-reference region.

Hence, the shapes of the pseudo-reference region were characterized by low amount of specific binding, as shown by the fast washout and low tail (Figure 7.9). This confirms that the cortical and cerebellar GM can be used as a prospective mask to define the pseudo-reference region. The total brain GM can also be used to define a SVCA-derive reference region with low specific binding. However, including subcortical regions with high TSPO expression, such as the thalamus, might results in a pseudo-reference region with a TAC more similar to high binding grey matter and, therefore not suitable as reference region. Likewise, the previous study that validated the SVCA approach for [^{18}F]-DPA-714 against the gold standard compartmental model with full AIF also used the cortical and cerebellar GM to identify low-binding voxels rather than the total brain GM (García-Lorenzo *et al.*, 2018). Of note, the scope of extracting a pseudo-reference region is to correct for non-specific binding, which is assumed to be the same in every brain region.

The significant DVR increase after LPS suggests that the SVCA could be a viable non-invasive technique for the estimation of putative microglial activation during systemic inflammation. These results add on and expand results from another study that showed a robust increase in brain TSPO density after LPS injection (1 ng/kg) in healthy subjects measured using the gold standard 2TCM with full AIF (Sandiego *et al.*, 2015). However, there is a substantial discrepancy between the effects of LPS on the brain TSPO estimated with the two methods. Here, I observed a 4.58% increase in brain DVR, mostly driven by the cortical regions and total GM, while Sandiego and colleagues reported a widespread 30-60% TSPO density (V_T) increase. Nevertheless, the more pronounced effect in cortical regions versus subcortical region is consistent between the two studies. A more robust effect of LPS on cortical versus subcortical regions was also shown by another study, in

which healthy subjects received a higher LPS dose (2 ng/kg) (Peters van Ton *et al.*, 2021). It is worth considering the potential factors that led to this difference in TSPO binding increase between studies. The results of the SVCA analysis could be affected by intrinsic limitations of a pseudo-reference region approach in a condition of widespread inflammation. Making use of a reference region enables correcting for non-specific binding when the region is completely devoid of specific binding. Such a reference region does not exist in the human brain for TSPO. Thus, SVCA-derived pseudo-reference region contains to some extent specific signal. The presence of specific signal contamination was confirmed by the higher [^{18}F]-DPA-714 uptake in the pseudo-reference region in HABs versus MABs, whilst the signal in a true reference region should not be affected by the genotype. Of note, a genotype effect within the SVCA-derived pseudo-reference region, reflecting the presence of specific signal, was also reported for [^{11}C]-PBR28 (Zanotti-Fregonara *et al.*, 2019). A specific signal in the reference region might have resulted in an underestimation of the TSPO expression in the target ROIs. In addition, since LPS is thought to cause a widespread increase in the brain, it might have also affected the amount of specific signal, which cannot be estimated, in the pseudo-reference region. Interestingly, however, a comparison of the pseudo-reference regions masks size in the saline and the LPS scans showed a trend ($p=0.076$) (data not shown) towards a smaller size in the LPS condition, suggesting that the algorithm was at least in part sensitive to the effect of inflammation, and identified fewer voxels with minimal specific binding in the LPS condition. Considering all of these aspects then, it is likely that, due to specific signal contamination in the pseudo-reference region, the DVR increase could only be observed in regions that more strongly respond to LPS, such as the cortical regions and total GM, whereas this technique may lack sensitivity for regions that

overexpress TSPO more weakly after LPS. Moreover, another potential factor that may result in different findings when TSPO density is estimated using a reference region approach, instead of a 2TCM, is the contribution of endothelial cells binding. A retrospective analysis of the first study that investigated TSPO density change after LPS in humas (Sandiego *et al.*, 2015) suggested that the substantial V_T increase initially reported ($p<0.001$) was also due to endothelial uptake. Indeed, when the same dataset (8 subjects) was analysed with a 2TCM-1k (a kinetic model that accounts for endothelial binding), the V_T change was more moderate ($p=0.03$) (Woodcock *et al.*, 2020). On the other hand, a pseudo-reference region approach to quantifying TSPO binding is likely less biased by the relative contribution of endothelial binding, as the effect of endothelial cells is assumed to be the same within the pseudo-reference region and in the target regions. It is also worth noting that while we adopted a 60 min scan, Sandiego et al. used a 120 min scan. It has been shown that a 60 min scans can provide [^{18}F]-DPA-714 binding quantification with >98% similarity to 90 min scans, as [^{18}F]-DPA-714 shows concentration equilibrium between compartments at 60 min under normal conditions (Lavisse *et al.*, 2015). However, it is not known whether this is valid during LPS-induced inflammation.

The lack of correlation between central and peripheral inflammation is consistent with previous data on TSPO density after LPS (Sandiego *et al.*, 2015), IFN-α treatment (Nettis *et al.*, 2020) and in MDD patients (J. J. Schubert *et al.*, 2021) that did not show associations between TSPO binding and circulating cytokines or CRP. This suggests that although peripheral and immune function are related (see Chapter 1), regulatory mechanisms in the brain may be independent of those in the periphery. In support of this, a recent study showed no correlations between plasma and CSF cytokines in patients after

orthopaedic surgery (Fertleman *et al.*, 2022). On the other hand, an LPS-induced increase in TSPO density correlated with serum cytokines in a small sample of nonhuman primates (N=6) (Hannestad *et al.*, 2012).

In the second phase of the study, I aimed to validate the SVCA method using standard kinetic modelling, and investigate the LPS effect on [^{18}F]-DPA-714 metabolism and distribution within the blood compartment. Interestingly, I did not find a significant correlation between absolute 2TCM V_T and SVCA-DVR. Due to the lack of blood measurements, in some sessions, it was not possible to assess the correlation between changes in the 2TCM V_T and SVCA-DVR. However, there was agreement between the two techniques, in the regional binding variation assessed using twelve ROIs within each dataset.

Establishing a radiochemistry laboratory, sampling arterial blood and quantifying the intact radiotracer concentration in it have proven to be challenging procedures. An accurate estimation of V_T depends on precise blood measurements. Here, it was only possible to obtain at least three blood samples in both conditions, in two subjects (one being the outlier previously described). A number of logistic and methodological issues affected the blood sampling procedures, preventing the implementation of a consistent protocol across sessions, and a more frequent sampling. However, although the blood sampling procedure could not be kept consistent across the sessions, it provided important information about LPS-induced changes in [^{18}F]-DPA-714 distribution and metabolism. Importantly, I observed a decrease in the POB ratio in the LPS condition in 4 subjects and a lower input function AUC. This suggests that systemic inflammation may increase specific binding (TSPO expression) in the periphery, resulting in a decreased [^{18}F]-DPA-

714 plasma concentration. In particular lower POB may reflect the increased expression of TSPO in blood cells, which is consistent with a previous PET study that quantified the LPS effect on [^{18}F]-DPA-714 concentration in blood pellets after centrifugation (Peters van Ton *et al.*, 2021). Moreover, the lower peak of the AIF after LPS, observed in four subjects, corroborate the hypothesis of a first-pass effect described above. Interestingly, LPS was associated with a reduction in the parent fraction in four of the five subjects tested with arterial blood sampling, suggesting that inflammation may increase the [^{18}F]-DPA-714 metabolism rate.

Given the technical difficulties in arterial blood radioactivity quantification and the inconsistent sampling between sessions I evaluated the impact that one extra blood sample (3 versus 4 time points) has on the final V_T. I repeated the same 2TCM analysis on datasets with 4 blood samples, excluding the latest sample. There was a mean ~10% difference across ROIs between the V_T estimated with 3 or 4 samples, suggesting that the precision of the [^{18}F]-DPA-714 V_T estimation is associated with the accuracy of the AIF and that an inconsistent sampling protocol between sessions may affect the quantification of the treatment effect. The paucity of blood samples and the variation of V_T based on the number of available samples have hampered the assessment of correlations between the SVCA analyses and the standard kinetic modelling outcomes.

The difficulty to accurately estimate the of free intact tracer in the plasma is a major obstacle in TSPO PET imaging with kinetic modelling. Moreover, even when numerous discrete samples are available, a metabolite-corrected plasma AIF should account for the free-plasma fraction (f_p) of radiotracer (i.e. fraction of radiotracer in the plasma not bound to plasma proteins) (Turkheimer *et al.*, 2015). A study that investigated the effect of IFN-

α treatment on brain TSPO binding in healthy humans showed that inflammation is associated with a reduction in the f_p. Changes in the f_p affected the tracer permeability in the brain (in fact, tracer bound to plasma proteins cannot enter the brain) and the TSPO binding estimation (Nettis *et al.*, 2020). It should be noted that none of the mentioned studies that measured LPS effect on TSPO binding in humans or baboons included free-plasma fraction correction. Hence, it is possible that the reported effect of LPS could be substantially biased, which is similar to what was observed in the IFN-α study.

One goal of this study was to test whether minocycline treatment could block LPS-induced microglial activation, indexed with TSPO density. I did not find any effect of minocycline versus placebo on [^{18}F]-DPA-714 TSPO binding. This suggests that a pre-treatment of 100mg bd for 3½ days does not affect the microglial response to LPS. Nevertheless, it is also possible that, considering the modest size of the group receiving minocycline pre-treatment included in the study (N=7), the SVCA analysis did not provide enough power to detect any minocycline effect. Two studies had previously investigated the minocycline effect on TSPO density in different pathologies. A recent study in treatment-resistance depressed patients showed no TSPO density change after minocycline treatment (100mg bd for 8 weeks) (Attwells *et al.*, 2021). Another study on traumatic brain injury reported a reduction in TSPO density after minocycline treatment (100mg bd for 12 weeks) compared to placebo (Scott *et al.*, 2018). Both studies used a substantially longer minocycline treatment, which complicates the comparison with the present data. These discrepancies could also be due to the different mechanisms leading to neuroinflammation and to the different duration of the neuroinflammatory process between each pathology and between chronic diseases and an acute immune challenge.

One limitation of TSPO imaging as a tool in assessing microglial activation is that of the relatively low cell specificity of the TSPO signal. TSPO brain density estimation can be affected by specific binding on endothelial cells, astrocytes and neurons (Hillmer *et al.*, 2017). The cellular sources of TSPO overexpression during inflammation have been suggested to be dependent on the type of pathology or inflammatory stimulus (Tournier *et al.*, 2020). Post-mortem analyses on neurodegenerative diseases have suggested that increased TSPO expression is related to glial density rather than proinflammatory activation (Nutma *et al.*, 2019; Tournier *et al.*, 2020). However, considering the rapid and transient inflammatory effect of LPS it is unlikely that the reported LPS-induced TSPO overexpression is due to glial cell proliferation. Hence, the relative cellular source of TSPO overexpression during endotoxemia, which is thought to be microglia, based on evidence from preclinical studies, remains an open question.

Age and sex are variables that can affect TSPO quantification, with females showing higher TSPO expression across the brain than males in healthy condition (Tuisku *et al.*, 2019). A limitation of this study was that, due to ethical constraints, only male subjects could be included. Cytokine release response during endotoxemia has been reported to be higher in female than in male (Wegner *et al.*, 2017). Although the role of sex in the TSPO overexpression during endotoxemia remains unknown, it cannot be overlooked, and additional data are needed to extend the present findings to the female population. Since the age range was restricted (20-30 years old), it was not considered in the analysis.

In summary, the implementation of an SVCA approach was sensitive to TSPO density change induced by LPS administration. This quantification method may be a non-invasive alternative to investigate TSPO expression change when an AIF is not available. Further

validation against modelling technique accounting for endothelial binding and f_p are warranted.

Chapter 8: Summary, conclusions and future directions

The overarching aim of this study was to investigate whether combining an experimental inflammatory challenge with neuroimaging (and cognitive) measurements of neuroinflammation could be used as a way of measuring target engagement of novel microglial-targeted therapies. A specific aim was to assess the effect of an immune challenge on the brain with two non-invasive neuroimaging methods and a cognitive test. Another objective was to test two non-invasive neuroimaging modalities against the gold-standard TSPO PET with an arterial input function. Finally, I aimed to assess whether the putative microglial inhibitor minocycline could attenuate LPS-induced neuroinflammation.

TSPO PET, the current state-of-the-art imaging technique for detecting neuroinflammation *in vivo*, suffers from a range of limitations. This includes poor cellular specificity, challenging tracer kinetics (particularly in the context of systemic inflammation) and challenging modelling (which often requires the use of atrial input functions) making it poorly suited for large-scale clinical or drug development studies. Consequently, the absence of a simple, reliable neuroimaging method for indexing neuroinflammation and quantifying human target engagement *in vivo* is also hindering the development of novel therapeutic compounds targeting microglial activation.

Endotoxemia is a well-established model of acute inflammation. In Chapter 4 I illustrated the effect of 1 ng/kg LPS injection on physiological parameters, differential white blood cell counts and the circulating cytokines concentration. The pro-inflammatory cytokines

IL-6, IL8 and TNF-α and the anti-inflammatory cytokine IL-10 showed a rapid and robust increase at 3hr, and a trend towards returning to baseline, although the values were still markedly elevated, at 6hr. Differential white cell counts showed significant changes at both 3hr and 6hr. The temporal evolution of the physiological data confirmed that inflammation persisted at the time of the scan (PET (3½ hr) and MRI (5-5½ hr)) and during the cognitive task (6 hr). The rationale for using minocycline to selectively target the central inflammatory response without altering peripheral inflammation was supported by the lack of minocycline effect on systemic inflammatory markers.

In the second analyses I reported the central effects of endotoxin challenge on subjective mood, sickness symptoms and reward/punishment learning measured using a reinforcement learning task. Self-reported questionnaires, completed at baseline and at 5 time points after saline/LPS injection, confirmed that LPS administration was associated with an acute deterioration in mood, an increase in subjective experience of fatigue and an increase in classical sickness symptoms recorded on the SicknessQ questionnaire. The temporal pattern of LPS-induced changes in mood, sickness and fatigue was consistent with previous data (Lasselin, Benson, *et al.*, 2020), showing a rapid peak at 1-2 hr post injection and then a gradual return toward baseline values. Mood changes, fatigue and sickness symptoms were still present at 6 hr post-injection, therefore all measurements (PET, MRI and cognitive) were collected at times that overlapped with the sickness symptoms. I hypothesized that minocycline, as putative inhibitor of neuroinflammation, would inhibit inflammation-associated mood deterioration. However, it no did not affect the self-reported questionnaires measurements during endotoxemia. This study might have been underpowered to detect the minocycline effect on these measurements.

Using a reinforcement learning task, I observed that LPS induces a motivational reorientation, impairing sensitivity to rewards versus punishments, as shown by significant condition (saline/LPS) × valence (reward/punishment) interaction. Specifically, inflammation was linked to a decrease in the correct selection of stimuli associated with reward outcomes, and an increased in the avoidance of stimuli associated with punishment outcomes. However, post-hoc t-test for each valence did not reach statistical significance. This replicated the previous finding with the same task, which used typhoid vaccination in healthy volunteers as a model of mild inflammation (Harrison *et al.*, 2016). Minocycline pre-treatment attenuated this inflammation-induced shift in reward versus punishment sensitivity.

In depression, inflammation was found to be associated with specific symptoms, including anhedonia (Milaneschi *et al.*, 2021). There is evidence that the relationship between inflammation and anhedonia may be mediated by alterations of reward circuitry in the ventral striatum (Eisenberger *et al.*, 2010; Harrison *et al.*, 2016). It was previously shown, using the same reinforcement learning task presented here, integrated with fMRI, that ventral striatal circuits play a central role in reward learning while activity of the insula was linked to avoidance of loss stimuli selection (Pessiglione *et al.*, 2006). These observations were replicated in the study that used the typhoid vaccination, which also showed that both striatal and insular activity were affected by inflammation (decreased ventral striatum activity and increased insula activity) (Harrison *et al.*, 2016). The present study provided preliminary evidence suggesting that minocycline modulated the effect of inflammation on reward versus punishment sensitivity. To investigate this further future studies may couple the present protocol with fMRI (similarly to the study using typhoid vaccination) to assess whether minocycline modulates the activity of the ventral striatum

and the insula. In light of the data presented here, it is possible that minocycline inhibits the effect of inflammation on both regions. fMRI studies could also be useful to investigate whether the effect of minocycline is restricted to specific brain areas.

To complement the data presented here, studies in animals may assess the downstream consequences of minocycline on neurotransmitters synaptic availability. In Chapter 1 I reviewed the possible mechanisms through which pro-inflammatory cytokines may affect the monoamine neurotransmitters and glutamate signalling. Thus, given the anti-inflammatory properties of minocycline, it could be investigated if it ultimately affects neurotransmitters turnover, synaptic vesicular formation, reuptake process or the expression of post-synaptic receptors.

The current findings provide preliminary evidence that the implementation of a cognitive task coupled with an immune challenge may be a useful approach in screening new compounds that target neuroinflammation. Nevertheless, these findings will need to be replicated with a larger sample size.

In Chapters 6 and 7, I reported the results from two neuroimaging studies that used non-invasive methods to index neuroinflammation. In the first, which used DW-MRS, a novel MRI technique that enables measuring of the diffusion properties of intracellular metabolites, I observed an increased diffusion of the predominantly glial metabolite, choline, during endotoxemia. The selective effect of LPS on glial cells was confirmed by the absence of any change in the diffusion of the neuronal marker NAA. I interpreted this finding as a measure of the inflammation-associated morphological changes of glial cells. Pending further replication, this finding suggests that choline diffusion may serve as a novel inflammatory marker of microglial activation. This constitutes an improvement for

MRI techniques in terms of cell specificity during neuroinflammatory processes. The availability of cost-effective and non-invasive MRI techniques sensitive to glial activation may facilitate studies that seek to assess the temporal evolution of neuroinflammation in both disease and experimental models. The practical advantage is particularly evident when compared with studies that employ the gold standard TSPO PET, in which, due to high costs and complex procedures, the study population is often limited. The possibility of implementing DW-MRS in large populations and in longitudinal studies may increase the sensitivity, enabling detection of the effect of a putative immunomodulant agent. The finding of this study will need to be complemented by future studies, for example by assessing the DW-MRS signal in a larger number of brain areas. The differential effect of LPS in grey versus white matter is consistent with TSPO PET results. However, this will need to be investigated further, including cortical and subcortical areas. Further studies may also employ DW-MRS in combination with other quantitative or functional MRI techniques to provide a more comprehensive description of the neuroinflammatory processes. Further investigations in larger cohorts of correlations between DW-MRS outcomes and circulating immune biomarkers are also warranted.

Interpretation of the DW-MRS data, particularly the choline signal, is complicated by the unknown relative contribution of each glial cell type. Here, it was speculated that the observed choline diffusion change was due to microglial activation rather than astrocytes (as explained in the discussion in Chapter 6). Indeed, in a study on a mouse model of multiple sclerosis, post-mortem histological analysis showed a correlation between choline diffusion and the microglial total area, whereas the astrocytes area was associated with myo-inositol diffusion (Genovese, Palombo, *et al.*, 2021). Future research will need to confirm this. It should be noted that, in the present study, it was not possible to measure

the myo-inositol diffusion. The cell-specificity of the choline and myo-inositol diffusion signals could be tested in animals, for example, by measuring their diffusion at different time points after microglial depletion. This would allow testing whether myo-inositol concentration is only related to astrocytes and whether choline would increase as microglial repopulate the brain.

In my last analysis set, I presented the results of a TSPO PET imaging study on 19 healthy subjects, each of whom was tested twice, once after saline and once after LPS. I showed that a simplified analysis method based on an SVCA-defined pseudo-reference region is sensitive to an LPS-induced change in TSPO availability in the grey matter and cortical regions. This finding confirms putative microglial activation during endotoxemia in humans and accords with previously reported findings that used the full kinetic modelling (Sandiego *et al.*, 2015). This previous study reported a more robust effect of LPS (30-60% V_T increase across different regions), which had been assessed using a two-tissue compartmental model (2TCM), while, in the present study, I observed a 4.58% DVR increase. This may be the result of using different modelling techniques to assess TSPO density. Implementing a pseudo-reference region approach could have resulted in an underestimation of the treatment effect, since the pseudo-reference region is not completely devoid of specific signal (radiotracer binding to TSPO) and therefore potentially subjected to changes induced by LPS. On the other hand, the 2TCM does not account for the specific endothelial binding. In fact, the increased V_T reported by Sandiego and colleagues was substantially smaller when corrected for endothelial binding (Woodcock *et al.*, 2020). The lack of consensus in TSPO PET imaging modelling analyses and the presence of confounders, such as TSPO expression in endothelial cells,

highlight the need to develop novel imaging techniques to assess microglial activation *in vivo*.

I then went on compare my SVCA findings against the gold standard kinetic modelling with full arterial blood sampling, in a subgroup of this population. The comparison between the gold-standard 2TCM V_T and the SVCA outcomes and between the findings of this study with those of previous studies was complicated by the inconsistency of the blood sampling between sessions. It should be noted that, the complicated arterial blood sampling process was further hindered by LPS-induced blood clotting.

In summary, this study provided further evidence that a non-invasive quantification approach based on a SVCA-derived pseudo-reference region can inform about neuroinflammation in humans. This experiment also highlighted the complications associated with arterial blood collection. Hence, the relevance of a non-invasive quantification approach that does not require complex blood analysis. Arterial blood sampling is an invasive and painful procedure that requires trained clinicians and can be challenging for specific populations, for example, the elderly. Moreover, a precise quantification of plasma radioligand concentration requires sophisticated equipment that only specialized PET sites have at their disposal. Even fewer groups have been able to include in their experiment the quantification of the free-plasma fraction, a measure that has been shown to be potentially crucial for an appropriate TSPO density quantification during acute inflammation (Nettis *et al.*, 2020).

Thus, a non-invasive quantification approach is an attractive alternative that may facilitate a widespread use of TSPO PET. A non-invasive approach to estimating TSPO availability may make it possible to design multi-centre studies on larger clinical populations. This is

complementary to what I have highlighted above about the benefit of non-invasive and cost-effective MRI techniques. Large-scale studies may make it possible to assess associations between neuroinflammation and disease progression or, in the context of a study that uses a putative immunomodulating therapy, clinical improvements.

However, the limitations of TSPO PET are not solely linked with practical disadvantages. Uncertainty exists regarding the cell-specificity of TSPO and regarding the interpretation of an increase in its expression in disease. TSPO is expressed in a variety of cell-types, including vascular endothelial cells, astrocytes and neurons (Lavisse *et al.*, 2012; Rizzo *et al.*, 2019; Notter *et al.*, 2020). An open question remains about the relative contribution of microglial cells in TSPO overexpression in different diseases. Post-mortem studies of neurodegenerative diseases samples have suggested that increased TSPO expression in the brain reflects microglial density rather than activation, and that TSPO is expressed by microglial cells irrespective of their pro- or anti-inflammatory phenotype (Nutma *et al.*, 2019; Tournier *et al.*, 2020). Future research will need to investigate the cellular source of TSPO in psychiatric disease.

It is important to note that no correlations were observed between the changes in neuroinflammatory markers assessed through DW-MRS in the thalamus and TSPO PET in the thalamus, total brain and total GM. It is worth considering the factors that could underlie the lack of agreement between the two techniques. First, the application of the SVCA approach to estimate TSPO density revealed no changes to putative microglial activation in the thalamus (as well as subcortical regions) and the change in the whole brain DVR was associated with a smaller effect size (Cohen's d=0.56) when compared to that observed for the changes in the ADC(tCho) in the thalamus (Cohen's d=1.22). As

discussed in the previous chapter, the limited sensitivity of TSPO PET in subcortical regions is likely due to the inherent limitations of a pseudo-reference region approach in detecting changes in brain regions in which TSPO is only moderately overexpressed (when compared to cortical regions). This suggests that DW-MRS could exhibit greater sensitivity in assessing the effect of LPS on subcortical grey matter regions than a non-invasive TSPO PET approach. The relationship between techniques should be evaluated in further studies examining a larger number of grey matter areas including cortical ROIs. However, it also possible that the pathway regulating TSPO expression level and microglial cell morphology are independently regulated. This latter hypothesis suggests that a combined approach using different imaging methods in parallel might provide a more comprehensive interpretation of the neuroinflammatory process and could better inform about anti-inflammatory properties of novel pharmacological agents.

The potential of employing multiple techniques to evaluate the effects of a putative drug is exemplified by the divergent outcomes observed with minocycline. While minocycline pre-treatment inhibited LPS-induced changes in reward versus punishment sensitivity within the reinforcement learning task, no discernible effects were captured by the two neuroimaging modalities when assessing the response to LPS. It could be possible that minocycline selectively affected pathways regulating neurotransmission, ultimately changing behavioural outcomes, while leaving unaffected the expression levels of TSPO or the morphological status as assessed by DW-MRS. Another plausible factor contributing to these disparate findings is that minocycline might differentially impact specific brain regions implicated in the behavioural outcomes, which were not measurable using TSPO PET and DW-MRS. Alternatively, it is possible that the neuroimaging modalities had limited sensitivity to the minocycline effect. Adopting a combined

approach to investigating drug effects could prove particularly advantageous when the specific molecular target and the affected pathways of a drug remain unknown, as is the case of minocycline. Moreover, the limited understanding of the precise biological role of TSPO during acute neuroinflammation further complicates the interpretation of the absence of treatment effects supporting the importance comprehensive approach to screen novel pharmacological agents.

In conclusion, my study demonstrates the viability of a cognitive task and non-invasive imaging techniques as a tool to detect the effect of experimentally-induced neuroinflammation. The results of my work are relevant to inform design and application of future experimental paradigms for the assessment of target engagement of novel immunomodulatory drugs in humans.

References

Agwuh, K.N. and MacGowan, A. (2006) 'Pharmacokinetics and pharmacodynamics of the tetracyclines including glycylcyclines', *The Journal of antimicrobial chemotherapy*, 58(2), pp. 256–265.

Akerele, M.I. *et al.* (2021) 'Population-based input function for TSPO quantification and kinetic modeling with [11C]-DPA-713', *EJNMMI Physics*, 8(1), pp. 1–17.

Albrecht, D.S. *et al.* (2018) 'Pseudoreference regions for glial imaging with 11 C-PBR28: Investigation in 2 clinical cohorts', *Journal of Nuclear Medicine*, 59(1), pp. 107–114.

Alesci, S. *et al.* (2005) 'Major depression is associated with significant diurnal elevations in plasma interleukin-6 levels, a shift of its circadian rhythm, and loss of physiological complexity in its secretion: clinical implications', *The Journal of clinical endocrinology and metabolism*, 90(5), pp. 2522–2530.

Almeida, P.G.C. *et al.* (2020) 'Neuroinflammation and glial cell activation in mental disorders', *Brain, Behavior, & Immunity - Health*, 2, p. 100034.

Andreasson, A. *et al.* (2018) 'A global measure of sickness behaviour: Development of the Sickness Questionnaire', *Journal of health psychology*, 23(11), pp. 1452–1463.

Anholt, R.R. *et al.* (1986) 'The peripheral-type benzodiazepine receptor. Localization to the mitochondrial outer membrane.', *Journal of Biological Chemistry* , 261(2), pp. 576–583. Available at: http://www.jbc.org/content/261/2/576.abstract.

Arakawa, S. *et al.* (2012) 'Minocycline produced antidepressant-like effects on the learned helplessness rats with alterations in levels of monoamine in the amygdala and no

changes in BDNF levels in the hippocampus at baseline', *Pharmacology Biochemistry and Behavior*, 100(3), pp. 601–606.

Arbour, N.C. *et al.* (2000) 'TLR4 mutations are associated with endotoxin hyporesponsiveness in humans', *Nature Genetics 2000 25:2*, 25(2), pp. 187–191.

Arlicot, N. *et al.* (2012) 'Initial evaluation in healthy humans of [18F]DPA-714, a potential PET biomarker for neuroinflammation', *Nuclear Medicine and Biology*, 39(4), pp. 570–578.

Attwells, S. *et al.* (2021) 'A double-blind placebo-controlled trial of minocycline on translocator protein distribution volume in treatment-resistant major depressive disorder', *Translational Psychiatry 2021 11:1*, 11(1), pp. 1–9.

Babcock, A.A. *et al.* (2003) 'Chemokine expression by glial cells directs leukocytes to sites of axonal injury in the CNS.', *The Journal of neuroscience : the official journal of the Society for Neuroscience*, 23(21), pp. 7922–30.

Bahador, M. and Cross, A.S. (2007) 'Review: From therapy to experimental model: a hundred years of endotoxin administration to human subjects', *Journal of Endotoxin Research*, 13(5), pp. 251–279.

Banati, R.B. (2002) 'Visualising microglial activation in vivo', *Glia*, 40(2), pp. 206–217.

Banister, S.D. *et al.* (2013) '[18F]DPA-714: Direct Comparison with [11C]PK11195 in a Model of Cerebral Ischemia in Rats', *PLoS ONE*, 8(2), p. e56441.

Banister, S.D. *et al.* (2015) 'Ether analogues of DPA-714 with subnanomolar affinity for the translocator protein (TSPO)', *European Journal of Medicinal Chemistry*, 93, pp. 392–400.

Banks, W. (2005) ‘Blood-brain barrier transport of cytokines: a mechanism for neuropathology’, *Current pharmaceutical design*, 11(8), pp. 973–984.

Banks, W.A., Kastin, A.J. and Gutierrez, E.G. (1994) ‘Penetration of interleukin-6 across the murine blood-brain barrier’, *Neuroscience letters*, 179(1–2), pp. 53–56.

Banks, W.A., Moinuddin, A. and Morley, J.E. (2001) ‘Regional transport of TNF-α across the blood-brain barrier in young ICR and young and aged SAMP8 mice’, *Neurobiology of Aging*, 22(4), pp. 671–676.

Banks, W.A., Niehoff, M.L. and Zalcman, S.S. (2004) ‘Permeability of the mouse blood-brain barrier to murine interleukin-2: Predominance of a saturable efflux system’, *Brain, Behavior, and Immunity*, 18(5), pp. 434–442.

Baumeister, D., Ciufolini, S. and Mondelli, V. (2016) ‘Effects of psychotropic drugs on inflammation: Consequence or mediator of therapeutic effects in psychiatric treatment?’, *Psychopharmacology*, 233(9), pp. 1575–1589.

Beckers, L. *et al.* (2018) ‘Increased Expression of Translocator Protein (TSPO) Marks Pro-inflammatory Microglia but Does Not Predict Neurodegeneration’, *Molecular Imaging and Biology*, 20(1), pp. 94–102.

Bekhbat, M. *et al.* (2020) ‘Gene signatures in peripheral blood immune cells related to insulin resistance and low tyrosine metabolism define a sub-type of depression with high CRP and anhedonia’, *Brain, Behavior, and Immunity*, 88, pp. 161–165.

Bekhbat, M. *et al.* (2022) ‘Functional connectivity in reward circuitry and symptoms of anhedonia as therapeutic targets in depression with high inflammation: evidence from a dopamine challenge study’, *Molecular Psychiatry 2022 27:10*, 27(10), pp. 4113–4121.

Betlazar, C. *et al.* (2020) 'The Translocator Protein (TSPO) in Mitochondrial Bioenergetics and Immune Processes', *Cells*, 9(2).

Bhattacharya, A. and Biber, K. (2016) 'The microglial ATP-gated ion channel P2X7 as a CNS drug target', *GLIA*, 64(10), pp. 1772–1787.

Bhattacharya, A. and Ceusters, M. (2020) 'Targeting neuroinflammation with brain penetrant P2X7 antagonists as novel therapeutics for neuropsychiatric disorders', *Neuropsychopharmacology*, 45(1), pp. 234–235.

Billones, R.R., Kumar, S. and Saligan, L.N. (2020) 'Disentangling fatigue from anhedonia: a scoping review', *Translational Psychiatry 2020 10:1*, 10(1), pp. 1–11.

Blecharz-Lang, K.G. *et al.* (2022) 'Minocycline Attenuates Microglia/Macrophage Phagocytic Activity and Inhibits SAH-Induced Neuronal Cell Death and Inflammation', *Neurocritical Care*, 37(2), pp. 410–423.

Bluthé, R.M., Dantzer, R. and Kelley, K.W. (1997) 'Central mediation of the effects of interleukin-1 on social exploration and body weight in mice', *Psychoneuroendocrinology*, 22(1), pp. 1–11.

Bodini, B. *et al.* (2018) 'Dysregulation of energy metabolism in multiple sclerosis measured in vivo with diffusion-weighted spectroscopy', *Multiple Sclerosis Journal*, 24(3), pp. 313–321.

Borden, E.C. and Parkinson, D. (1998) 'A perspective on the clinical effectiveness and tolerance of interferon-alpha.', *Seminars in Oncology*, 25(1 Suppl 1), pp. 3–8. Available at: https://europepmc.org/article/med/9482534 (Accessed: 19 December 2022).

Breen, E.C. *et al.* (2011) 'Multisite Comparison of High-Sensitivity Multiplex Cytokine

Assays', *Clinical and Vaccine Immunology : CVI*, 18(8), p. 1229.

Bremner, J.D. *et al.* (1997) 'Positron Emission Tomography Measurement of Cerebral Metabolic Correlates of Tryptophan Depletion—Induced Depressive Relapse', *Archives of General Psychiatry*, 54(4), pp. 364–374.

Briley, M. and Lépine (2011) 'The increasing burden of depression', *Neuropsychiatric Disease and Treatment*, 7(Suppl 1), p. 3.

Brydon, L. *et al.* (2008) 'Peripheral Inflammation is Associated with Altered Substantia Nigra Activity and Psychomotor Slowing in Humans', *Biological Psychiatry*, 63(11), pp. 1022–1029.

Buttini, M., Limonta, S. and Boddeke, H.W.G.M. (1996) 'Peripheral administration of lipopolysaccharide induces activation of microglial cells in rat brain', *Neurochemistry International*, 29(1), pp. 25–35.

Cagnin, A. *et al.* (2001) 'In-vivo measurement of activated microglia in dementia', *Lancet*, 358(9280), pp. 461–467.

Calcia, M.A. *et al.* (2016) 'Stress and neuroinflammation: A systematic review of the effects of stress on microglia and the implications for mental illness', *Psychopharmacology*. Springer Verlag, pp. 1637–1650.

Camara, M. Lou *et al.* (2015) 'Effects of centrally administered etanercept on behavior, microglia, and astrocytes in mice following a peripheral immune challenge', *Neuropsychopharmacology : official publication of the American College of Neuropsychopharmacology*, 40(2), pp. 502–512.

Canat, X. *et al.* (1993) 'Distribution profile and properties of peripheral-type

benzodiazepine receptors on human hemopoietic cells', *Life Sciences*, 52(1), pp. 107–118.

Capuron, L. *et al.* (2002) 'Association between decreased serum tryptophan concentrations and depressive symptoms in cancer patients undergoing cytokine therapy', *Molecular Psychiatry*, 7(5), pp. 468–473.

Capuron, Lucile *et al.* (2002) 'Neurobehavioral effects of interferon-alpha in cancer patients: phenomenology and paroxetine responsiveness of symptom dimensions', *Neuropsychopharmacology : official publication of the American College of Neuropsychopharmacology*, 26(5), pp. 643–652.

Capuron, L. *et al.* (2003) 'Association of exaggerated HPA axis response to the initial injection of interferon-alpha with development of depression during interferon-alpha therapy', *American Journal of Psychiatry*, 160(7), pp. 1342–1345.

Capuron, L. (2012) 'Dopaminergic Mechanisms of Reduced Basal Ganglia Responses to Hedonic Reward During Interferon Alfa Administration.', *Changes*, 29(6), pp. 997–1003.

Capuron, L. *et al.* (2012) 'Dopaminergic Mechanisms of Reduced Basal Ganglia Responses to Hedonic Reward During Interferon Alfa Administration', *Archives of general psychiatry*, 69(10), p. 1044.

Capuron, L. and Miller, A.H. (2004) 'Cytokines and psychopathology: Lessons from interferon-α', *Biological Psychiatry*, 56(11), pp. 819–824.

Capuron, L. and Miller, A.H. (2011) 'Immune System to Brain Signaling: Neuropsychopharmacological Implications', *Pharmacology & therapeutics*, 130(2), p. 226.

Carlyle Clawson, C., Francis Hartmann, J. and Vernier, R.L. (1966) 'Electron microscopy of the effect of gram-negative endotoxin on the blood-brain barrier', *Journal of Comparative Neurology*, 127(2), pp. 183–197.

Cattaneo, A. *et al.* (2012) 'Candidate Genes Expression Profile Associated with Antidepressants Response in the GENDEP Study: Differentiating between Baseline "Predictors" and Longitudinal "Targets"', *Neuropsychopharmacology 2013 38:3*, 38(3), pp. 377–385.

Cattaneo, A. *et al.* (2020) 'Whole-blood expression of inflammasome- and glucocorticoid-related mRNAs correctly separates treatment-resistant depressed patients from drug-free and responsive patients in the BIODEP study', *Translational Psychiatry 2020 10:1*, 10(1), pp. 1–14.

Chamberlain, S.R. *et al.* (2019) 'Treatment-resistant depression and peripheral C-reactive protein', *The British Journal of Psychiatry*, 214(1), pp. 11–19.

Chauveau, F. *et al.* (2008) 'Nuclear imaging of neuroinflammation: A comprehensive review of [11C]PK11195 challengers', *European Journal of Nuclear Medicine and Molecular Imaging*, 35(12), pp. 2304–2319.

Chauveau, F. *et al.* (2009) 'Comparative evaluation of the translocator protein radioligands 11C-DPA-713, 18F-DPA-714, and 11C-PK11195 in a rat model of acute neuroinflammation.', *Journal of nuclear medicine : official publication, Society of Nuclear Medicine*, 50(3), pp. 468–76.

Chen, M.K. and Guilarte, T.R. (2008) 'Translocator protein 18 kDa (TSPO): Molecular sensor of brain injury and repair', *Pharmacology and Therapeutics*, 118(1), pp. 1–17.

Cherry, J.D., Olschowka, J.A. and Banion, M.K.O. (2014) 'Neuroinflammation and M2 microglia : the good , the bad , and the inflamed', pp. 1–15.

Colasanti, A. *et al.* (2014) 'In Vivo Assessment of Brain White Matter Inflammation in Multiple Sclerosis with (18)F-PBR111 PET', *Journal of nuclear medicine : official publication, Society of Nuclear Medicine*, 55(7), pp. 1112–1118.

Colasanti, A. *et al.* (2016) 'Hippocampal Neuroinflammation, Functional Connectivity, and Depressive Symptoms in Multiple Sclerosis', *Biological Psychiatry*, 80(1), p. 62.

Cowen, P.J., Parry-Billings, M. and Newsholme, E.A. (1989) 'Decreased plasma tryptophan levels in major depression', *Journal of Affective Disorders*, 16(1), pp. 27–31.

Critchley, H.D. and Harrison, N.A. (2013) 'Visceral Influences on Brain and Behavior', *Neuron*. Elsevier, pp. 624–638.

D'Mello, C., Le, T. and Swain, M.G. (2009) 'Cerebral Microglia Recruit Monocytes into the Brain in Response to Tumor Necrosis Factor Signaling during Peripheral Organ Inflammation', *Journal of Neuroscience*, 29(7), pp. 2089–2102.

Dantzer, R. (2001) 'Cytokine-Induced Sickness Behavior: Where Do We Stand?', *Brain, Behavior, and Immunity*, 15(1), pp. 7–24.

Dantzer, R. *et al.* (2008) 'From inflammation to sickness and depression: When the immune system subjugates the brain', *Nature Reviews Neuroscience*, 9(1), pp. 46–56.

Davies, K.A. *et al.* (2020) 'Interferon and anti-TNF therapies differentially modulate amygdala reactivity which predicts associated bidirectional changes in depressive symptoms', *Molecular Psychiatry*, pp. 1–11.

Davis, E.J., Foster, T.D. and Thomas, W.E. (1994) 'Cellular forms and functions of brain microglia', *Brain Research Bulletin*. Elsevier, pp. 73–78.

Dean, O.M. *et al.* (2017) 'Adjunctive minocycline treatment for major depressive disorder: A proof of concept trial', *The Australian and New Zealand journal of psychiatry*, 51(8), pp. 829–840.

Delgado, P.L. (2000) 'Depression: The Case for a Monoamine Deficiency', *The Journal of Clinical Psychiatry*, 61(suppl 6), p. 4165. Available at: https://www.psychiatrist.com/jcp/depression/depression-case-monoamine-deficiency (Accessed: 10 December 2022).

DellaGioia, N. *et al.* (2013) 'Bupropion pre-treatment of endotoxin-induced depressive symptoms', *Brain, behavior, and immunity*, 31, pp. 197–204.

Demir, S. *et al.* (2015) 'Neutrophil–lymphocyte ratio in patients with major depressive disorder undergoing no pharmacological therapy', *Neuropsychiatric Disease and Treatment*, 11, p. 2253.

Dickens, A.M. *et al.* (2014) 'Detection of microglial activation in an acute model of neuroinflammation using PET and radiotracers 11C-(R)-PK11195 and 18F-GE-180', *Journal of nuclear medicine : official publication, Society of Nuclear Medicine*, 55(3), pp. 466–472.

Dipasquale, O. *et al.* (2016) 'Interferon-α acutely impairs whole-brain functional connectivity network architecture – A preliminary study', *Brain, Behavior, and Immunity*, 58, pp. 31–39.

Dowell, N.G. *et al.* (2016) 'Acute changes in striatal microstructure predict the

development of interferon-Alpha induced fatigue', *Biological Psychiatryl*, 79(4), pp. 320–328.

Dowell, N.G. *et al.* (2019) 'Interferon-alpha-Induced Changes in NODDI Predispose to the Development of Fatigue', *Neuroscience*, 403, pp. 111–117.

Dowlati, Y. *et al.* (2010) 'A Meta-Analysis of Cytokines in Major Depression', *Biological Psychiatry*, 67(5), pp. 446–457.

Draper, A. *et al.* (2017) 'Effort but not Reward Sensitivity is Altered by Acute Sickness Induced by Experimental Endotoxemia in Humans', *Neuropsychopharmacology 2018 43:5*, 43(5), pp. 1107–1118.

Drevets, W.C. *et al.* (2022) 'Immune targets for therapeutic development in depression: towards precision medicine', *Nature Reviews Drug Discovery 2022 21:3*, 21(3), pp. 224–244.

Eggerstorfer, B. *et al.* (2022) 'Meta-analysis of molecular imaging of translocator protein in major depression', *Frontiers in Molecular Neuroscience*, 15.

Eisenberger, N.I. *et al.* (2010) 'Inflammation-induced anhedonia: Endotoxin reduces ventral striatum responses to reward', *Biological Psychiatry*, 68(8), pp. 748–754.

Emadi-Kouchak, H. *et al.* (2016) 'Therapeutic effects of minocycline on mild-to-moderate depression in HIV patients: A double-blind, placebo-controlled, randomized trial', *International Clinical Psychopharmacology*, 31(1), pp. 20–26.

Enache, D., Pariante, C.M. and Mondelli, V. (2019) 'Markers of central inflammation in major depressive disorder: A systematic review and meta-analysis of studies examining cerebrospinal fluid, positron emission tomography and post-mortem brain tissue', *Brain,*

Behavior, and Immunity, 81, pp. 24–40.

Engler, H. *et al.* (2017) 'Selective increase of cerebrospinal fluid IL-6 during experimental systemic inflammation in humans: association with depressive symptoms', *Molecular Psychiatry 2017 22:10*, 22(10), pp. 1448–1454.

Ercan, E. *et al.* (2016) 'Glial and axonal changes in systemic lupus erythematosus measured with diffusion of intracellular metabolites.', *Brain : a journal of neurology*, 139(Pt 5), pp. 1447–57.

Erickson, M.A. and Banks, W.A. (2018) 'Neuroimmune Axes of the Blood–Brain Barriers and Blood–Brain Interfaces: Bases for Physiological Regulation, Disease States, and Pharmacological Interventions', *Pharmacological Reviews*, 70(2), pp. 278–314.

Evans, S.S., Repasky, E.A. and Fisher, D.T. (2015) 'System Feels the Heat', *Nature Reviews Immunology*, 15(6), pp. 335–349.

Fang, Y.H.D. *et al.* (2022) 'Image Quantification for TSPO PET with a Novel Image-Derived Input Function Method', *Diagnostics*, 12(5).

Felger, J.C., Mun, J., *et al.* (2013) 'Chronic Interferon-α Decreases Dopamine 2 Receptor Binding and Striatal Dopamine Release in Association with Anhedonia-Like Behavior in Nonhuman Primates', *Neuropsychopharmacology*, 38(11), p. 2179.

Felger, J.C., Li, L., *et al.* (2013) 'Tyrosine Metabolism During Interferon-alpha Administration: Association with Fatigue and CSF Dopamine Concentrations', *Brain, behavior, and immunity*, 31, p. 153.

Felger, J.C. *et al.* (2016) 'Inflammation is associated with decreased functional connectivity within corticostriatal reward circuitry in depression', *Molecular psychiatry*,

21(10), pp. 1358–1365.

Felger, J.C. and Miller, A.H. (2012) 'Cytokine Effects on the Basal Ganglia and Dopamine Function: the Subcortical Source of Inflammatory Malaise', *Frontiers in neuroendocrinology*, 33(3), p. 315.

Felten, D.L. *et al.* (1985) 'Noradrenergic and peptidergic innervation of lymphoid tissue.', *Journal of Immunology (Baltimore, Md. : 1950)*, 135(2 Suppl), pp. 755s-765s. Available at: https://europepmc.org/article/med/2861231 (Accessed: 24 January 2023).

Fernandes, B.S. *et al.* (2015) 'C-reactive protein is increased in schizophrenia but is not altered by antipsychotics: meta-analysis and implications', *Molecular Psychiatry 2016 21:4*, 21(4), pp. 554–564.

Fertleman, M. *et al.* (2022) 'Cytokine changes in cerebrospinal fluid and plasma after emergency orthopaedic surgery', *Scientific Reports*, 12(1), p. 2221.

Franco-Bocanegra, D.K. *et al.* (2019) 'Molecular Mechanisms of Microglial Motility: Changes in Ageing and Alzheimer's Disease', *Cells*, 8(6), p. 639.

Friedrich, M.J. (2017) 'Depression Is the Leading Cause of Disability Around the World', *JAMA*, 317(15), pp. 1517–1517.

Fujita, M. *et al.* (2008) 'Kinetic Analysis in Healthy Humans of a Novel Positron Emission Tomography Radioligand to Image the Peripheral Benzodiazepine Receptor, a Potential Biomarker for Inflammation', *NeuroImage*, 40(1), p. 43.

Fukui, S. *et al.* (1991) 'Blood–Brain Barrier Transport of Kynurenines: Implications for Brain Synthesis and Metabolism', *Journal of Neurochemistry*, 56(6), pp. 2007–2017.

Gabbay, V. *et al.* (2012) 'The possible role of the kynurenine pathway in anhedonia in adolescents', *Journal of Neural Transmission*, 119(2), pp. 253–260.

Garcia-Hernandez, R. *et al.* (2020) 'Imaging Microglia and Astrocytes non-invasively using Diffusion MRI', *bioRxiv*, p. 2020.02.07.938910.

García-Lorenzo, D. *et al.* (2018) 'Validation of an automatic reference region extraction for the quantification of [18 F]DPA-714 in dynamic brain PET studies', *Journal of Cerebral Blood Flow and Metabolism*, 38(2), pp. 333–346.

Gavish, M. *et al.* (1999) 'Enigma of the Peripheral Benzodiazepine Receptor', *Pharmacol. Rev.*, 51(4), pp. 629–650.

Genovese, G., Marjańska, M., *et al.* (2021) 'In vivo diffusion-weighted MRS using semi-LASER in the human brain at 3 T: Methodological aspects and clinical feasibility', *NMR in Biomedicine*, 34(5).

Genovese, G., Palombo, M., *et al.* (2021) 'Inflammation-driven glial alterations in the cuprizone mouse model probed with diffusion-weighted magnetic resonance spectroscopy at 11.7 T', *NMR in Biomedicine* [Preprint].

Gibertini, M. *et al.* (1995) 'Spatial Learning Impairment in Mice Infected with Legionella pneumophila or Administered Exogenous Interleukin-1-β', *Brain, Behavior, and Immunity*, 9(2), pp. 113–128.

Goldstein, L.E. *et al.* (2000) '3-Hydroxykynurenine and 3-hydroxyanthranilic acid generate hydrogen peroxide and promote alpha-crystallin cross-linking by metal ion reduction', *Biochemistry*, 39(24), pp. 7266–7275.

Golla, S.S.V. *et al.* (2015) 'Quantification of [18 F]DPA-714 binding in the human brain:

Initial studies in healthy controls and Alzheimer's disease patients', *Journal of Cerebral Blood Flow and Metabolism*, 35(5), pp. 766–772.

González-Reyes, R.E. *et al.* (2017) 'Involvement of astrocytes in Alzheimer's disease from a neuroinflammatory and oxidative stress perspective', *Frontiers in Molecular Neuroscience*. Frontiers Media S.A.

Gorwood, P. (2008) 'Neurobiological mechanisms of anhedonia', *Dialogues in Clinical Neuroscience*, 10(3), p. 291.

Goshen, I. *et al.* (2007) 'Brain interleukin-1 mediates chronic stress-induced depression in mice via adrenocortical activation and hippocampal neurogenesis suppression', *Molecular Psychiatry 2008 13:7*, 13(7), pp. 717–728.

Greuter, H.N.J.M. *et al.* (2005) 'Optimizing an online SPE–HPLC method for analysis of (R)-[11C]1-(2-chlorophenyl)-N-methyl-N-(1-methylpropyl)-3-isoquinolinecarboxamide [(R)-[11C]PK11195] and its metabolites in humans', *Nuclear Medicine and Biology*, 32(3), pp. 307–312.

Grigoleit, J.S. *et al.* (2011) 'Dose-Dependent Effects of Endotoxin on Neurobehavioral Functions in Humans', *PLoS ONE*, 6(12), p. 28330.

Grisanti, L.A. *et al.* (2011) 'Pro-inflammatory responses in human monocytes are beta1-adrenergic receptor subtype dependent.', 47(6), pp. 1244–1254.

Gruetter, R. and Tkáč, I. (2000) *Field Mapping Without Reference Scan Using Asymmetric Echo-Planar Techniques*.

Gunn, R., Coello, C. and Searle, G. (2016) 'Molecular Imaging And Kinetic Analysis Toolbox (MIAKAT) - A Quantitative Software Package for the Analysis of PET

Neuroimaging Data', *Journal of Nuclear Medicine*, 57(supplement 2).

Gupta, R. *et al.* (2016) 'Effect of Mirtazapine Treatment on Serum Levels of Brain-Derived Neurotrophic Factor and Tumor Necrosis Factor-α in Patients of Major Depressive Disorder with Severe Depression', *Pharmacology*, 97(3–4), pp. 184–188.

Gut, P., Zweckstetter, M. and Banati, R.B. (2015) 'Lost in translocation: The function of the 18 kD translocator protein', *Trends in endocrinology and metabolism: TEM*, 26(7), p. 349.

Haapakoski, R. *et al.* (2015) 'Cumulative meta-analysis of interleukins 6 and 1β, tumour necrosis factor α and C-reactive protein in patients with major depressive disorder', *Brain, behavior, and immunity*, 49, pp. 206–215.

Hannestad, J. *et al.* (2012) 'Endotoxin-induced systemic inflammation activates microglia: [11C]PBR28 positron emission tomography in nonhuman primates', *NeuroImage*, 63(1), pp. 232–239.

Hannestad, J., Dellagioia, N. and Bloch, M. (2011) 'The Effect of Antidepressant Medication Treatment on Serum Levels of Inflammatory Cytokines: A Meta-Analysis', *Neuropsychopharmacology 2011 36:12*, 36(12), pp. 2452–2459.

Harmer, C.J., Duman, R.S. and Cowen, P.J. (2017) 'How do antidepressants work? New perspectives for refining future treatment approaches', *The lancet. Psychiatry*, 4(5), p. 409.

Haroon, E. *et al.* (2014) 'IFN-Alpha-Induced Cortical and Subcortical Glutamate Changes Assessed by Magnetic Resonance Spectroscopy', *Neuropsychopharmacology*, 39(7), p. 1777.

Haroon, E. *et al.* (2016) ‘Conceptual convergence: increased inflammation is associated with increased basal ganglia glutamate in patients with major depression’, *Molecular Psychiatry*, 21(10), p. 1351.

Harrison, N.A. *et al.* (2009) ‘Inflammation Causes Mood Changes Through Alterations in Subgenual Cingulate Activity and Mesolimbic Connectivity’, *Biological Psychiatry*, 66(5), pp. 407–414.

Harrison, N.A. *et al.* (2015) ‘Quantitative magnetization transfer imaging as a biomarker for effects of Systemic inflammation on the brain’, *Biological Psychiatry*, 78(1), pp. 49–57.

Harrison, N.A. *et al.* (2016) ‘A Neurocomputational Account of How Inflammation Enhances Sensitivity to Punishments Versus Rewards’, *Biological Psychiatry*, 80(1), p. 73.

Harrison, N.A. (2017) ‘Brain structures implicated in inflammation-associated depression’, in *Current Topics in Behavioral Neurosciences*. Springer Verlag, pp. 221–248.

Hart, B.L. (1988) ‘Biological basis of the behavior of sick animals’, *Neuroscience & Biobehavioral Reviews*, 12(2), pp. 123–137.

Hashimoto, K. (2019) ‘Rapid-acting antidepressant ketamine, its metabolites and other candidates: A historical overview and future perspective’, *Psychiatry and Clinical Neurosciences*, 73(10), p. 613.

Helmut, K. *et al.* (2011) ‘Physiology of microglia’, *Physiological Reviews*, 91(2), pp. 461–553.

Heneka, M.T., Kummer, M.P. and Latz, E. (2014) 'Innate immune activation in neurodegenerative disease', *Nature Reviews Immunology*. Nature Publishing Group, pp. 463–477.

Henry, C.J. *et al.* (2008) 'Minocycline attenuates lipopolysaccharide (LPS)-induced neuroinflammation, sickness behavior, and anhedonia', *Journal of Neuroinflammation*, 5(1), pp. 1–14.

Herder, C. *et al.* (2017) 'Association between pro- and anti-inflammatory cytokines and depressive symptoms in patients with diabetes-potential differences by diabetes type and depression scores', *Translational Psychiatry*, 7(11).

Heuser, I., Yassouridis, A. and Holsboer, F. (1994) 'The combined dexamethasone/CRH test: A refined laboratory test for psychiatric disorders', *Journal of Psychiatric Research*, 28(4), pp. 341–356.

Heyes, M.P. *et al.* (1991) 'Quinolinic acid in cerebrospinal fluid and serum in HIV-1 infection: relationship to clinical and neurological status', *Annals of neurology*, 29(2), pp. 202–209.

Hillmer, A.T. *et al.* (2017) 'Microglial depletion and activation: A [11C]PBR28 PET study in nonhuman primates', *EJNMMI Research*, 7(1), p. 59.

Himmerich, H. *et al.* (2019) 'Cytokine Research in Depression: Principles, Challenges, and Open Questions', *Frontiers in Psychiatry*, 10(FEB), p. 30.

Hinwood, M. *et al.* (2013) 'Chronic stress induced remodeling of the prefrontal cortex: Structural re-organization of microglia and the inhibitory effect of minocycline', *Cerebral Cortex*, 23(8), pp. 1784–1797.

Hirschfeld, R.M. (2000) ‘History and evolution of the monoamine hypothesis of depression.’, *The Journal of clinical psychiatry*, 61 Suppl 6, pp. 4–6.

Holmes, S.E. *et al.* (2018) ‘Elevated Translocator Protein in Anterior Cingulate in Major Depression and a Role for Inflammation in Suicidal Thinking: A Positron Emission Tomography Study’, *Biological Psychiatry*, 83(1), pp. 61–69.

Husain, M.I. *et al.* (2017) ‘Minocycline as an adjunct for treatment-resistant depressive symptoms: A pilot randomised placebo-controlled trial’, *Journal of psychopharmacology (Oxford, England)*, 31(9), pp. 1166–1175.

Husain, M.I. *et al.* (2020) ‘Minocycline and celecoxib as adjunctive treatments for bipolar depression: a multicentre, factorial design randomised controlled trial’, *The lancet. Psychiatry*, 7(6), pp. 515–527.

Ida, T. *et al.* (2008) ‘Cytokine-induced enhancement of calcium-dependent glutamate release from astrocytes mediated by nitric oxide’, *Neuroscience Letters*, 432(3), pp. 232–236.

Imura, H. and Fukata, J.I. (1994) ‘Endocrine–paracine interaction in communication between the immune and endocrine systems. Activation of the hypothalamic-pituitary-adrenal axis in inflammation’, *European Journal of Endocrinology*, 130(1), pp. 32–37.

Ingo, C. *et al.* (2018) ‘Studying neurons and glia non-invasively via anomalous subdiffusion of intracellular metabolites’, *Brain Structure and Function*, 223(8), pp. 3841–3854.

Innis, R.B. *et al.* (2007) ‘Consensus nomenclature for in vivo imaging of reversibly binding radioligands’, *Journal of Cerebral Blood Flow and Metabolism*. SAGE

PublicationsSage UK: London, England, pp. 1533–1539.

Ishikawa, Y. and Furuyashiki, T. (2021) ‘The impact of stress on immune systems and its relevance to mental illness’, *Neuroscience research* [Preprint].

Jacobs, B.L., Van Praag, H. and Gage, F.H. (2000) ‘Adult brain neurogenesis and psychiatry: a novel theory of depression’, *Molecular Psychiatry 2000 5:3*, 5(3), pp. 262–269.

James, M.L. *et al.* (2008) ‘DPA-714, a New Translocator Protein–Specific Ligand: Synthesis, Radiofluorination, and Pharmacologic Characterization’, *Journal of Nuclear Medicine*, 49(5), pp. 814–822.

Kappelmann, N. *et al.* (2021) ‘Dissecting the Association Between Inflammation, Metabolic Dysregulation, and Specific Depressive Symptoms: A Genetic Correlation and 2-Sample Mendelian Randomization Study’, *JAMA psychiatry*, 78(2), pp. 161–170.

Kast, R.E. (2003) ‘Anti- and pro-inflammatory considerations in antidepressant use during medical illness: bupropion lowers and mirtazapine increases circulating tumor necrosis factor-alpha levels’, *General Hospital Psychiatry*, 25(6), pp. 495–496.

Kazumori, H. *et al.* (2004) ‘Transforming growth factor-α directly augments histidine decarboxylase and vesicular monoamine transporter 2 production in rat enterochromaffin-like cells’, *American Journal of Physiology - Gastrointestinal and Liver Physiology*, 286(3 49-3), pp. 508–514.

Kenis, G. and Maes, M. (2002) ‘Effects of antidepressants on the production of cytokines’, *International Journal of Neuropsychopharmacology*, 5(4), pp. 401–412.

Kent, S. *et al.* (1996) ‘Mechanisms of sickness-induced decreases in food-motivated

behavior', *Neuroscience & Biobehavioral Reviews*, 20(1), pp. 171–175.

Kettenmann, H. *et al.* (2011) 'Physiology of Microglia', *Physiological Reviews*, 91(2), pp. 461–553.

Khandaker, G. *et al.* (eds) (2021) *Textbook of Immunopsychiatry*. Cambridge University Press.

Kitzbichler, M.G. *et al.* (2021) 'Peripheral inflammation is associated with micro-structural and functional connectivity changes in depression-related brain networks', *Molecular Psychiatry 2021 26:12*, 26(12), pp. 7346–7354.

Kobayashi, K. *et al.* (2013) 'Minocycline selectively inhibits M1 polarization of microglia', *Cell Death & Disease 2013 4:3*, 4(3), pp. e525–e525.

Köhler, O. *et al.* (2014) 'Effect of Anti-inflammatory Treatment on Depression, Depressive Symptoms, and Adverse Effects: A Systematic Review and Meta-analysis of Randomized Clinical Trials', *JAMA Psychiatry*, 71(12), pp. 1381–1391.

Kraynak, T.E. *et al.* (2018) 'Functional neuroanatomy of peripheral inflammatory physiology: A meta-analysis of human neuroimaging studies', *Neuroscience and Biobehavioral Reviews*. Elsevier Ltd, pp. 76–92.

Kreisl, W.C. *et al.* (2020) 'PET Imaging of Neuroinflammation in Neurological Disorders', *The Lancet. Neurology*, 19(11), p. 940.

Kreutzberg, G.W. (1996) 'Microglia: A sensor for pathological events in the CNS', *Trends in Neurosciences*, 19(8), pp. 312–318.

Kristiansson, M. *et al.* (2015) 'Urban air pollution, poverty, violence and health--

Neurological and immunological aspects as mediating factors', *Environmental research*, 140, pp. 511–513.

Kronfol, Z. (2002) 'Immune dysregulation in major depression: a critical review of existing evidence.', *The International Journal of Neuropsychopharmacology*, 5(4), pp. 333–343.

Krügel, U. *et al.* (2013) 'Antidepressant effects of TNF- a blockade in an animal model of depression', *Journal of Psychiatric Research*, 47(5), pp. 611–616.

Kuwabara, T. *et al.* (2017) 'The Role of IL-17 and Related Cytokines in Inflammatory Autoimmune Diseases', *Mediators of Inflammation*, 2017.

Lam, D., Lively, S. and Schlichter, L.C. (2017) 'Responses of rat and mouse primary microglia to pro- and anti-inflammatory stimuli: Molecular profiles, K+channels and migration', *Journal of Neuroinflammation*, 14(1), pp. 1–30.

Lanquillon, S. *et al.* (2000) 'Cytokine production and treatment response in major depressive disorder', *Neuropsychopharmacology*, 22(4), pp. 370–379.

Lasselin, J., Treadway, M.T., *et al.* (2016) 'Lipopolysaccharide Alters Motivated Behavior in a Monetary Reward Task: a Randomized Trial', *Neuropsychopharmacology 2017 42:4*, 42(4), pp. 801–810.

Lasselin, J., Elsenbruch, S., *et al.* (2016) 'Mood disturbance during experimental endotoxemia: Predictors of state anxiety as a psychological component of sickness behavior', *Brain, behavior, and immunity*, 57, pp. 30–37.

Lasselin, J., Schedlowski, M., *et al.* (2020) 'Comparison of bacterial lipopolysaccharide-induced sickness behavior in rodents and humans: Relevance for symptoms of anxiety

and depression', *Neuroscience and biobehavioral reviews*, 115, pp. 15–24.

Lasselin, J., Benson, S., *et al.* (2020) 'Immunological and behavioral responses to in vivo lipopolysaccharide administration in young and healthy obese and normal-weight humans', *Brain, Behavior, and Immunity*, 88, pp. 283–293.

Lasselin, J., Lekander, M., *et al.* (2020) 'Sick for science: experimental endotoxemia as a translational tool to develop and test new therapies for inflammation-associated depression', *Molecular Psychiatry* [Preprint].

Lavisse, S. *et al.* (2012) 'Reactive Astrocytes Overexpress TSPO and Are Detected by TSPO Positron Emission Tomography Imaging', *The Journal of Neuroscience*, 32(32), p. 10809.

Lavisse, S. *et al.* (2015) 'Optimized Quantification of Translocator Protein Radioligand 18F-DPA-714 Uptake in the Brain of Genotyped Healthy Volunteers', *Journal of Nuclear Medicine*, 56(7), pp. 1048–1054.

Laye, S. *et al.* (1995) 'Subdiaphragmatic vagotomy blocks induction of IL-1 beta mRNA in mice brain in response to peripheral LPS', *The American journal of physiology*, 268(5 Pt 2).

Li, Q. and Barres, B.A. (2017) 'Microglia and macrophages in brain homeostasis and disease', *Nature Reviews Immunology 2017 18:4*, 18(4), pp. 225–242.

Liddelow, S.A. *et al.* (2017) 'Neurotoxic reactive astrocytes are induced by activated microglia', *Nature*, 541(7638), pp. 481–487.

Ligneul, C. *et al.* (2019) 'Diffusion-weighted magnetic resonance spectroscopy enables cell-specific monitoring of astrocyte reactivity in vivo', *NeuroImage*, 191, pp. 457–469.

Lively, S. and Schlichter, L.C. (2018) 'Microglia responses to pro-inflammatory stimuli (LPS, IFNγ+TNFα) and reprogramming by resolving cytokines (IL-4, IL-10)', *Frontiers in Cellular Neuroscience*, 12.

Lockhart, A. *et al.* (2003) 'The peripheral benzodiazepine receptor ligand PK11195 binds with high affinity to the acute phase reactant α1-acid glycoprotein: implications for the use of the ligand as a CNS inflammatory marker', *Nuclear Medicine and Biology*, 30(2), pp. 199–206.

Logan, J. *et al.* (1996) 'Distribution volume ratios without blood sampling from graphical analysis of PET data', *Journal of Cerebral Blood Flow and Metabolism*, 16(5), pp. 834–840.

Loggia, M.L. *et al.* (2015) 'Evidence for brain glial activation in chronic pain patients', *Brain*, 138(3), p. 604.

Lowry, S.F. (2005) 'Human endotoxemia: A model for mechanistic insight and therapeutic targeting', *Shock*, 24(SUPPL. 1), pp. 94–100.

Lucido, M.J. *et al.* (2021) 'Aiding and Abetting Anhedonia: Impact of Inflammation on the Brain and Pharmacological Implications', *Pharmacological Reviews*, 73(3), pp. 1084–1117.

Luheshi, G.N. *et al.* (2000) 'Vagotomy attenuates the behavioural but not the pyrogenic effects of interleukin-1 in rats', *Autonomic neuroscience : basic & clinical*, 85(1–3), pp. 127–132.

Lyoo, C.H. *et al.* (2015) 'Cerebellum can serve as a pseudo-reference region in Alzheimer disease to detect neuroinflammation measured with PET radioligand binding to

translocator protein', *Journal of Nuclear Medicine*, 56(5), pp. 701–706.

Mabrouk, R. *et al.* (2017) 'Feasibility study of TSPO quantification with [18F]FEPPA using population-based input function', *PLOS ONE*. Edited by P. Garg, 12(5), p. e0177785.

Maes, M. *et al.* (1990) 'The decreased availability of L-tryptophan in depressed females: Clinical and biological correlates', *Progress in Neuro-Psychopharmacology and Biological Psychiatry*, 14(6), pp. 903–919.

Maes, M., Lambrechts, J., *et al.* (1992) 'Evidence for a systemic immune activation during depression: results of leukocyte enumeration by flow cytometry in conjunction with monoclonal antibody staining', *Psychological medicine*, 22(1), pp. 45–53.

Maes, M., Scharpé, S., *et al.* (1992) 'Higher α1-antitrypsin, haptoglobin, ceruloplasmin and lower retinol binding protein plasma levels during depression: Further evidence for the existence of an inflammatory response during that illness', *Journal of Affective Disorders*, 24(3), pp. 183–192.

Maes, M. *et al.* (1993) 'Relationships between interleukin-6 activity, acute phase proteins, and function of the hypothalamic-pituitary-adrenal axis in severe depression', *Psychiatry Research*, 49(1), pp. 11–27.

Maes, M. *et al.* (1997) 'Increased serum IL-6 and IL-1 receptor antagonist concentrations in major depression and treatment resistant depression', *Cytokine*, 9(11), pp. 853–858.

Maes, M. *et al.* (2011) 'Progress in Neuro-Psychopharmacology & Biological Psychiatry The new " 5-HT " hypothesis of depression : Cell-mediated immune activation induces indoleamine 2 , 3-dioxygenase , which leads to lower plasma tryptophan and an increased

synthesis of detriment', *Progress in Neuropsychopharmacology & Biological Psychiatry*, 35(3), pp. 702–721.

Mak, J.C. and Barnes, P.J. (1990) 'Peripheral type benzodiazepine receptors in human and guinea pig lung: characterization and autoradiographic mapping.', *Journal of Pharmacology and Experimental Therapeutics*, 252(2).

Maness, L.M. *et al.* (1995) 'Selective transport of blood-borne interleukin-1α into the posterior division of the septum of the mouse brain', *Brain Research*, 700(1–2), pp. 83–88.

Maness, L.M., Kastin, A.J. and Banks, W.A. (1998) 'Relative contributions of a CVO and the microvascular bed to delivery of blood-borne IL-1alpha to the brain', *The American journal of physiology*, 275(2).

Marin, I.A. and Kipnis, J. (2017) 'Central Nervous System: (Immunological) Ivory Tower or Not', *Neuropsychopharmacology*, 42(1), pp. 28–35.

Marques, F. *et al.* (2009) 'The choroid plexus response to a repeated peripheral inflammatory stimulus', *BMC Neuroscience*, 10, p. 135.

Mazza, M.G. *et al.* (2018) 'Neutrophil/lymphocyte ratio and platelet/lymphocyte ratio in mood disorders: A meta-analysis', *Progress in neuro-psychopharmacology & biological psychiatry*, 84(Pt A), pp. 229–236.

McGeer, P.L. and McGeer, E.G. (2002) 'Inflammatory processes in amyotrophic lateral sclerosis', *Muscle and Nerve*, pp. 459–470.

Meyer, J.H. *et al.* (2020) 'Neuroinflammation in psychiatric disorders: PET imaging and promising new targets', *The lancet. Psychiatry*, 7(12), p. 1064.

Michopoulos, V. *et al.* (2015) 'CRP genetic variation and CRP levels are associated with increased PTSD symptoms and physiological responses in a highly traumatized civilian population', *The American journal of psychiatry*, 172(4), p. 353.

Milaneschi, Y. *et al.* (2021) 'Association of inflammation with depression and anxiety: evidence for symptom-specificity and potential causality from UK Biobank and NESDA cohorts', *Molecular Psychiatry*, 26(12), p. 7393.

Mildner, A. *et al.* (2008) 'Ly-6G+CCR2- Myeloid Cells Rather Than Ly-6ChighCCR2+ Monocytes Are Required for the Control of Bacterial Infection in the Central Nervous System', *The Journal of Immunology*, 181(4), pp. 2713–2722.

Miller, A.H., Maletic, V. and Raison, C.L. (2009) 'Inflammation and Its Discontents: The Role of Cytokines in the Pathophysiology of Major Depression', *Biological psychiatry*, 65(9), p. 732.

Miller, A.H. and Pariante, C.M. (2020) 'Trial failures of anti-inflammatory drugs in depression', *The Lancet Psychiatry*, 7(10), p. 837.

Miller, A.H. and Raison, C.L. (2016) 'The role of inflammation in depression: From evolutionary imperative to modern treatment target', *Nature Reviews Immunology*, 16(1), pp. 22–34.

Moieni, M. *et al.* (2019) 'Sex differences in the relationship between inflammation and reward sensitivity: A randomized controlled trial of endotoxin', *Biological psychiatry. Cognitive neuroscience and neuroimaging*, 4(7), p. 619.

Mukherjee, S. *et al.* (2009) 'Lipopolysaccharide-driven Th2 cytokine production in macrophages is regulated by both MyD88 and TRAM', *Journal of Biological Chemistry*, 225

284(43), pp. 29391–29398.

Muscatell, K.A. *et al.* (2016) 'Exposure to an inflammatory challenge enhances neural sensitivity to negative and positive social feedback', *Brain, behavior, and immunity*, 57, pp. 21–29.

Musselman, D.L. *et al.* (2001) 'Paroxetine for the Prevention of Depression Induced by High-Dose Interferon Alfa', *New England Journal of Medicine*, 344(13), pp. 961–966.

Najjar, S. *et al.* (2013) 'Neuroinflammation and psychiatric illness', *Journal of Neuroinflammation*. BioMed Central, pp. 1–24.

Nam, H.Y. *et al.* (2018) 'Ibrutinib suppresses LPS-induced neuroinflammatory responses in BV2 microglial cells and wild-type mice', *Journal of Neuroinflammation*, 15(1), pp. 1–22.

Nava Catorce, M. and Gevorkian, G. (2016) 'LPS-induced Murine Neuroinflammation Model: Main Features and Suitability for Pre-clinical Assessment of Nutraceuticals', *Current Neuropharmacology*, 14(2), pp. 155–164.

Nestler, E.J. and Carlezon, W.A. (2006) 'The Mesolimbic Dopamine Reward Circuit in Depression', *Biological Psychiatry*, 59(12), pp. 1151–1159.

Nettis, M.A. *et al.* (2020) 'PET imaging shows no changes in TSPO brain density after IFN-α immune challenge in healthy human volunteers', *Translational Psychiatry*, 10(1), pp. 1–11.

Nettis, M.A. *et al.* (2021) 'Augmentation therapy with minocycline in treatment-resistant depression patients with low-grade peripheral inflammation: results from a double-blind randomised clinical trial', *Neuropsychopharmacology 2021 46:5*, 46(5), pp. 939–948.

Nettis, M.A. (2021) ‘Minocycline in Major Depressive Disorder: And overview with considerations on treatment-resistance and comparisons with other psychiatric disorders’, *Brain, Behavior, & Immunity - Health*, 17, p. 100335.

Neumann, H., Kotter, M.R. and Franklin, R.J.M. (2009) ‘Debris clearance by microglia: an essential link between degeneration and regeneration’, *Brain*, 132(2), p. 288.

Neurauter, G. *et al.* (2008) ‘Chronic Immune Stimulation Correlates with Reduced Phenylalanine Turnover’, *Current Drug Metabolism*, 9(7), pp. 622–627.

Nikodemova, M., Duncan, I.D. and Watters, J.J. (2006) ‘Minocycline exerts inhibitory effects on multiple mitogen-activated protein kinases and IκBα degradation in a stimulus-specific manner in microglia’, *Journal of Neurochemistry*, 96(2), pp. 314–323.

Nimmerjahn, A., Kirchhoff, F. and Helmchen, F. (2005) ‘Resting Microglial Cells Are Highly Dynamic Surveillants of Brain Parenchyma in Vivo’, 308(May), pp. 1314–1319.

Noble, W. *et al.* (2009) ‘Minocycline reduces the development of abnormal tau species in models of Alzheimer’s disease’, *FASEB journal : official publication of the Federation of American Societies for Experimental Biology*, 23(3), pp. 739–750.

Notter, T. *et al.* (2020) ‘Neuronal activity increases translocator protein (TSPO) levels’, *Molecular Psychiatry*, pp. 1–13.

Nutma, E. *et al.* (2019) ‘A quantitative neuropathological assessment of translocator protein expression in multiple sclerosis’, *Brain*, 142(11), pp. 3440–3455.

O’Connor, J.C., Lawson, M.A., Andre, C., *et al.* (2009) ‘Induction of IDO by Bacille Calmette-Guerin Is Responsible for Development of Murine Depressive-Like Behavior’, *The Journal of Immunology*, 182(5), pp. 3202–3212.

O'Connor, J.C., Lawson, M.A., André, C., *et al.* (2009) 'Lipopolysaccharide-induced depressive-like behavior is mediated by indoleamine 2,3-dioxygenase activation in mice', *Molecular psychiatry*, 14(5), p. 511.

Orihuela, R., McPherson, C.A. and Harry, G.J. (2016) 'Microglial M1/M2 polarization and metabolic states', *British Journal of Pharmacology*, 173(4), pp. 649–665.

Owen, D.R. *et al.* (2017) 'TSPO mutations in rats and a human polymorphism impair the rate of steroid synthesis', *The Biochemical journal*, 474(23), pp. 3985–3999.

Owen, D.R.J. *et al.* (2011) 'Mixed-Affinity Binding in Humans with 18-kDa Translocator Protein Ligands', *Journal of nuclear medicine : official publication, Society of Nuclear Medicine*, 52(1), p. 24.

Owens, M.J. and Nemeroff, C.B. (1993) 'The Role of Corticotropin-Releasing Factor in the Pathophysiology of Affective and Anxiety Disorders: Laboratory and Clinical Studies', *Ciba Foundation symposium*, 172, pp. 296–316.

Palombo, M. *et al.* (2018) 'Insights into brain microstructure from in vivo DW-MRS', *NeuroImage*. Academic Press Inc., pp. 97–116.

Pandey, G.N. *et al.* (2019) 'Innate immunity in the postmortem brain of depressed and suicide subjects: role of Toll-like receptors', *Brain, behavior, and immunity*, 75, p. 101.

Papadopoulos, V. *et al.* (2006) 'Translocator protein (18 kDa): new nomenclature for the peripheral-type benzodiazepine receptor based on its structure and molecular function', *Trends in Pharmacological Sciences*, 27(8), pp. 402–409.

Pariante, C.M. *et al.* (1999) 'The Proinflammatory Cytokine, Interleukin-1α, Reduces Glucocorticoid Receptor Translocation and Function', *Endocrinology*, 140(9), pp. 4359–

4366.

Pariante, C.M. (2017) ‘Why are depressed patients inflamed? A reflection on 20 years of research on depression, glucocorticoid resistance and inflammation’, *European Neuropsychopharmacology*, 27(6), pp. 554–559.

Paugh, S.W. *et al.* (2015) ‘NALP3 inflammasome upregulation and CASP1 cleavage of the glucocorticoid receptor cause glucocorticoid resistance in leukemia cells’, *Nature genetics*, 47(6), pp. 607–614.

Pavlov, V.A. and Tracey, K.J. (2012) ‘The vagus nerve and the inflammatory reflex—linking immunity and metabolism’, *Nature reviews. Endocrinology*, 8(12), p. 743.

Perrin, A.J. *et al.* (2019) ‘Glucocorticoid resistance: Is it a requisite for increased cytokine production in depression? A systematic review and meta-analysis.’, *Frontiers in Psychiatry*, 10(MAY), p. 423.

Perry, V.H. and Holmes, C. (2014) ‘Microglial priming in neurodegenerative disease’, *Nature Reviews Neurology*. Nature Publishing Group, pp. 217–224.

Pessiglione, M. *et al.* (2006) ‘Dopamine-dependent prediction errors underpin reward-seeking behaviour in humans’, *Nature 2006 442:7106*, 442(7106), pp. 1042–1045.

Peters van Ton, A.M. *et al.* (2021) ‘Human in vivo neuroimaging to detect reprogramming of the cerebral immune response following repeated systemic inflammation’, *Brain, Behavior, and Immunity*, 95, pp. 321–329.

Petrulli, J.R. *et al.* (2017) ‘Systemic inflammation enhances stimulant-induced striatal dopamine elevation’, *Translational Psychiatry*, 7(3), p. e1076.

Peyronneau, M.A. *et al.* (2013) 'Metabolism and quantification of [18F]DPA-714, a new TSPO positron emission tomography radioligand', *Drug Metabolism and Disposition*, 41(1), pp. 122–131.

Pierpaoli, C. and Basser, P.J. (1996) *Toward a Quantitative Assessment of Diffusion Anisotropy*.

Plane, J.M. *et al.* (2010) 'Prospects for Minocycline Neuroprotection', *Archives of neurology*, 67(12), p. 1442.

Plotkin, S.R., BanksP, W.A. and Kastin, A.J. (1996) 'Comparison of saturable transport and extracellular pathways in the passage of interleukin-1 alpha across the blood-brain barrier', *Journal of neuroimmunology*, 67(1), pp. 41–47.

Pugh, C.R. *et al.* (1998) 'Selective effects of peripheral lipopolysaccharide administration on contextual and auditory-cue fear conditioning', *Brain, Behavior, and Immunity*, 12(3), pp. 212–229.

Quan, N., Whiteside, M. and Herkenham, M. (1998) 'Time course and localization patterns of interleukin-1β messenger RNA expression in brain and pituitary after peripheral administration of lipopolysaccharide', *Neuroscience*, 83(1), pp. 281–293.

Raison, C.L. *et al.* (2009) 'Activation of CNS Inflammatory Pathways by Interferon-alpha: Relationship to Monoamines and Depression', *Biological psychiatry*, 65(4), p. 296.

Raison, C.L. *et al.* (2013) 'A Randomized Controlled Trial of the Tumor Necrosis Factor-alpha Antagonist Infliximab in Treatment Resistant Depression: Role of Baseline Inflammatory Biomarkers', *JAMA psychiatry*, 70(1), p. 31.

Raison, C.L., Capuron, L. and Miller, A.H. (2006) 'Cytokines sing the blues :

inflammation and the pathogenesis of depression', 27(1).

Reis, D.J., Casteen, E.J. and Ilardi, S.S. (2019) 'The antidepressant impact of minocycline in rodents: A systematic review and meta-analysis', *Scientific Reports 2019 9:1*, 9(1), pp. 1–11.

Reischauer, C. *et al.* (2018) 'In-vivo evaluation of neuronal and glial changes in amyotrophic lateral sclerosis with diffusion tensor spectroscopy', *NeuroImage: Clinical*, 20, pp. 993–1000.

Richards, E.M. *et al.* (2018) 'PET radioligand binding to translocator protein (TSPO) is increased in unmedicated depressed subjects', *EJNMMI Research*, 8.

Rivest, S. (2003) 'Molecular insights on the cerebral innate immune system', *Brain, Behavior, and Immunity*, 17(1), pp. 13–19.

Rizzo, G. *et al.* (2019) 'Generalization of endothelial modelling of TSPO PET imaging:Considerations on tracer affinities', *Journal of Cerebral Blood Flow & Metabolism*, 39(5), p. 874.

Rupprecht, R. *et al.* (2010) 'Translocator protein (18 kDa) (TSPO) as a therapeutic target for neurological and psychiatric disorders', *Nature Reviews Drug Discovery 2010 9:12*, 9(12), pp. 971–988.

Ryu, K.Y. *et al.* (2019) 'Dasatinib regulates LPS-induced microglial and astrocytic neuroinflammatory responses by inhibiting AKT/STAT3 signaling', *Journal of Neuroinflammation*, 16(1), p. 190.

Sanacora, G., Treccani, G. and Popoli, M. (2012) 'Towards a glutamate hypothesis of depression: an emerging frontier of neuropsychopharmacology for mood disorders.',

Neuropharmacology, 62(1), pp. 63–77.

Sandiego, C.M. *et al.* (2015) 'Imaging robust microglial activation after lipopolysaccharide administration in humans with PET', *Proceedings of the National Academy of Sciences*, 112(40), pp. 12468–12473.

Dos Santos, S.E. *et al.* (2020) 'Similar Microglial Cell Densities across Brain Structures and Mammalian Species: Implications for Brain Tissue Function', *Journal of Neuroscience*, 40(24), pp. 4622–4643.

Sapolsky, R.M., Romero, L.M. and Munck, A.U. (2000) 'How Do Glucocorticoids Influence Stress Responses? Integrating Permissive, Suppressive, Stimulatory, and Preparative Actions*'. Available at: https://academic.oup.com/edrv/article-abstract/21/1/55/2423840 (Accessed: 15 December 2022).

Savage, J.C. *et al.* (2019) 'Microglial Ultrastructure in the Hippocampus of a Lipopolysaccharide-Induced Sickness Mouse Model', *Frontiers in Neuroscience*, 13, p. 1340.

Savitz, J. *et al.* (2013) 'Inflammation and Neurological Disease-Related Genes are Differentially Expressed in Depressed Patients with Mood Disorders and Correlate with Morphometric and Functional Imaging Abnormalities', *Brain, behavior, and immunity*, 31, p. 161.

Savitz, J. *et al.* (2015) 'Activation of the kynurenine pathway is associated with striatal volume in major depressive disorder', *Psychoneuroendocrinology*, 62, p. 54.

Schafer, D. *et al.* (2012) 'Microglia sculpt postnatal neuronal circuits in an activivty and complement-dependent manner', *Neuron*, 74(4), pp. 691–705.

Schetters, S.T.T. *et al.* (2018) 'Neuroinflammation: Microglia and T cells get ready to tango', *Frontiers in Immunology*, 8(JAN), p. 1905.

Schmidt, F.M. *et al.* (2015) 'Inflammatory cytokines in general and central obesity and modulating effects of physical Activity', *PLoS ONE*, 10(3).

Schubert, J. *et al.* (2021) 'Supervised clustering for TSPO PET imaging', *European Journal of Nuclear Medicine and Molecular Imaging* [Preprint].

Schubert, J.J. *et al.* (2021) 'A Modest Increase in 11C-PK11195-Positron Emission Tomography TSPO Binding in Depression Is Not Associated With Serum C-Reactive Protein or Body Mass Index', *Biological Psychiatry. Cognitive Neuroscience and Neuroimaging*, 6(7), p. 716.

Schultz, W., Dayan, P. and Montague, P.R. (1997) 'A neural substrate of prediction and reward', *Science (New York, N.Y.)*, 275(5306), pp. 1593–1599.

Schwarcz, R. and Pellicciari, R. (2002) 'Manipulation of Brain Kynurenines: Glial Targets, Neuronal Effects, and Clinical Opportunities', *Journal of Pharmacology and Experimental Therapeutics*, 303(1), pp. 1–10.

Scott, G. *et al.* (2018) 'Minocycline reduces chronic microglial activation after brain trauma but increases neurodegeneration', *Brain*, 141(2), pp. 459–471.

Setiawan, E. *et al.* (2015) 'Role of translocator protein density, a marker of neuroinflammation, in the brain during major depressive episodes', *JAMA Psychiatry*, 72(3), pp. 268–275.

Shelton, R.C. *et al.* (2011) 'ALTERED EXPRESSION OF GENES INVOLVED IN INFLAMMATION AND APOPTOSIS IN FRONTAL CORTEX IN MAJOR

DEPRESSION', *Molecular psychiatry*, 16(7), p. 751.

Shore, P.A., Silver, S.L. and Brodie, B.B. (1955) 'Interaction of Reserpine, Serotonin, and Lysergic Acid Diethylamide in Brain', *Science*, 122(3163), pp. 284–285.

Silverman, M.N. and Sternberg, E.M. (2012) 'Glucocorticoid regulation of inflammation and its functional correlates: from HPA axis to glucocorticoid receptor dysfunction', *Annals of the New York Academy of Sciences*, 1261(1), pp. 55–63.

Smith, S.M. and Vale, W.W. (2006) 'The role of the hypothalamic-pituitary-adrenal axis in neuroendocrine responses to stress', *Dialogues in Clinical Neuroscience*, 8(4), p. 383.

Soczynska, J.K. *et al.* (2012) 'Novel therapeutic targets in depression: Minocycline as a candidate treatment', *Behavioural Brain Research*, 235, pp. 302–317.

Sofroniew, M. V. and Vinters, H. V. (2010) 'Astrocytes: Biology and pathology', *Acta Neuropathologica*. Springer, pp. 7–35.

Spahn, J.D. *et al.* (1996) 'A novel action of IL-13: induction of diminished monocyte glucocorticoid receptor-binding affinity.', *The Journal of Immunology*, 157(6), pp. 2654–2659.

Steiner, J. *et al.* (2011) 'Severe depression is associated with increased microglial quinolinic acid in subregions of the anterior cingulate gyrus: Evidence for an immune-modulated glutamatergic neurotransmission?', *Journal of Neuroinflammation*, 8(1), p. 94.

Stone, T.W. (2001) *Kynurenines in the CNS: From endogenous obscurity to therapeutic importance*, *Progress in Neurobiology*.

Stratoulias, V. *et al.* (2019) 'Microglial subtypes: diversity within the microglial community', *The EMBO Journal*, 38(17), p. e101997.

Strike, P.C., Wardle, J. and Steptoe, A. (2004) 'Mild acute inflammatory stimulation induces transient negative mood', *Journal of Psychosomatic Research*, 57(2), pp. 189–194.

Suffredini, A.F. and Noveck, R.J. (2014) 'Human Endotoxin Administration as an Experimental Model in Drug Development', *Clinical Pharmacology and Therapeutics*, 96(4), pp. 418–422.

Sullivan, P.F., Neale, M.C. and Kendler, K.S. (2000) 'Genetic epidemiology of major depression: Review and meta-analysis', *American Journal of Psychiatry*, 157(10), pp. 1552–1562.

Tai, K. *et al.* (2013) 'Minocycline modulates cytokine and chemokine production in lipopolysaccharide-stimulated THP-1 monocytic cells by inhibiting IκB kinase α/β phosphorylation', *Translational Research*, 161(2), pp. 99–109.

Tavares, R.G. *et al.* (2002) 'Quinolinic acid stimulates synaptosomal glutamate release and inhibits glutamate uptake into astrocytes', *Neurochemistry International*, 40(7), pp. 621–627.

Taylor, J.L. and Grossberg, S.E. (1998) 'The effects of interferon-alpha on the production and action of other cytokines', *Seminars in oncology*, 25(1 Suppl 1), pp. 23–29. Available at: https://pubmed.ncbi.nlm.nih.gov/9482537/ (Accessed: 19 December 2022).

Tilleux, S. and Hermans, E. (2007) 'Neuroinflammation and regulation of glial glutamate uptake in neurological disorders', *Journal of neuroscience research*, 85(10), pp. 2059–235

2070.

Torres-Platas, S.G. *et al.* (2014) 'Evidence for increased microglial priming and macrophage recruitment in the dorsal anterior cingulate white matter of depressed suicides', *Brain, Behavior, and Immunity*, 42, pp. 50–59.

Tournier, B.B. *et al.* (2020) 'Fluorescence-activated cell sorting to reveal the cell origin of radioligand binding', *Journal of Cerebral Blood Flow and Metabolism*, 40(6), pp. 1242–1255.

Tracey, K.J. (2007) 'Physiology and immunology of the cholinergic antiinflammatory pathway', *Journal of Clinical Investigation*. American Society for Clinical Investigation, pp. 289–296.

Tuisku, J. *et al.* (2019) 'Effects of age, BMI and sex on the glial cell marker TSPO — a multicentre [11C]PBR28 HRRT PET study', *European Journal of Nuclear Medicine and Molecular Imaging*, 46(11), pp. 2329–2338.

Turkheimer, F.E. *et al.* (2015) 'The methodology of TSPO imaging with positron emission tomography', *Biochemical Society Transactions*. Portland Press Ltd, pp. 586–592.

Tziortzi, A.C. *et al.* (2011) 'Imaging dopamine receptors in humans with [11C]-(+)-PHNO: Dissection of D3 signal and anatomy', *NeuroImage*, 54(1), pp. 264–277.

Udina, M. *et al.* (2012) 'Interferon-induced depression in chronic hepatitis C: a systematic review and meta-analysis', *The Journal of clinical psychiatry*, 73(8), pp. 1128–1138.

Urenjak, J. *et al.* (1993) *Proton Nuclear Magnetic Resonance Spectroscopy Unambiguously Identifies Different Neural Cell Types*.

Varatharaj, A. and Galea, I. (2017) 'The blood-brain barrier in systemic inflammation', *Brain, Behavior, and Immunity*. Academic Press Inc., pp. 1–12.

Veiga, S. *et al.* (2007) 'Translocator protein (18 kDa) is involved in the regulation of reactive gliosis', *GLIA*, 55(14), pp. 1426–1436.

Venneti, S., Lopresti, B.J. and Wiley, C.A. (2006) 'The peripheral benzodiazepine receptor (Translocator protein 18 kDa) in microglia: From pathology to imaging', *Progress in Neurobiology*, 80(6), pp. 308–322.

Vereker, E., O'Donnell, E. and Lynch, M.A. (2000) 'The inhibitory effect of interleukin-1beta on long-term potentiation is coupled with increased activity of stress-activated protein kinases', *The Journal of Neuroscience*, 20(18), pp. 6811–6819.

Vicente-Rodríguez, M. *et al.* (2021) 'Resolving the cellular specificity of TSPO imaging in a rat model of peripherally-induced neuroinflammation', *Brain, Behavior, and Immunity* [Preprint].

Vignal, N. *et al.* (2018) '[18F]FEPPA a TSPO radioligand: Optimized radiosynthesis and evaluation as a PET radiotracer for brain inflammation in a peripheral LPS-injected mouse model', *Molecules*, 23(6).

Voineskos, D., Daskalakis, Z.J. and Blumberger, D.M. (2020) 'Management of Treatment-Resistant Depression: Challenges and Strategies', *Neuropsychiatric Disease and Treatment*, 16, p. 221.

van Wageningen, T.A. *et al.* (2021) 'Viscoelastic properties of white and gray matter-derived microglia differentiate upon treatment with lipopolysaccharide but not upon treatment with myelin', *Journal of Neuroinflammation*, 18(1), pp. 1–15.

Walker, A.K. *et al.* (2013) 'NMDA receptor blockade by ketamine abrogates lipopolysaccharide-induced depressive-like behavior in C57BL/6J mice', *Neuropsychopharmacology*, 38(9), pp. 1609–1616.

Wan, W. *et al.* (1994) 'Neural and biochemical mediators of endotoxin and stress-induced c-fos expression in the rat brain', *Brain Research Bulletin*, 34(1), pp. 7–14.

Wang, L. *et al.* (2019) 'Effects of SSRIs on peripheral inflammatory markers in patients with major depressive disorder: A systematic review and meta-analysis', *Brain, Behavior, and Immunity*, 79, pp. 24–38.

Webster, J.I. and Sternberg, E.M. (2004) 'Role of the hypothalamic-pituitary-adrenal axis, glucocorticoids and glucocorticoid receptors in toxic sequelae of exposure to bacterial and viral products', *The Journal of endocrinology*, 181(2), pp. 207–221.

Wegner, A. *et al.* (2017) 'Sex differences in the pro-inflammatory cytokine response to endotoxin unfold in vivo but not ex vivo in healthy humans', *Innate immunity*, 23(5), pp. 432–439.

Wimberley, C. *et al.* (2021) 'Kinetic modeling and parameter estimation of TSPO PET imaging in the human brain', *European Journal of Nuclear Medicine and Molecular Imaging*, 49(1), pp. 246–256.

Wohleb, E.S. *et al.* (2013) 'Stress-Induced Recruitment of Bone Marrow-Derived Monocytes to the Brain Promotes Anxiety-Like Behavior', 33(34), pp. 13820–13833.

Wohleb, E.S. *et al.* (2015) 'Monocyte trafficking to the brain with stress and inflammation : a novel axis of immune-to-brain communication that influences mood and behavior', 8(January), pp. 1–17.

Woodcock, E.A. *et al.* (2020) 'Quantification of [11C]PBR28 data after systemic lipopolysaccharide challenge', *EJNMMI Research*, 10(1), p. 19.

Woodcock, E.A. *et al.* (2021) 'Acute neuroimmune stimulation impairs verbal memory in adults: A PET brain imaging study', *Brain, behavior, and immunity*, 91, p. 784.

Yang, Q. *et al.* (2020) 'Chronic minocycline treatment exerts antidepressant effect, inhibits neuroinflammation, and modulates gut microbiota in mice', *Psychopharmacology*, 237(10), pp. 3201–3213.

Yang, X. *et al.* (2019) 'Bacterial Endotoxin Activates the Coagulation Cascade through Gasdermin D-Dependent Phosphatidylserine Exposure Activation of GSDMD by caspase-11 triggers Ca 2+-dependent PS exposure through TMEM16F', *Immunity*, 51, pp. 983-996.e6.

Yaqub, M. *et al.* (2012) 'Optimization of supervised cluster analysis for extracting reference tissue input curves in (R)-[11C]PK11195 brain PET studies', *Journal of Cerebral Blood Flow & Metabolism*, 32(8), p. 1600.

Yaqub, M. *et al.* (2018) 'In vivo assessment of neuroinflammation in progressive multiple sclerosis: a proof of concept study with [18F]DPA714 PET', *Journal of Neuroinflammation*, 15(1), pp. 4–13.

Yirmiya, R. (1996) 'Endotoxin produces a depressive-like episode in rats', *Brain Research*, 711(1–2), pp. 163–174.

Yirmiya, R., Rimmerman, N. and Reshef, R. (2015) 'Depression as a Microglial Disease', *Trends in Neurosciences*, 38(10), pp. 637–658.

Yoder, K.K. *et al.* (2015) 'Comparison of standardized uptake values with volume of

distribution for quantitation of [11C]PBR28 brain uptake', *Nuclear Medicine and Biology*, 42(3), pp. 305–308.

Yrjänheikki, J. *et al.* (1998) 'Tetracyclines inhibit microglial activation and are neuroprotective in global brain ischemia', *Proceedings of the National Academy of Sciences of the United States of America*, 95(26), p. 15769.

Zanotti-Fregonara, P. *et al.* (2011) 'Image-derived input function for brain PET studies: Many challenges and few opportunities', *Journal of Cerebral Blood Flow and Metabolism*, pp. 1986–1998.

Zanotti-Fregonara, P. *et al.* (2019) 'Automatic Extraction of a Reference Region for the Noninvasive Quantification of Translocator Protein in Brain Using 11C-PBR28', *Journal of Nuclear Medicine*, 60(7), pp. 978–984.

Zhang, L. *et al.* (2019) 'The effect of minocycline on amelioration of cognitive deficits and pro-inflammatory cytokines levels in patients with schizophrenia', *Schizophrenia Research*, 212, pp. 92–98.

Zhu, C. Bin *et al.* (2010) 'Interleukin-1 Receptor Activation by Systemic Lipopolysaccharide Induces Behavioral Despair Linked to MAPK Regulation of CNS Serotonin Transporters', *Neuropsychopharmacology 2010 35:13*, 35(13), pp. 2510–2520.

Zhu, C., Blakely, R.D. and Hewlett, W.A. (2006) 'The Proinflammatory Cytokines Interleukin-1beta and Tumor Necrosis Factor-Alpha Activate Serotonin Transporters', pp. 2121–2131.

Ziv, Y. *et al.* (2006) 'Immune cells contribute to the maintenance of neurogenesis and spatial learning abilities in adulthood', *Nature Neuroscience*, 9(2), pp. 268–275.

Zürcher, N.R. *et al.* (2020) '[11C]PBR28 MR–PET imaging reveals lower regional brain expression of translocator protein (TSPO) in young adult males with autism spectrum disorder', *Molecular Psychiatry 2020 26:5*, 26(5), pp. 1659–1669.

Appendix A: Self-reported questionnaires

Profile of Mood states (POMS)

Participant Id:

Directions: Read each statement and then circle the appropriate number to the right of the statement to indicate **HOW YOU FEEL RIGHT NOW**:

	Not at all	**A little**	**Moderately**	**Quite a bit**	**Extremely**
1. Tense	0	1	2	3	4
2. Feverish	0	1	2	3	4
3. Worn out	0	1	2	3	4
4. Angry	0	1	2	3	4
5. Lively	0	1	2	3	4
6. Confused	0	1	2	3	4
7. Shaky	0	1	2	3	4
8. Aching joints	0	1	2	3	4
9. Sad	0	1	2	3	4

10. Grouchy	0	1	2	3	4
11. Active	0	1	2	3	4
12. On edge	0	1	2	3	4
13. Annoyed	0	1	2	3	4
14. Energetic	0	1	2	3	4
15. Hopeless	0	1	2	3	4
16. Relaxed	0	1	2	3	4
17. Resentful	0	1	2	3	4
18. Unworthy	0	1	2	3	4
19. Uneasy	0	1	2	3	4
20. Can’t concentrate	0	1	2	3	4
21. Fatigued	0	1	2	3	4
22. Nauseated	0	1	2	3	4
23. Listless	0	1	2	3	4
24. Nervous	0	1	2	3	4
25. Lonely	0	1	2	3	4
	Not at all	**A little**	**Moderately**	**Quite a bit**	**Extremely**
26. Muddled	0	1	2	3	4
27. Furious	0	1	2	3	4

28. Cheerful	0	1	2	3	4
29. Exhausted	0	1	2	3	4
30. Gloomy	0	1	2	3	4
31. Sluggish	0	1	2	3	4
32. Headache	0	1	2	3	4
33. Weary	0	1	2	3	4
34. Bewildered	0	1	2	3	4
35. Alert	0	1	2	3	4
36. Bitter	0	1	2	3	4
37. Efficient	0	1	2	3	4
38. Hungry	0	1	2	3	4
39. Forgetful	0	1	2	3	4
40. Guilty	0	1	2	3	4
41. Vigorous	0	1	2	3	4
42. Thirsty	0	1	2	3	4

Participant Id:

Visual Analogue Scale (VAS) of Fatigue

Please score below how fatigued you currently feel

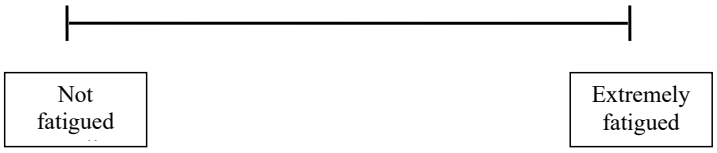

Sickness Questionnaire (SicknessQ)

INSTRUCTION: Read the statements below and then circle the number that best corresponds to *how you currently feel, in this very moment*. There are no right or wrong answers. Don't use too much time at each statement, just pick the answer you think best describes how you feel right now.

		Disagree	**Agree somewhat**	**Mostly agree**	**Agree**
0.	I want to keep still	0	1	2	3
2.	My body feels sore	0	1	2	3
3.	I wish to be alone	0	1	2	3
4.	I don't wish to do anything at all	0	1	2	3
5.	I feel depressed	0	1	2	3
6.	I feel drained	0	1	2	3
7.	I feel nauseous	0	1	2	3
8.	I feel shaky	0	1	2	3
9.	I feel tired	0	1	2	3
10.	I have a headache	0	1	2	3